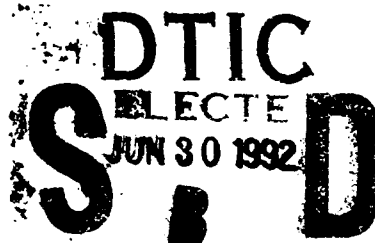CONTRACTOR REPORT BRL-CR-693

BRL

AD-A252 375

MEASUREMENT OF CLOSE-IN BLAST
AND SHOCK LOADS

JAMES K. GRAN
BAYARD S. HOLMES
SRI INTERNATIONAL

DTIC
ELECTE
JUN 30 1992
S B D

JULY 1992

U.S. ARMY LABORATORY COMMAND

BALLISTIC RESEARCH LABORATORY
ABERDEEN PROVING GROUND, MARYLAND

92-17032

92 6

NOTICES

REPORT DOCUMENTATION PAGE

1. AGENCY USE ONLY (Leave blank)	2. REPORT DATE July 1992	3. REPORT TYPE AND DATES COVERED Final, 31 Mar 89–29 May 92

4. TITLE AND SUBTITLE
Measurement of Close-In Blast and Shock Loads

5. FUNDING NUMBERS
PR: 1L162618AH80
C: DAAA15-89-C-0009

6. AUTHOR(S)
James K. Gran and Bayard S. Holmes

7. PERFORMING ORGANIZATION NAME(S) AND ADDRESS(ES)
SRI International
333 Ravenswood Avenue
Menlo Park, CA 94025

8. PERFORMING ORGANIZATION REPORT NUMBER
SRI Project 7422

9. SPONSORING / MONITORING AGENCY NAME(S) AND ADDRESS(ES)
U.S. Army Ballistic Research Laboratory
ATTN: SLCBR-DD-T
Aberdeen Proving Ground, MD 21005-5066

10. SPONSORING / MONITORING AGENCY REPORT NUMBER
BRL-CR-693

11. SUPPLEMENTARY NOTES
The Technical Monitor for this report is Mr. Robert Bitting, U.S. Army Ballistic Research Laboratory, ATTN: SLCBR-TB-B, Aberdeen Proving Ground, MD 21005-5066.

12a. DISTRIBUTION / AVAILABILITY STATEMENT
Approved for public release; distribution is unlimited.

12b. DISTRIBUTION CODE

13. ABSTRACT (Maximum 200 words)

On this contract, SRI International is developing a "flatpack" stress gage for BRL to use for measuring blast pressure histories on armored vehicles very near explosive charges. A flatpack stress gage comprises piezoresistance foil elements, such as manganin or ytterbium, encapsulated in a thin polymer layer and sandwiched between two steel strips welded at the edges. This gage is very well suited for measuring blast pressure loads on the surface of an armored vehicle because it can be attached to the target with no penetrations (by welding or bonding with epoxy) and it presents a very low profile obstacle to blast waves. In this project, we accomplished two major developments to make flatpacks usable for this application. First, the flatpack design was improved by using a very-high-strength steel case, confining the piezoresistance elements in a shallow cavity to mitigate strains, incorporating three piezoresistance elements in a single gage to measure inplane strains, and reducing the size of the gage so that all the elements fit within a 5-mm radius. Second, an analytical procedure was derived and a computer code was written to interpret resistance histories from three piezoresistance elements under nonuniaxial strain conditions based on the constitutive and piezoresistance properties of the elements. With these developments, the flatpack gage is now a usable tool for many blast-load measurement problems although additional calibration and validation experiments are recommended.

14. SUBJECT TERMS
piezoresistance, measurement, explosives, flatpack gage, blast

15. NUMBER OF PAGES
139

16. PRICE CODE

17. SECURITY CLASSIFICATION OF REPORT UNCLASSIFIED	18. SECURITY CLASSIFICATION OF THIS PAGE UNCLASSIFIED	19. SECURITY CLASSIFICATION OF ABSTRACT UNCLASSIFIED	20. LIMITATION OF ABSTRACT UL

INTENTIONALLY LEFT BLANK.

SUMMARY

The objective of this project was to provide Ballistic Research Laboratory (BRL) with a capability to measure explosively generated blast pressure histories at the surface of a structure very near the explosive. An example of a situation of interest is a 1-kg explosive charge spaced 100 mm from a steel surface. The peak blast pressure on the surface directly under this charge is about 25 kbar (2.5 GPa).

Our approach was to adapt the "flatpack" stress gage to this environment. A flatpack stress gage comprises piezoresistance foil elements encapsulated in a thin polymer layer and sandwiched between two steel strips welded at the edges. The steel case allows the gage to be welded to steel armored vehicles and enhances the survivability of the gage elements under severe loading conditions. However, the loading environment in this application is so severe that the gage elements stretch significantly and these "in-plane strains" reduce gage accuracy. In the current effort, we built flatpack stress gages containing three piezoresistance elements: a manganin (or ytterbium) element to measure normal stress and two constantan elements to measure in-plane strains. That is, the measured in-plane strains were used to more accurately interpret the resistance history from the manganin (or ytterbium) element.

This approach required the development of a new flatpack gage design and the development of an analytical method for interpreting the piezoresistance element resistance histories. The flatpack gages contain a manganin (or ytterbium) element and two constantan elements arranged as shown in Figure 1. All three sensing elements lie within a 5-mm radius. Figure 2 shows the configuration of an explosive blast test with a manganin flatpack gage 10.6 cm from a 904-g HE charge. The resistance histories from this test are plotted in Figure 3.

The method for interpreting these resistance histories combines the piezoresistance relations and the constitutive relations for the three elements to determine stresses and strains from the three simultaneous measurements of resistance change. The piezoresistance and constitutive properties of the element materials are taken from previous work by Gupta and colleagues.[1-4] In addition to the requirement that the piezoresistance properties and constitutive properties of each element be known, the analysis relies on the assumptions that (1) all three elements experience the same normal stress, (2) the elements are aligned in the principal directions,* and (3) the coupling of the in-plane strains from the matrix (the insulating material inside the flatpack) to the elements is known. The piezoresistance relations, constitutive relations, and coupling relations form a system of 21 scalar equations. The unknowns are the normal stress and in-plane strains in the matrix and the six principal stresses and strains in each element. A computer program named PIEZOR was written to iteratively solve these equations.

The data recorded in explosive blast experiments were analyzed with PIEZOR to determine the stresses and strains inside flatpack gages. For the data shown in Figure 3, three analyses were performed so that the sensitivity of the result to two parameters could be observed. These parameters are the coupling of transverse in-plane strain into the piezoresistance elements $[(\lambda_{33})_n]$ and the coefficient relating resistance change to plastic strain (η_n). The solid lines in Figure 4 are computed with $\lambda_{33} = 0$ and $\eta = 0$ for all three elements. The assumption of zero coupling is

---

*This assumption is consistent with the notion that the principal directions inside the flatpack are controlled by the flatpack case. It does not require that the flatpack itself be aligned with the principal loading directions.
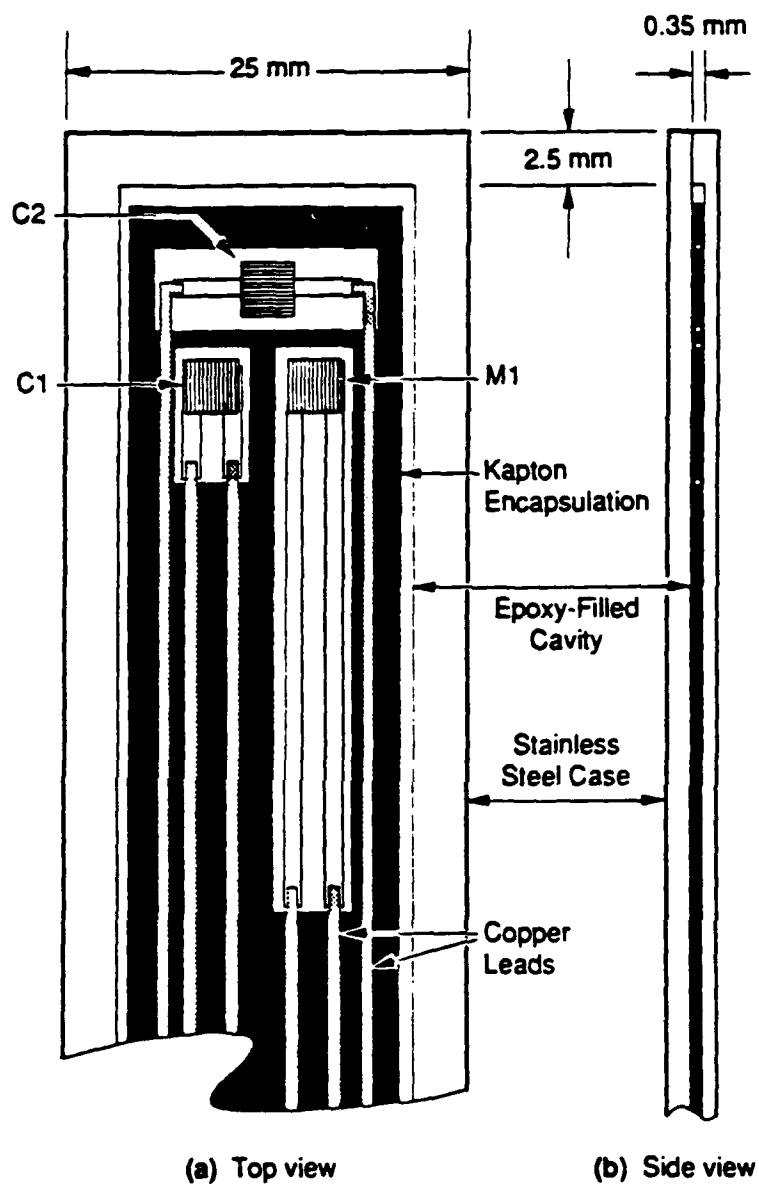
Figure 1. Layout of the three-element flatpack, with one manganin element (M1) and two constantan elements (C1 and C2) in a shallow flat-bottom cavity.
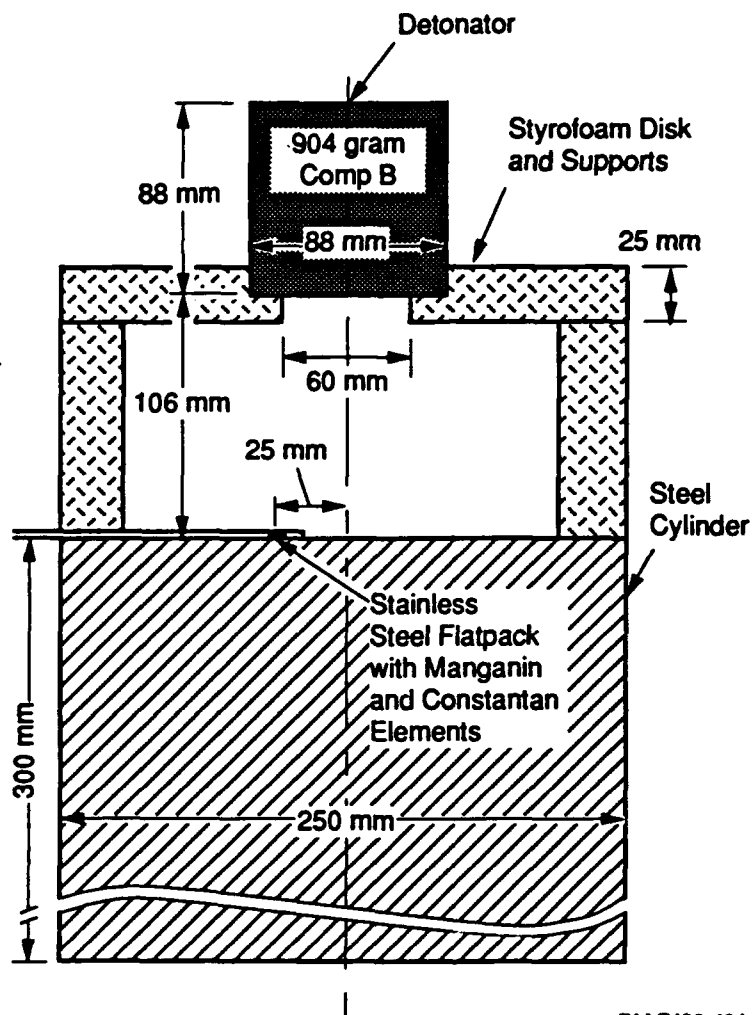
Figure 2. Explosive blast test configuration.

Figure 3.   Resistance histories from a three-element flatpack gage
in an explosive blast experiment.

RA-7422-58A

(a) Sensitivity to transverse strain coupling

$\lambda_{33} = 0, \eta = 0$
$\lambda_{33} = 1, \eta = 0$

(b) Sensitivity to plastic strain coefficient

$\lambda_{33} = 0, \eta = 0$
$\lambda_{33} = 0, \eta \neq 0$
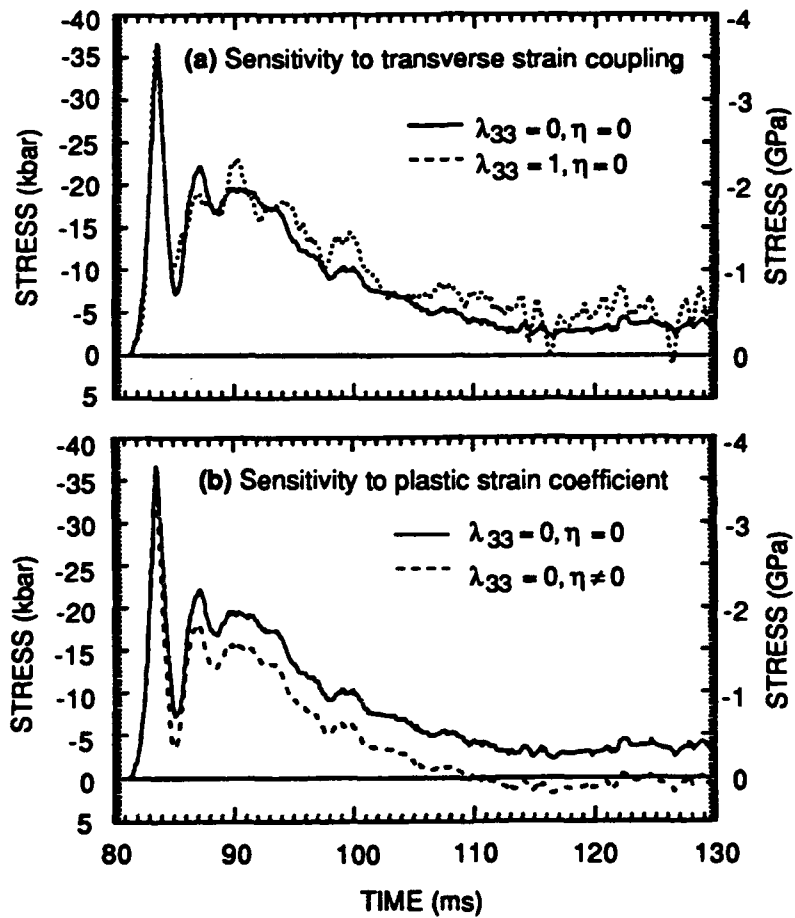
RM-7422-59A

Figure 4.   Flatpack stress determined with PIEZOR.
Compression stress is negative.

consistent with the very low (<1%) coupling coefficient for the constantan elements for surface-mounted conditions with no normal stress.[10] Zero dependence on plastic strain is consistent with the static properties of manganin and constantan.[1]

The dotted curve in Figure 4(a) is computed with $\lambda_{33} = 1$ and $\eta = 0$ for all three elements. For this case, the dependence of the computed stress on the transverse strain coupling is small because the stress produces a large resistance change in the manganin and the flatpack limits the transverse strains.

The dashed curve in Figure 4(b) is computed with $\lambda_{33} = 0$ for all three elements, $\eta = 0$ for the constantan elements, but η for manganin taken as the function of plastic strain determined in shock wave experiments (200 ns duration).[4] The comparison shows a significant dependence of the computed stress on η.

In summary, a flatpack stress gage containing piezoresistance foil elements is very well suited for measuring blast pressure loads on the surface of an armored vehicle because it can be attached to the target with no penetrations (by welding or bonding with epoxy) and it presents a very-low-profile obstacle to blast waves. Two important developments were used in this project to make flatpacks usable for this application. First, the flatpack design was improved by using a very-high-strength steel case, incorporating three piezoresistance elements in a single gage, confining the piezoresistance elements in a shallow cavity to mitigate strains, and reducing the size of the gage so that all the elements fit within a 5-mm radius. Second, an analytical procedure was derived and a computer code was written to interpret resistance histories from the piezoresistance elements in non-uniaxial strain conditions based on the constitutive and piezoresistance properties of the elements. With these developments, the flatpack gage is now a useful tool for many blast-load measurement problems.

A good next step in the advancement of the flatpack gage at BRL is to continue to use it in explosive blast environments. A repeat of the experiment shown here would provide a measure of reproducibility of the results, and a detailed calculation of this experiment would help determine the range of uncertainty in the mechanical and piezoresistance parameters of the elements (especially λ_{33} and η). Other experiments for which the pressures can be calculated or measured, such as contact explosives or explosively driven flyer-plate impacts, should aslo be performed. To further the gage's utility, the flatpack should be tested under fragmenting rounds and hardened as necessary to perform in that application.

Additional basic work is also needed to eliminate some of the uncertainties in the properties of the piezoresistance elements, and to determine in more detail the mechanical response of the gage case, the insulation, and the elements.

PREFACE

CONTENTS

LIST OF ILLUSTRATIONS

LIST OF SYMBOLS

ρ	density
c	sound speed
K	bulk modulus
G	shear modulus
E	Young's modulus
ν	Poisson's ratio
H	hardening modulus (slope of uniaxial tension test stress-strain curve)
σ	stress
ε	stain
σ_y	yield strength
$\bar{\sigma}$	effective stress
$\bar{\varepsilon}^p$	equivalent plastic strain
R	resistance
α	piezoresistance coefficient for principal stresses
β	piezoresistance coefficient for stress parallel to current flow
η	piezoresistance coefficient for plastic strain
A	factor of functional form for η
g	factor of functional form for η
Ω	transformation matrix for stresses and strains from flatpack to element reference
f	vector containing matrix material normal stress and in-plane strains
s	vector containing element normal stress and in-plane strains
t	vector containing element in-plane stresses and normal strain
N	parameter in incremental plasticity analysis
Λ	coupling matrix relating matrix material and element stresses and strains
λ	element of Λ

SECTION 1

INTRODUCTION

The objective of this project was to provide BRL with a capability to measure explosively generated blast pressure histories at the surface of a structure very near the explosive. An example of a situation of interest is a 1-kg explosive charge spaced 100 mm from a steel surface. The peak blast pressure on the surface directly under this charge is about 25 kbar (2.5 GPa).

Our approach was to adapt the "flatpack" stress gage to this environment. A flatpack stress gage comprises piezoresistance foil elements, such as manganin or ytterbium, and copper foil leads encapsulated in a thin insulating layer and sandwiched between two steel strips welded at the edges. This package enhances the survivability of the elements and leads, and it helps to mitigate the in-plane strains in two- and three-dimensional loading conditions. Historically, piezoresistance elements have been used only in uniaxial strain conditions (no in-plane strain) for which the relation between normal stress and resistance change has been established in gas-gun impact experiments. However, the large in-plane strains produced in the loading environment near an explosive charge degrade the accuracy of a flatpack gage significantly. To overcome this problem, we built flatpack stress gages containing constantan strain gages to measure the in-plane strains, and we used this additional information to more accurately interpret the resistance history from the manganin or ytterbium elements.

This approach required the development of a new flatpack gage design and the development of an analytical method for interpreting the piezoresistance element resistance histories. In the new flatpack gages, one predominantly stress-sensitive element (manganin or ytterbium) and two predominantly strain-sensitive elements (constantan) were arranged within a 5-mm radius. The gage packages measured 25 mm wide, 1.3 mm thick, and about 300 mm long. The new analytical interpretation method is more than a simple correction for strain. A numerical algorithm named PIEZOR was developed to solve simultaneously the combined set of piezoresistance equations and elastic-plastic constitutive equations for the three piezoresistance elements in a flatpack. Thus, in addition to determining the normal stress, the algorithm provides all three principal stresses and strains in all three elements as functions of time.

Several gage-development experiments were performed and two major gage-demonstration experiments were performed. In the demonstration experiments, flatpacks containing ytterbium elements were loaded in a gas-gun impact, and flatpacks containing manganin elements were loaded with an explosive blast. The records from these experiments were interpreted with the PIEZOR algorithm and compared with calculated environments. In general, the three-element flatpack gages performed well and the PIEZOR algorithm provided a straightforward method for interpreting the resistance histories for non-uniaxial elastic-plastic response.

The remainder of the report is organized as follows: Sections 2 and 3 describe the design of the flatpack gages and the derivation of the analytical procedure for interpreting their resistance histories. Sections 4 and 5 describe results of an explosive blast test and a plate impact test on flatpack gages. Section 6 presents our conclusions and offers recommendations for future work. These sections are followed by Appendices A through E, which describe the piezoresistance material models, the PIEZOR computer program, finite-difference computations of explosive blast loads, preliminary experiments, and electronics considerations for using flatpack gages.

1

SECTION 2

FLATPACK GAGES

A drawing of a three-element flatpack gage is shown in Figure 5; photographs of flatpacks without covers are shown in Figure 6. All three sensing elements are roughly 3-mm-square grids and lie within a 5-mm radius. The case is made of heat-treated 17-7PH stainless steel ($R_c = 48$) and comprises a base and a cover, each measuring 25 mm wide, 1.3 mm thick, and 300 mm long. The base has a 0.36-mm-deep, 20-mm-wide cavity into which the elements and insulation are placed. The elements and their 0.05-mm-thick by 1.3-mm-wide soldered copper leads are first encapsulated between layers of 0.025-mm-thick Kapton; this sandwich is then potted in Shell Epon 815 epoxy in the cavity. Finally, the base and cover are welded together at their edges.

Specific assembly procedures are as follows:

(1) Bond the elements to one layer of Kapton with Shell Epon 815 epoxy.

(2) Solder the copper leads to the solder tabs.

(3) Bond the other layer of Kapton over the elements and leads with 815.

(4) Bond the Kapton/element sandwich to the bottom of the cavity in the 17-7PH steel case with 815, then fill the cavity with 815.

(5) Lap the top surface of the epoxy to make it flat and flush with the rim of the steel.

(6) Clamp the two steel pieces between copper chill bars. These can be square-section bars with one hole down the center and cold water circulating through the hole. The edges of the steel should protrude from between the chill bars by about 2 mm for welding.

(7) Weld the edges with a TIG welder. The welder used in this work is a Miller Dialarc HF-P with the following settings: Argon 98%, Oxygen 2%, Straight Polarity, 10-55 DC, Ampere Adjustment 100, Remote Amperage Off, Remote Contactor On, High Frequency Start, Electrode Size 15-16. The weld is made with a Gullco Kat II tractor feed set at 10 ipm.

The piezoresistance elements used in the three-element flatpack gages are listed in Table 1. These elements are all commercially available, they all have approximately the same grid geometry, and they are all encapsulated in polyimide.

We performed a three-dimensional finite-element analysis of this flatpack design in a blast environment, using the DYNA3D finite-element code.[12] In this calculation, the gage was bonded to the top surface of a thick steel plate, and a surface pressure was applied. The spatial dependence of the load was defined with the Gaussian distribution $P_{peak} = P_0 e^{-(r/r_0)^2}$, where P_{peak} is the peak pressure at radius r, $P_0 = 43$ kbar (4.3 GPa), and $r_0 = 29$ mm. The pressure pulse shape at every

2

0.35 mm

25 mm

2.5 mm

C2

C1 — M1

Kapton
Encapsulation

Epoxy-Filled
Cavity

Stainless
Steel Case

Copper
Leads

(a) Top view (b) Side view
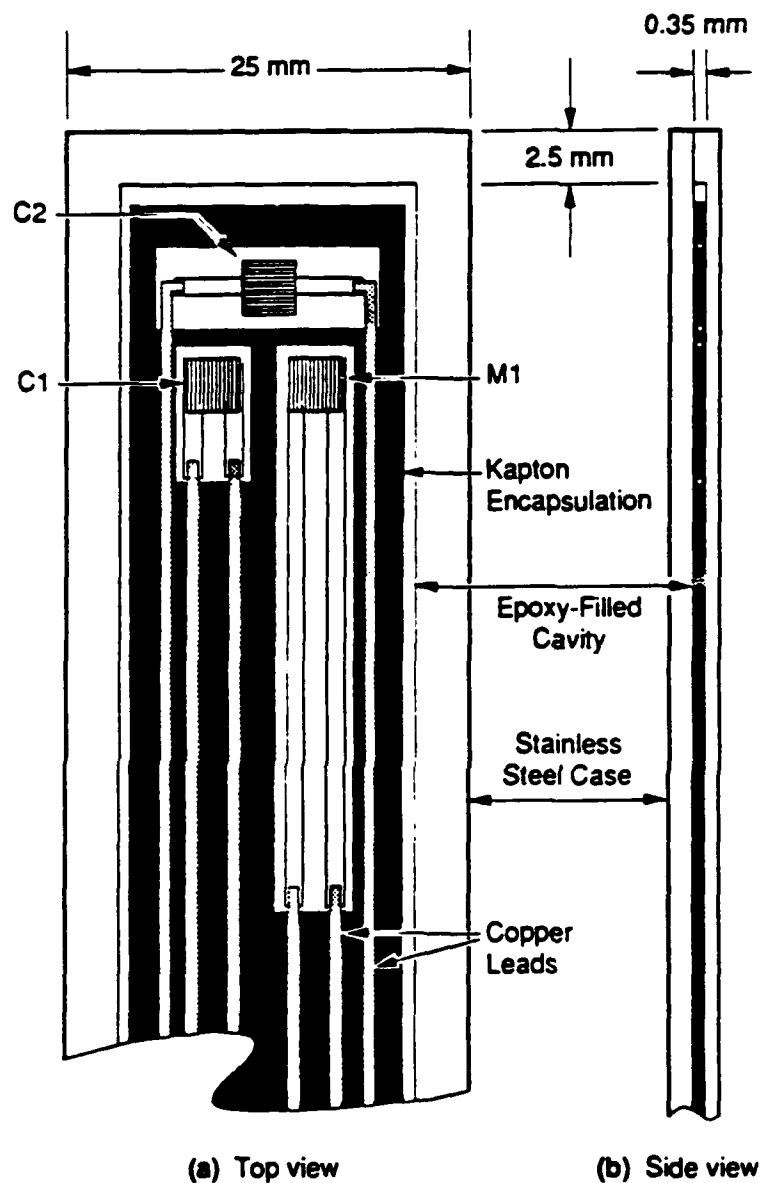
RA-7422-38D

Figure 5.   Layout of the three-element flatpack, with one manganin
element (M1) and two constantan elements (C1 and C2)
in a shallow flat-bottom cavity.

3
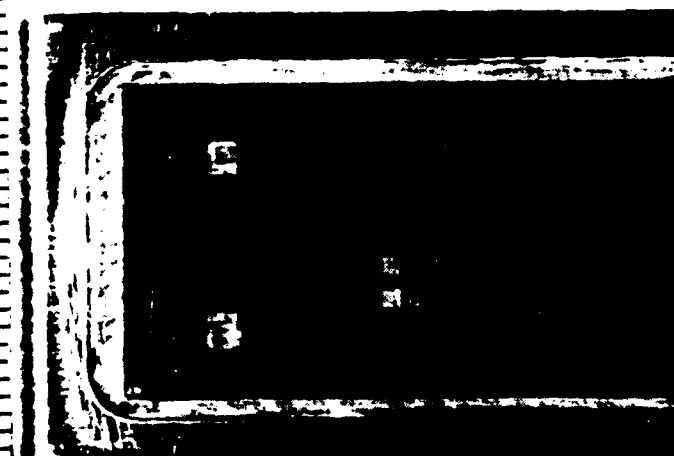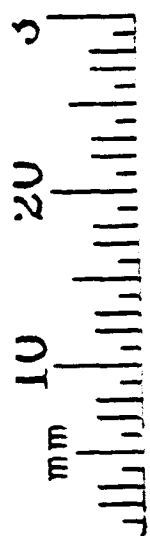
RP-7422 46

(a) Ytterbium
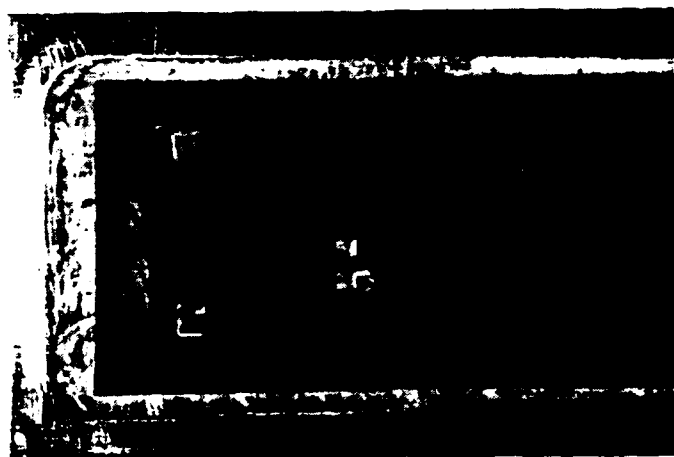
(b) Manganin

Figure 6.   Three-element flatpack gages.

4

Table 1. Piezoresistance elements for flatpack gages.

Element	Model	Resistance (ohms)	Overall Width (mm)	Number of Grid Legs	Grid Leg Length (mm)	Grid Leg Width (mm)	Thickness* (mm)
Manganin	Micromeasurements J2M-SS-110FB-048	48	2.8	12	3.1	0.062	0.005
Ytterbium	Dynasen Yb4-50-EK	50	3.1	18	3.1	0.075	0.006
Longitudinal Constantan	Micromeasurements CEA-06-125UN-350	350	3.1	24	2.8	0.025	0.005
Transverse Constantan	Micromeasurements CEA-06-125UE-350	350	3.1	24	2.8	0.025	0.005

*The thickness is estimated from the grid leg length and width, the element resistance, and the nominal resistivity of the material.

radius was a triangle with zero rise time and a 20-μs duration.* The flatpack was oriented in the radial direction and was located with the center of the sensing area 27.8 mm from the center of the plate. The steel plate, the flatpack case, and the epoxy were modeled as simple elastic-plastic materials with yield strengths of 1 GPa, 1.2 GPa, and 100 MPa, respectively. The piezoresistance elements, leads, and Kapton were not modeled explicitly because the very small elements required to model them would have greatly increased computing time; instead, the cavity within the flatpack was assumed to be filled entirely with epoxy. Figure 7 shows the normal stress and in-plane strains computed in the epoxy layer in the flatpack gage at the 27.8-mm radius. At this location, the peak pressure applied to the surface of the gage was 17.2 kbar (1.72 GPa). The calculation indicates that the gage responds in a damped oscillatory mode with a period of about 5 μs. This oscillation was also observed in the blast experiments, described in Section 4 and Appendix D. The calculated in-plane strains are less than 1%, also consistent with experimental observation.

The oscillation in the gage stress is caused by the motion of the cover plate on the epoxy-filled cavity. The formula for the period of this motion is

$$T = 2\pi \sqrt{\frac{\rho h d}{K + \frac{4}{3}G}}$$

where ρ and h are the density and thickness of the cover plate, and K, G, and d are the bulk modulus, shear modulus, and depth of the epoxy layer. (Using ρ = 7.9 g/cm^3, h = 1.27 mm, K = 3.9 GPa,[5] G = 1.5 GPa,[5] and d = 0.36 mm, we calculate the period as 4.9 μs). The oscillation of the gage stress is accentuated in the finite-element calculation for two reasons. First, the rise time

*This pressure loading was based on the results of a finite-difference computation of a 165-g C-4 explosive charge over a steel plate (see Appendix C).
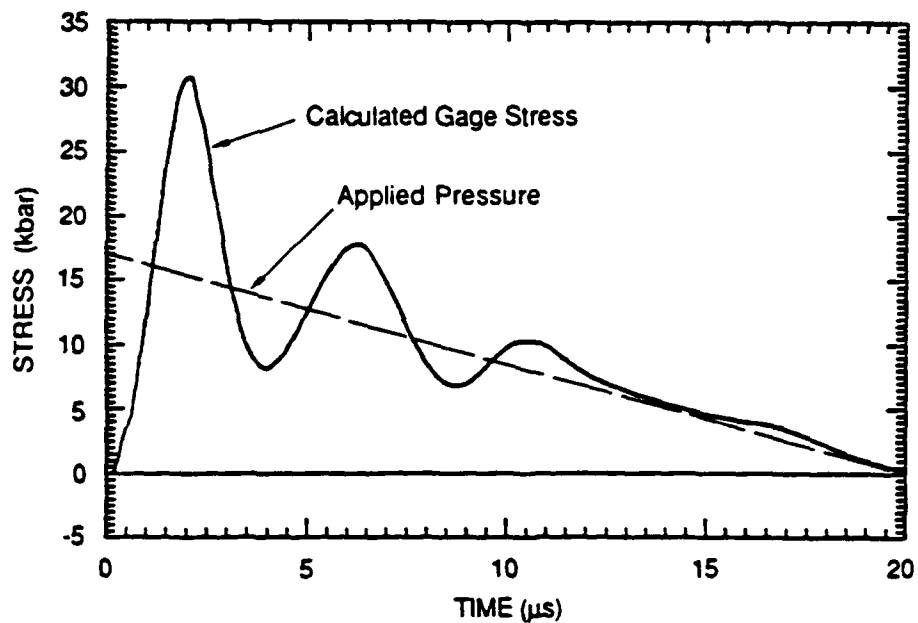
(a) Normal stress (compression positive)
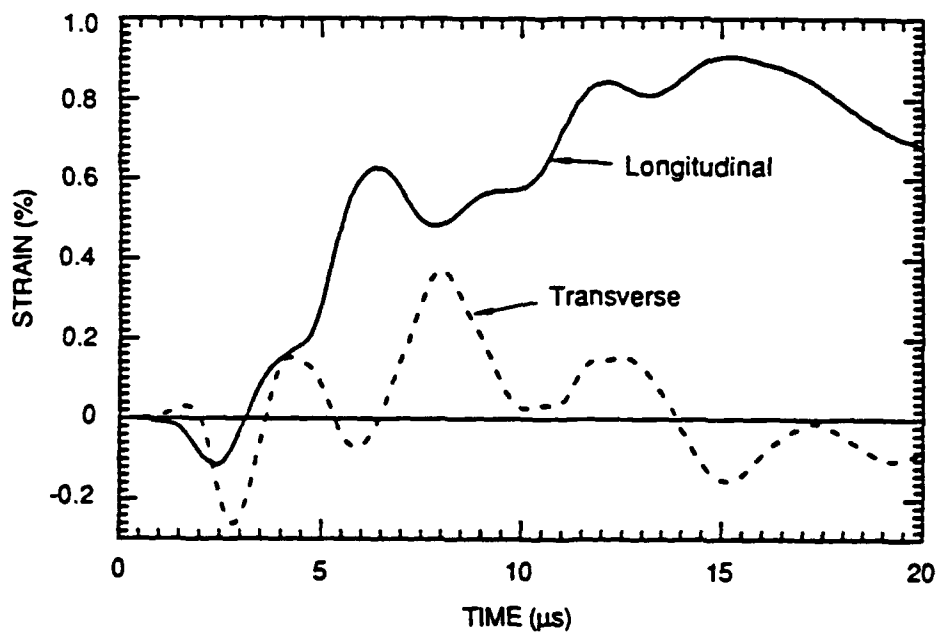
(b) In-plane strains (tension positive)

RA-7422-47B

Figure 7.   Three-dimensional finite-element analysis of a flatpack gage under blast loading.

6

of the blast pressure in the calculation was zero, whereas an actual blast pressure loading has a finite rise time. Second, this gage is designed for use in larger scale blast environments for which the duration will be a factor of 2 or more longer than in the calculation, which corresponds to our sub-scale developmental experiments.

In theory, the magnitude of stress oscillations could be reduced by increasing the natural frequency of the gage. One way to accomplish this would be to decrease the cover thickness and cavity depth (h and d) and to increase the stiffness of the insulating layers (K and G). Other options would be to decrease the density of the cover plate (ρ), by replacing the high-strength stainless steel cover with titanium, or to miniaturize the entire package.

In an attempt to reduce the magnitude of the stress record oscillations, we built two gages with the cavity depth cut in half to 0.18 mm (0.007 inch). In addition, the Kapton insulation was replaced with mica, which has an elastic modulus similar to that of steel. In one gage, the cover thickness was also reduced by a factor of 2 to 0.64 mm (0.025 inch). In an explosive blast experiment (Test 6, Section 4) the mica-insulated gage with the standard cover showed less overshoot than a Kapton-insulated gage, but the in-plane strains were larger and the gage failed before the measurement was complete. The larger strains were not expected, and this may not be a general result. However, mica is a layered, anisotropic mineral and it may allow more shear deformation between layers than assumed in this design. The gage with the thin cover failed at the time of arrival of the blast.

7

SECTION 3

PIEZORESISTANCE ANALYSIS

Because some in-plane strain in the manganin and ytterbium elements is inevitable, a method is needed to account for these strains when interpreting the resistance histories to determine stresses. Furthermore, because the elements will undergo plastic deformation, the analysis of piezoresistance gage records must include elastic-plastic element response. This section describes the PIEZOR algorithm, an analytical procedure developed in this project to interpret piezoresistance flatpack gage records.

As described earlier, the measurement strategy adopted here is to record resistance histories from three independent piezoresistance elements positioned at the same "point" within the flatpack and oriented in the principal directions of the insulation matrix stress and strain fields. In the example shown in Figure 8, one manganin element and two constantan elements oriented at right angles to one another are used to measure normal stress and two in-plane strains. The manganin element is primarily sensitive to stress normal to the element; the constantan elements are primarily sensitive to strain in the direction of the element grid. Each element, however, has sensitivity to all three principal stresses and strains. The analysis simultaneously solves the piezoresistance equations and the elastic-plastic constitutive equations for the three elements to determine stresses and strains from three simultaneous measurements of resistance change.

In addition to the requirement that the piezoresistance properties and constitutive properties of each element be known, the analysis relies on the assumptions that (1) all three elements experience the same normal stress, (2) the elements are aligned in the principal directions, and (3) the coupling of the in-plane strains from the matrix (the insulating material inside the flatpack) to the elements is known. The piezoresistance and constitutive properties of the element materials are taken from previous work by Gupta and colleagues.[1-4] The first assumption is supported by the results of finite-element calculations performed by Ito and Muki.[6] The second assumption is consistent with the notion that the principal directions inside the flatpack are normal to the planes of symmetry of the case, i.e., longitudinal, transverse, and through-the-thickness. The third assumption is a statement of the so-called inclusion problem, for which a general solution is not available. For strains in the direction of the element grid legs, one-to-one coupling is safely assumed because of the tremendous aspect ratio of the grid legs. Although the coupling of transverse strain to the element grids is much less certain, the analysis suggests that the resolved stress is not terribly sensitive to this relation.

As shown in Figure 8, an x, y, z coordinate system is fixed in the flatpack, and a 1, 2, 3 coordinate system fixed in each element with the 1 direction parallel to the element grid, the 2 direction transverse to the element grid, and the 3 direction normal to the element grid. The increments of principal stress and strain in the nth element are grouped into two one-dimensional arrays s_n and t_n, and a one-dimensional array f contains the increments in normal stress and in-plane strains in the matrix.

$$s_n = \begin{bmatrix} \Delta\sigma_3 \\ \Delta\varepsilon_1 \\ \Delta\varepsilon_2 \end{bmatrix}_n \qquad t_n = \begin{bmatrix} \Delta\sigma_1 \\ \Delta\sigma_2 \\ \Delta\varepsilon_3 \end{bmatrix}_n \qquad f = \begin{bmatrix} \Delta\sigma_z \\ \Delta\varepsilon_x \\ \Delta\varepsilon_y \end{bmatrix} \qquad (1)$$

8
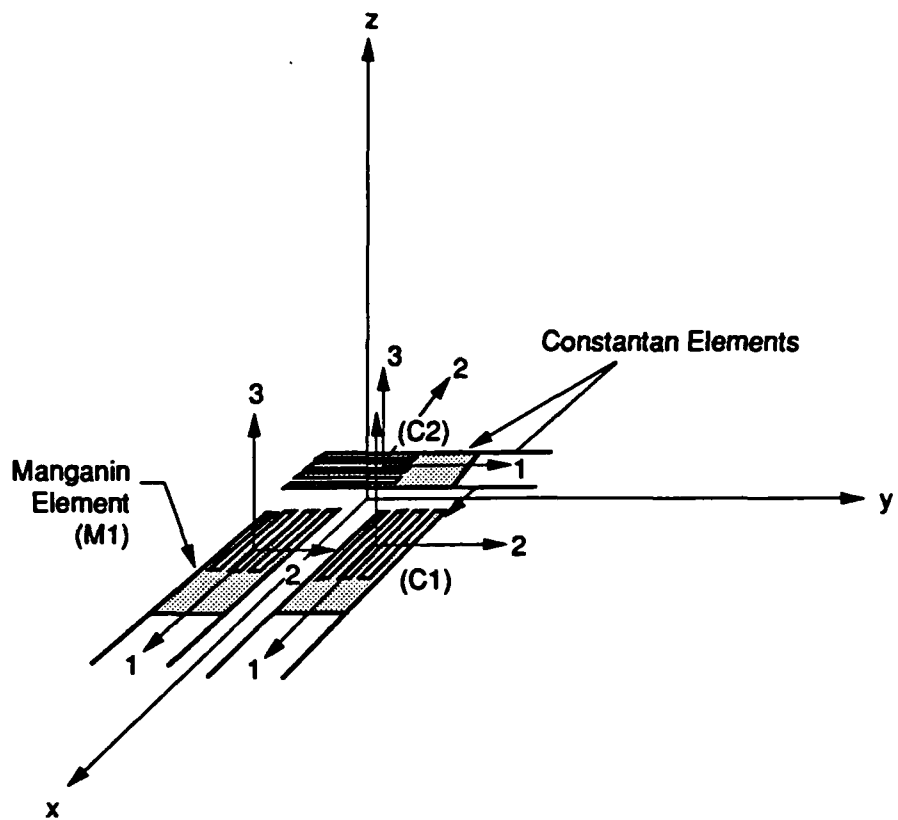
Figure 8. Orientation of three piezoresistance elements in a plane.

RM-7422-30A

9

The rotation matrix Ω_n relates the matrix stresses and strains in the flatpack coordinate system to those in the n-th element coordinate system. From Mohr's circle for two-dimensional strain,[11]

$$\Omega_n = \begin{bmatrix} 1 & 0 & 0 \\ 0 & \cos^2\theta_n & \sin^2\theta_n \\ 0 & \sin^2\theta_n & \cos^2\theta_n \end{bmatrix} \tag{2}$$

where θ_n is the angle between the X-axis and the 1_n-axis.

The coupling matrix Λ_n relates the normal stress and in-plane strain increments in the nth element to those in the matrix.

$$\Lambda_n = \begin{bmatrix} 1 & 0 & 0 \\ 0 & 1 & 0 \\ 0 & 0 & \lambda_{33} \end{bmatrix}_n \tag{3}$$

Thus, the normal stress and in-plane strain increments in the nth element are related to those in the matrix by

$$s_n = \Lambda_n \, \Omega_n \, f \tag{4}$$

The form of Λ_n implies that the normal stress and in-plane strain increments along the length of the element grid are identical to the matrix stress and strain increments in those directions, but the transverse in-plane strain increment in the element is coupled to the matrix strain increment by the factor λ_{33}. The Λ_n matrix could be made more general to represent an inclusion analysis of the element in the matrix. (By setting $\lambda_{22} = \lambda_{33} = 0$, we impose uniaxial strain conditions.)

The incremental elastic-plastic constitutive relation for the nth element is (with the subscript n omitted for clarity)[7]

$$\Delta\sigma_1 = (K + \tfrac{4}{3}GN) \, \Delta\varepsilon_1 + (K - \tfrac{2}{3}GN) \, \Delta\varepsilon_2 + (K - \tfrac{2}{3}GN) \, \Delta\varepsilon_3 + \sigma'_{1o}(N - 1)$$

$$\Delta\sigma_2 = (K - \tfrac{2}{3}GN) \, \Delta\varepsilon_1 + (K + \tfrac{4}{3}GN) \, \Delta\varepsilon_2 + (K - \tfrac{2}{3}GN) \, \Delta\varepsilon_3 + \sigma'_{2o}(N - 1)$$

$$\Delta\sigma_3 = (K - \tfrac{2}{3}GN) \, \Delta\varepsilon_1 + (K - \tfrac{2}{3}GN) \, \Delta\varepsilon_2 + (K + \tfrac{4}{3}GN) \, \Delta\varepsilon_3 + \sigma'_{3o}(N - 1) \tag{5}$$

where $\Delta\sigma_i$ and $\Delta\varepsilon_i$ are principal stress and strain increments, σ_{io} and σ'_{io} are initial values of the principal stresses and stress deviators, and K and G are the bulk and shear moduli. N is given by

10

$(H + 3G\frac{\bar{\sigma}_0}{\bar{\sigma}^N})/(H + 3G)$, where H is the hardening modulus, $\bar{\sigma}_0$ is the initial value of the effective

stress expressed as $\sqrt{\frac{3}{2}[(\sigma'_{1o})^2 + (\sigma'_{2o})^2 + (\sigma'_{3o})^2]}$, and $\bar{\sigma}^N$ is the effective stress computed

with entirely elastic strain increments, for which the stress deviators are $\sigma'^N_i = \sigma'_{io} + 2G\Delta\epsilon'_i$.

Using matrix notation and rearranging terms, we can rewrite the constitutive relation

$$\begin{bmatrix} \Delta\sigma_1 \\ \Delta\sigma_2 \\ \Delta\sigma_3 \end{bmatrix} - (N-1)\begin{bmatrix} \sigma'_{1o} \\ \sigma'_{2o} \\ \sigma'_{3o} \end{bmatrix} = \begin{bmatrix} m_{11} & m_{12} & m_{13} \\ m_{21} & m_{22} & m_{23} \\ m_{31} & m_{32} & m_{33} \end{bmatrix}\begin{bmatrix} \Delta\epsilon_1 \\ \Delta\epsilon_2 \\ \Delta\epsilon_3 \end{bmatrix} \tag{6}$$

and make the independent quantities increments in normal stress and in-plane strains

$$\begin{bmatrix} \Delta\sigma_1 \\ \Delta\sigma_2 \\ \Delta\epsilon_3 \end{bmatrix} = M^*\begin{bmatrix} \Delta\sigma_3 \\ \Delta\epsilon_1 \\ \Delta\epsilon_2 \end{bmatrix} + \begin{bmatrix} (N-1)\sigma'_{1o} \\ (N-1)\sigma'_{2o} \\ 0 \end{bmatrix} - M^*\begin{bmatrix} (N-1)\sigma'_{3o} \\ 0 \\ 0 \end{bmatrix} \tag{7}$$

where

$$M^* = \begin{bmatrix} (\frac{m_{13}}{m_{33}}) & (m_{11} - \frac{m_{13}m_{31}}{m_{33}}) & (m_{12} - \frac{m_{13}m_{32}}{m_{33}}) \\ (\frac{m_{23}}{m_{33}}) & (m_{21} - \frac{m_{23}m_{31}}{m_{33}}) & (m_{22} - \frac{m_{23}m_{32}}{m_{33}}) \\ (\frac{1}{m_{33}}) & (-\frac{m_{31}}{m_{33}}) & (-\frac{m_{32}}{m_{33}}) \end{bmatrix} \tag{8}$$

For the nth element, this equation condenses to

$$t_n = M^*_n s_n + b_n \tag{9}$$

where

$$b_n = \begin{bmatrix} (N-1)\sigma'_{1o} \\ (N-1)\sigma'_{2o} \\ 0 \end{bmatrix}_n - M^*_n\begin{bmatrix} (N-1)\sigma'_{3o} \\ 0 \\ 0 \end{bmatrix}_n \tag{10}$$

11

The piezoresistance equation that relates the incremental change in resistance of the nth element ΔR_n, normalized by the initial value of resistance $(R_o)_n$, to an increment in principal stresses and strains is

$$\frac{\Delta R_n}{(R_o)_n} = \alpha_i\,\Delta\sigma_{3n} + \Delta\varepsilon_{1n} - \Delta\varepsilon_{2n} + (\alpha_n + 2\beta_n)\Delta\sigma_{1n} + \alpha_n\,\Delta\sigma_{2n} - \Delta\varepsilon_{3n} + \eta_n\frac{\sqrt{3}}{2}\,\Delta\bar{\varepsilon}^p_n \qquad (11)$$

where α_n, β_n, and η_n are piezoresistance properties of the nth element and $\Delta\bar{\varepsilon}^p_n$ is the increment in the plastic strain in the nth element. This relation can be written in the form

$$r_n = \begin{bmatrix} \alpha_n & 1 & -1 \end{bmatrix}\begin{bmatrix} \Delta\sigma_{3n} \\ \Delta\varepsilon_{1n} \\ \Delta\varepsilon_{2n} \end{bmatrix} + \begin{bmatrix} (\alpha_n + 2\beta_n) & \alpha_n & -1 \end{bmatrix}\begin{bmatrix} \Delta\sigma_{1n} \\ \Delta\sigma_{2n} \\ \Delta\varepsilon_{3n} \end{bmatrix} + \eta_n\frac{\sqrt{3}}{2}\,\Delta\bar{\varepsilon}^p_n \qquad (12)$$

or

$$r_n = P_n\,s_n + Q_n\,t_n + \eta_n\frac{\sqrt{3}}{2}\,\Delta\bar{\varepsilon}^p_n \qquad (13)$$

Equations (4), (9), and (13) form a system of 21 scalar equations. The unknowns are the normal stress and in-plane strains in the matrix, contained in f, and the 6 principal stresses and strains in each element, contained in s_n and t_n. These are solved by substituting (4) and (9) into (13) to get

$$r_n = P_n\,\Lambda_n\,\Omega_n\,f + Q_n\,M_n^*\,\Lambda_n\,\Omega_n\,f + Q_n b_n + \eta_n\frac{\sqrt{3}}{2}\,\Delta\bar{\varepsilon}^p_n \qquad (14)$$

which can be rewritten as

$$r_n - \eta_n\frac{\sqrt{3}}{2}\,\Delta\bar{\varepsilon}^p_n - Q_n b_n = [P_n\,\Lambda_n\,\Omega_n + Q_n\,M_n^*\,\Lambda_n\,\Omega_n]\,f \qquad (15)$$

or, condensing further

$$r^* = W\,f \qquad (16)$$

where r^* is a 3 x 1 array whose nth element is $r_n - \eta_n\frac{\sqrt{3}}{2}\,\Delta\bar{\varepsilon}^p_n - Q_n b_n$ and W is a 3 x 3 array whose nth row is given by $P_n\,\Lambda_n\,\Omega_n + Q_n\,M_n^*\,\Lambda_n\,\Omega_n$. Equation (16) is solved iteratively for f; then equations (4) and (9) provide s_n and t_n. A computer program named PIEZOR was written to perform this task.

12

The PIEZOR program was tested with a sample problem generated with a NIKE2D finite-element computation. In this problem, constantan and manganin elements aligned like those in Figure 8 were subjected to the boundary conditions plotted in Figures 9(a) and (b). The normal stress ramped linearly to 10 kbar (1 GPa) and remained at that level; the longitudinal strain oscillated in a saw-tooth wave form with an amplitude of ±1%; the transverse strain remained zero. Because these boundary conditions were applied directly to each element (not through a matrix material), Λ_n is the identity matrix for each element. The stresses and strains computed with NIKE2D were used in equation (13) to obtain resistance histories for each element. These are shown in Figure 9(c). Note that for these conditions the output of the manganin gage is far from constant during the phase of constant stress.

The resistance histories were input to PIEZOR, which calculated the element stresses and strains. Comparisons of the output from PIEZOR with the output from NIKE2D are shown in Figures 10 through 13. All the stresses and strains in each element were computed with very good accuracy (<1% error).
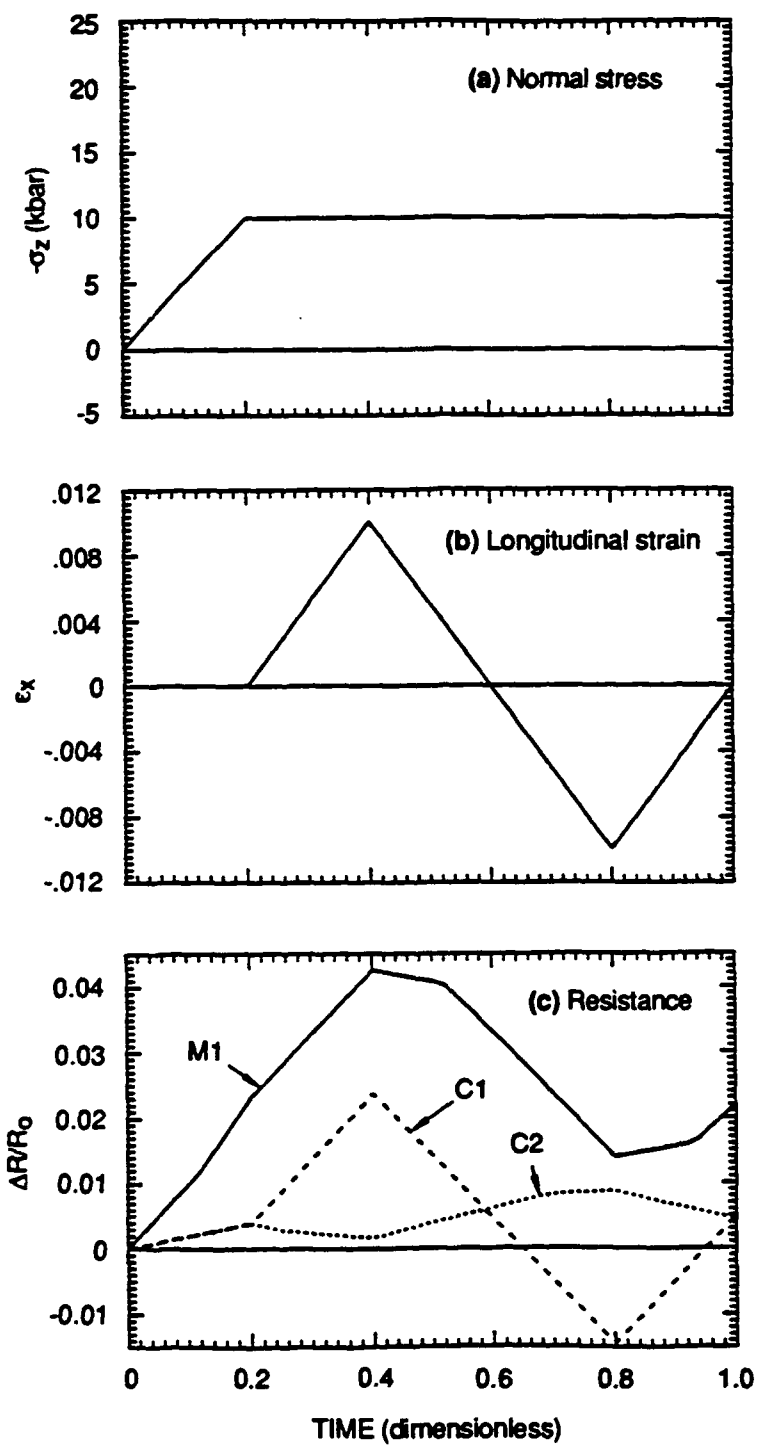
Figure 9. Applied boundary conditions and computed resistance histories for sample piezoresistance analysis problem ($\eta = 0$).
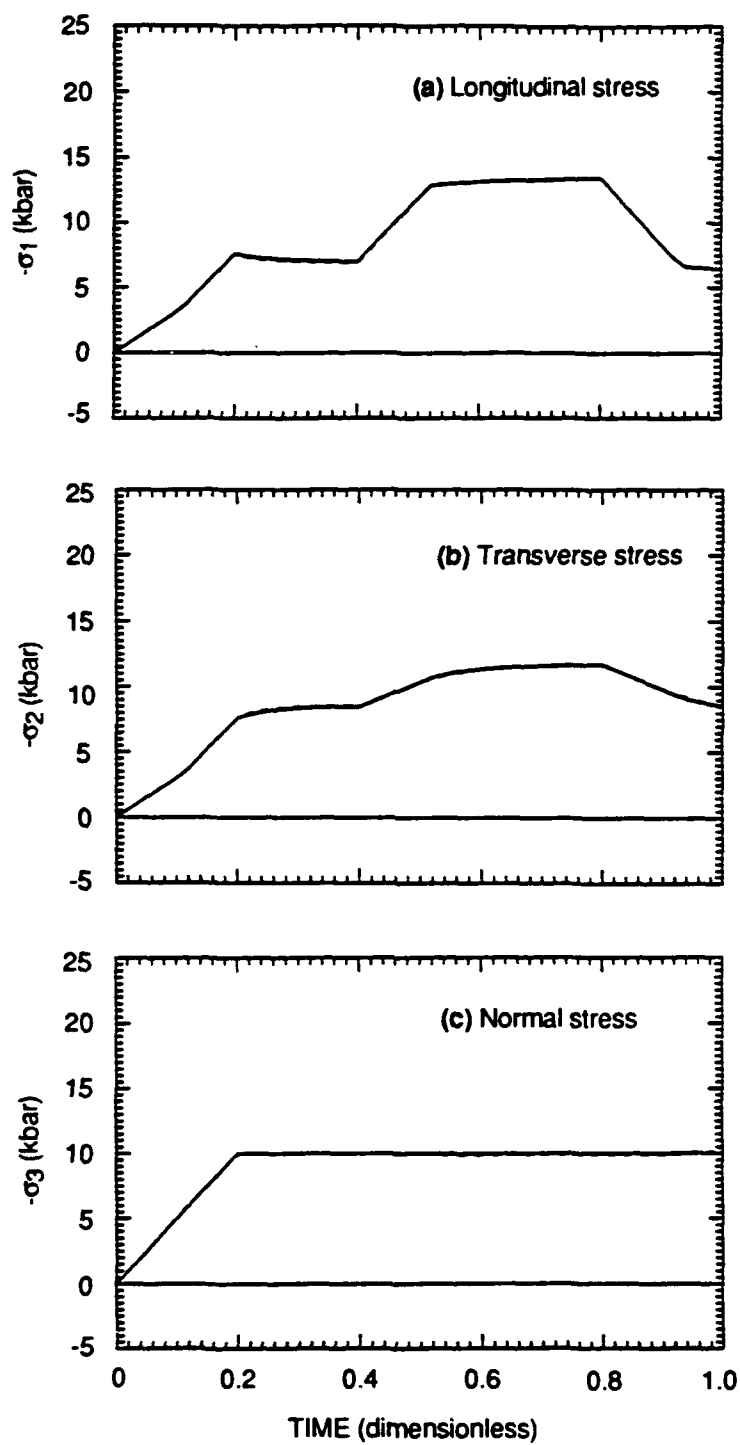
RA-7422-31

Figure 10. Manganin element (M1) stresses computed with NIKE2D finite element code (solid) and PIEZOR piezoresistance analysis (dashed).

15
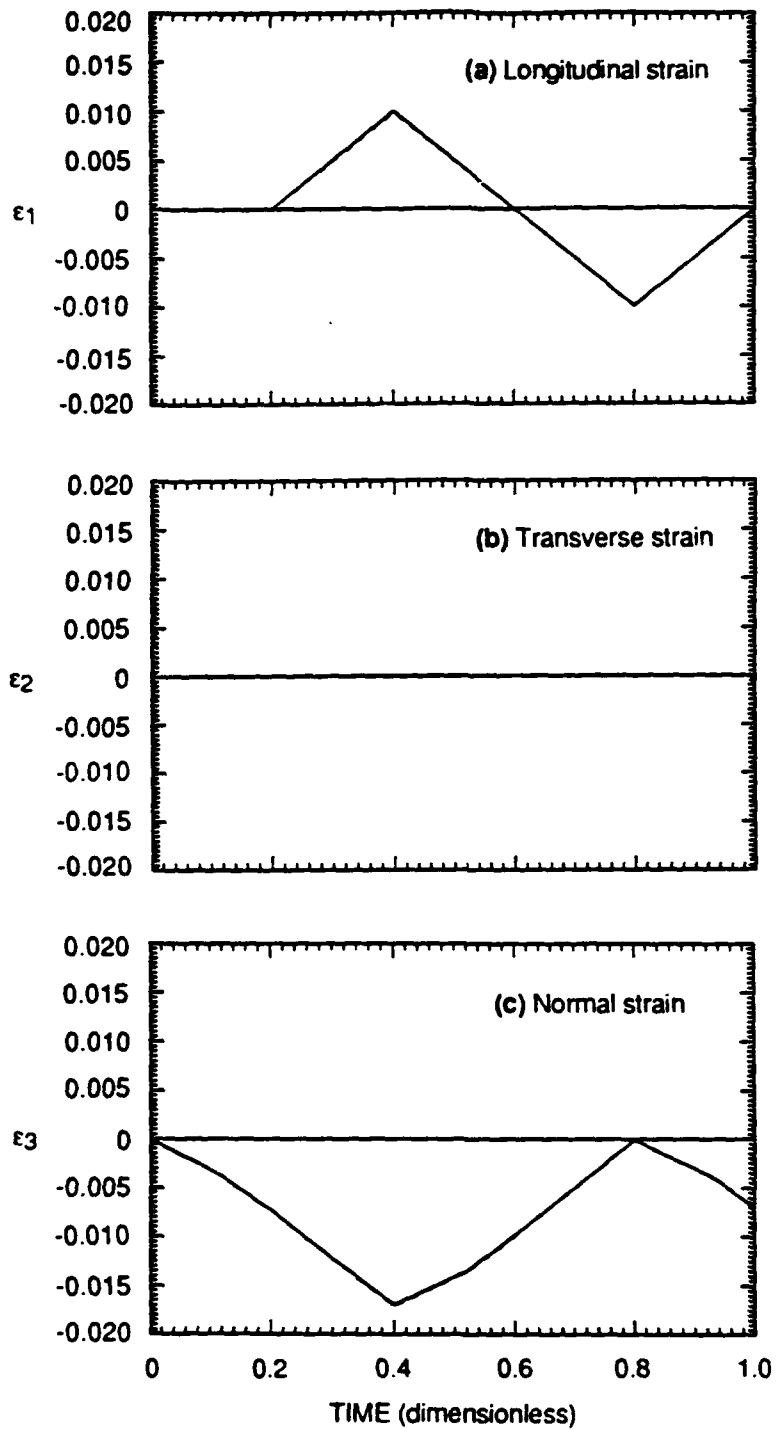
Figure 11. Manganin element (M1) strains computed with NIKE2D
finite-element code (solid) and PIEZOR piezoresistance
analysis (dashed).

16
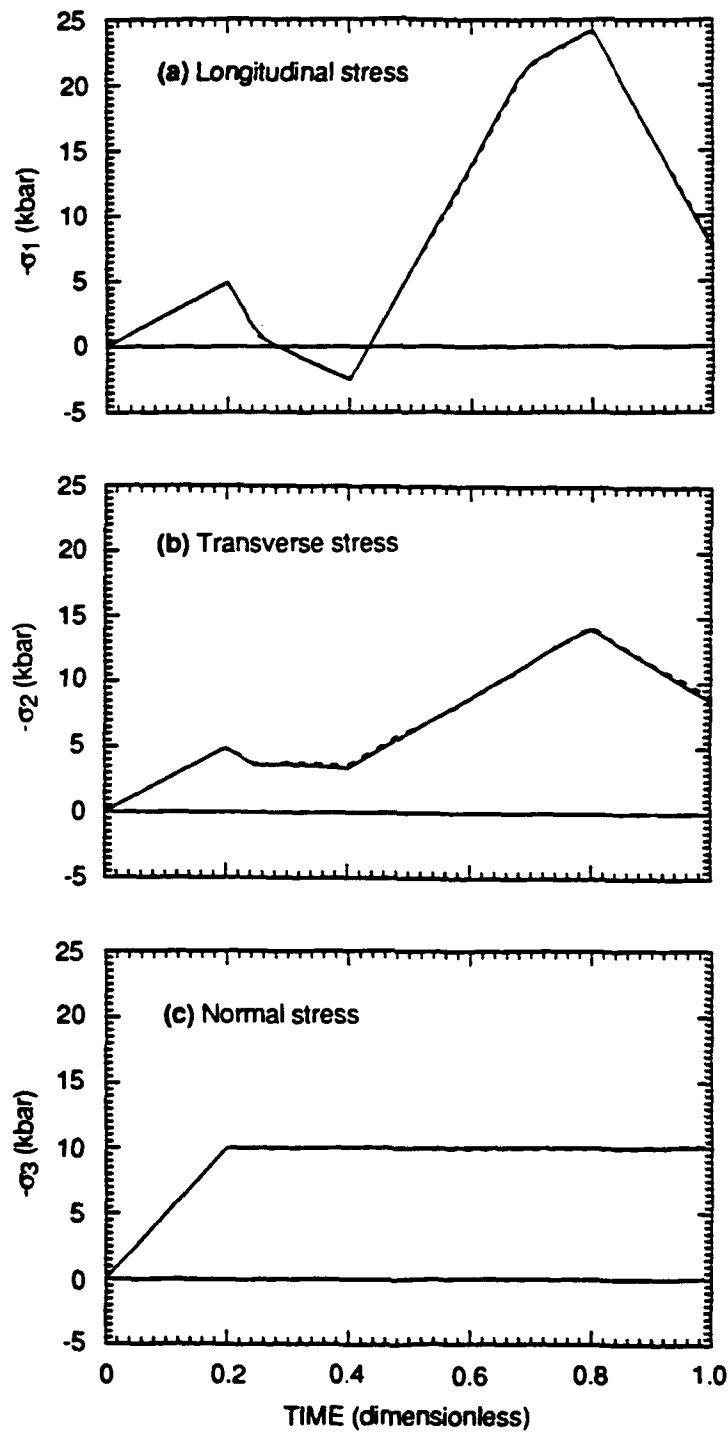
Figure 12. Constantan element (C1) stresses computed with NIKE2D
finite element code (solid) and PIEZOR piezoresistance
analysis (dashed).

17
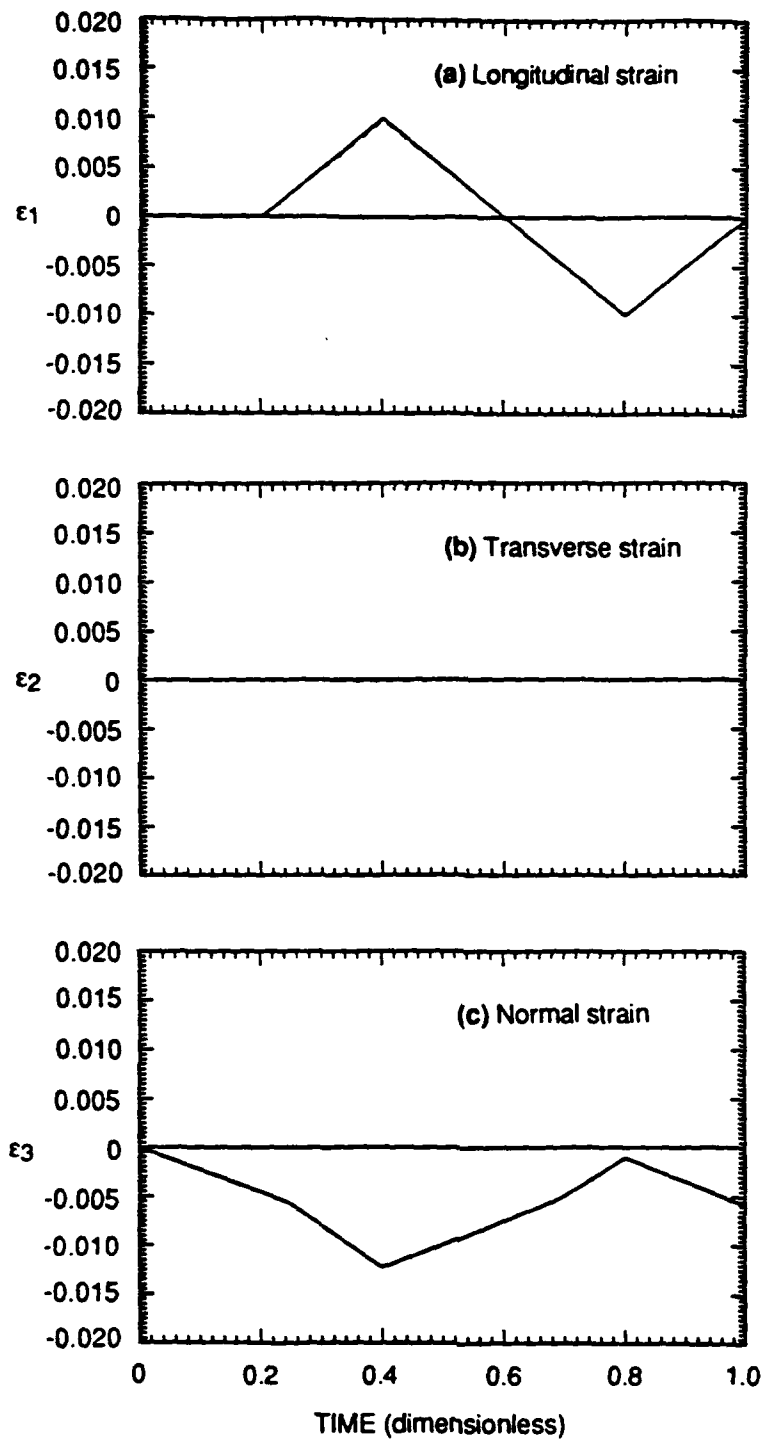
Figure 13. Constantan element (C1) strains computed with NIKE2D
finite element code (solid) and PIEZOR piezoresistance
analysis (dashed).

18

SECTION 4

CLOSE-IN BLAST EXPERIMENT

Four flatpack gages of three different designs were used in the close-in blast experiment (Test 6). Each flatpack contained a manganin element and two constantan elements in an epoxy-filled cavity. The four flatpack gages were welded to the top surface of a 25-cm-diameter steel cylinder in the positions shown in Figure 14. Flatpacks FP-1, FP-2, and FP-3 were positioned at a 2.54-cm radius (measured to the center of the manganin element); flatpack FP-4 was positioned at a 5.08-cm radius.

The differences in the designs were in the insulating material, the depth of the cavity, and the thickness of the stainless steel cover plate. In two of the flatpacks (FP-1 and FP-4) the elements were insulated with Kapton film and placed in a 0.35-mm-deep cavity (0.014 in.) filled with epoxy. These flatpacks both used 1.27-mm-thick cover plates. In the other two flatpacks (FP-2 and FP-3), the elements were insulated with mica film and placed in a 0.18-mm-deep cavity (0.007 in) filled with epoxy. One of these (FP-2) also used a 1.27-mm-thick cover plate; the other (FP-3) used 0.64-mm-thick cover plate.

Figure 15 shows the configuration of the explosive blast test. The 904-gram explosive charge was an 8.8-cm-diameter by 8.8-cm-tall cylinder of Composition B, provided by BRL (ID No. ABY 90A0E1S027). The charge was positioned over the 25-cm-diameter steel cylinder at a standoff of 15 cm, measured to the center of gravity of the charge (10.6-cm to the bottom of the charge). The charge was supported by a 2.54-cm-thick disk of styrofoam having a 6-cm-diameter central hole and an 8.8-cm-diameter, 1.27-cm-deep counter bore. Detonation was initiated with a Reynolds RP-1 detonator placed at the top center point of the charge. This configuration was chosen to match a test performed on an instrumented target plate at FMC Corporation.[8] The nominal peak pressure on the target directly under the charge was expected to be about 27 kbar (2.7 GPa), based on calculations performed at Southwest Research Institute (SWRI).[9]

The histories of resistance change were recorded on digital oscilloscopes at a sampling rate of 10 points per μs, which provided a recording window extending to about 190 μs after time of arrival (TOA). FP-1 provided signals for about 100 μs after TOA, FP-2 provided signals for about 20 μs after TOA, FP-3 failed within 5 μs after TOA, and FP-4 provided signals for the full duration of the recording window. The resistance histories from the elements in FP-1, FP-2, and FP-4 are plotted in Figures 16 through 18. In the time scale of these plots, the detonator was triggered at t = 0.

The data from FP-1, FP-2, and FP-4 were analyzed with the PIEZOR computer program to determine the actual stresses and strains inside the flatpack gages. Recall that in the PIEZOR analysis an assumption must be made regarding the coupling of transverse in-plane strain into the piezoresistance elements (see Section 3 for the definition of the Λ matrix). A very low (<1%) coupling coefficient is quoted by Micromeasurements for the strain gage elements, but this coefficient is determined only for surface-mounted gages with no normal stress. The solid curves plotted in Figures 19 through 23 use the assumption that transverse strain is fully coupled ($\lambda_{33} = 1$); the dashed curves use the assumption that transverse strain is completely uncoupled ($\lambda_{33} = 0$).

19

5.08-cm Radius

2.54-cm Radius

Charge Radius (4.4-cm)

Kapton Insulation
0.35-mm Cavity
0.127-mm Cover

Mica Insulation
0.18-mm Cavity
0.064-mm Cover

Kapton Insulation
0.35-mm Cavity
0.127-mm Cover

Mica Insulation
0.18-mm Cavity
0.127-mm Cover

FP-1

FP-2

FP-3

FP-4
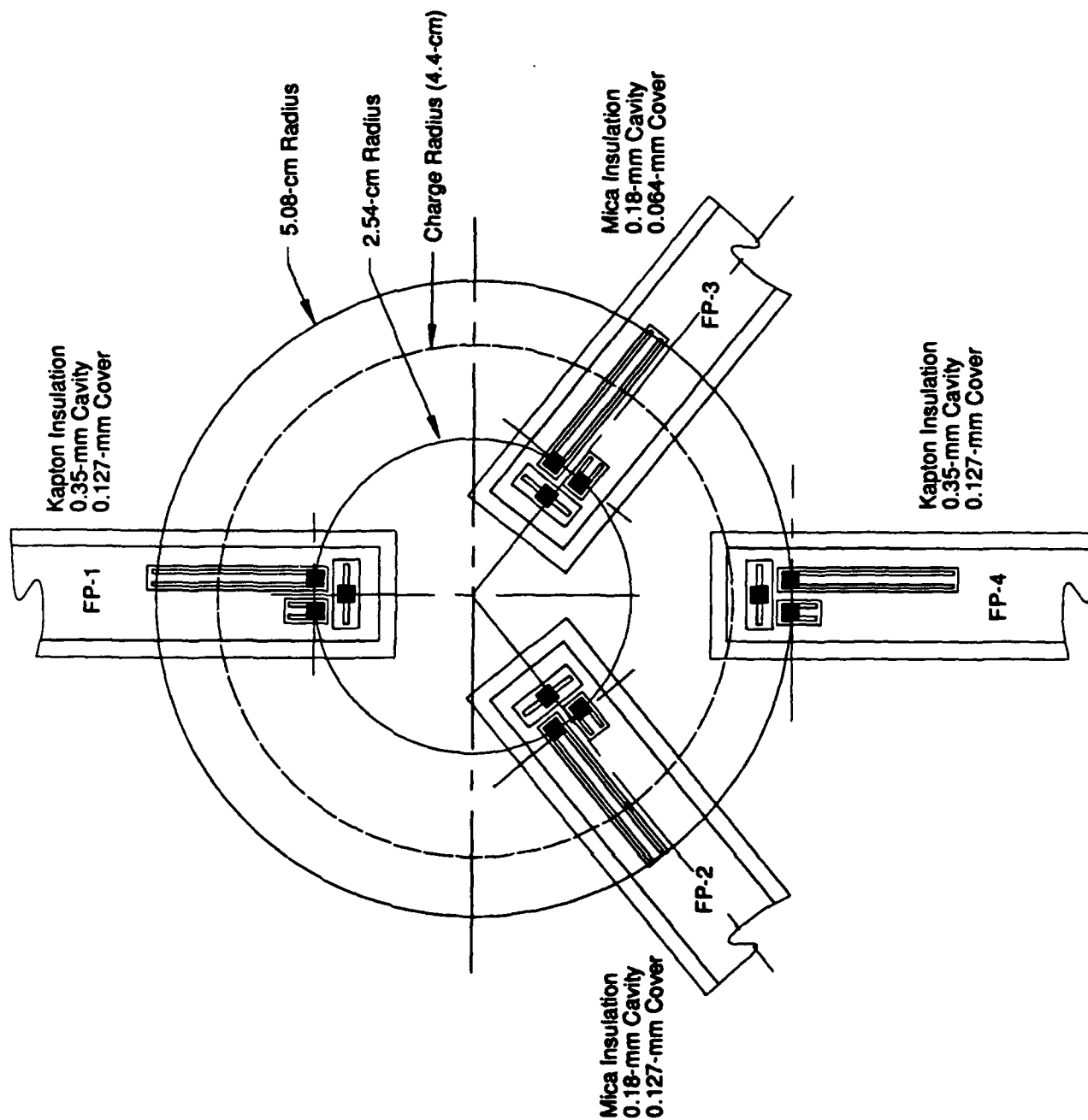
RM-7422-48

Figure 14.   Flatpack position in Test 6.

20

Detonator

904 gram
Comp B

8.8 cm

8.8 cm

Styrofoam
Disk

2.54 cm

6 cm

10.6 cm

2.54 cm

5.08 cm

Steel
Cylinder

Steel Flatpacks
With Manganin
and Strain
Gages

30 cm

25 cm
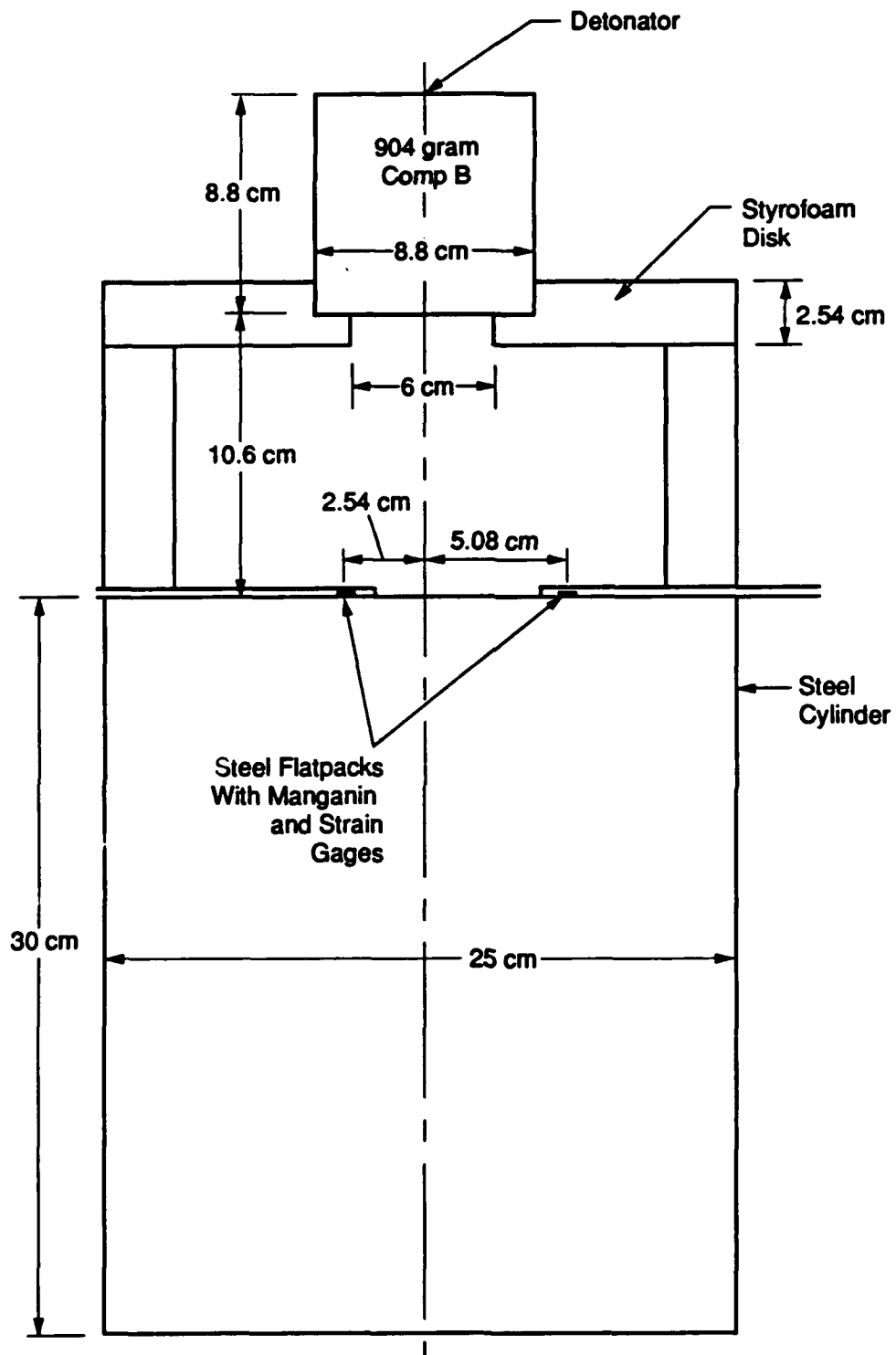
RM-7422-49

Figure 15.   Configuration of Test 6.

21
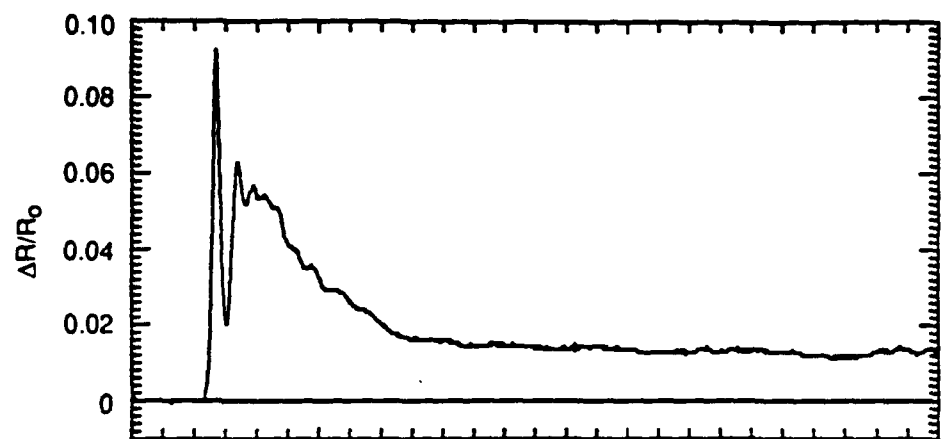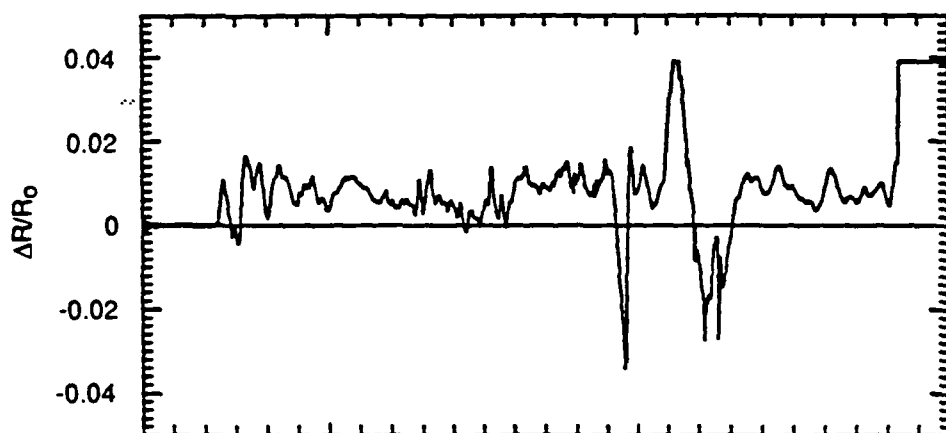
(a) Manganin
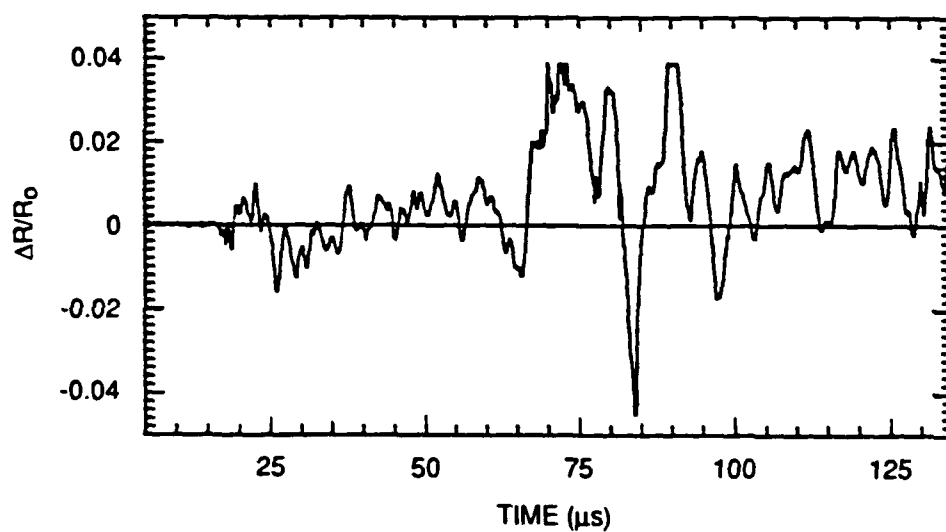
(b) Constantan 1

(c) Constantan 2

R-7422-50A

Figure 16.   Resistance histories from FP-1.

22
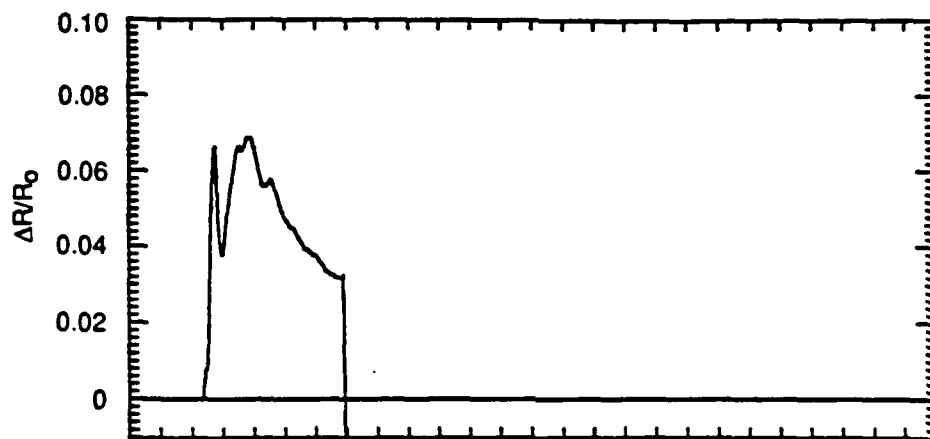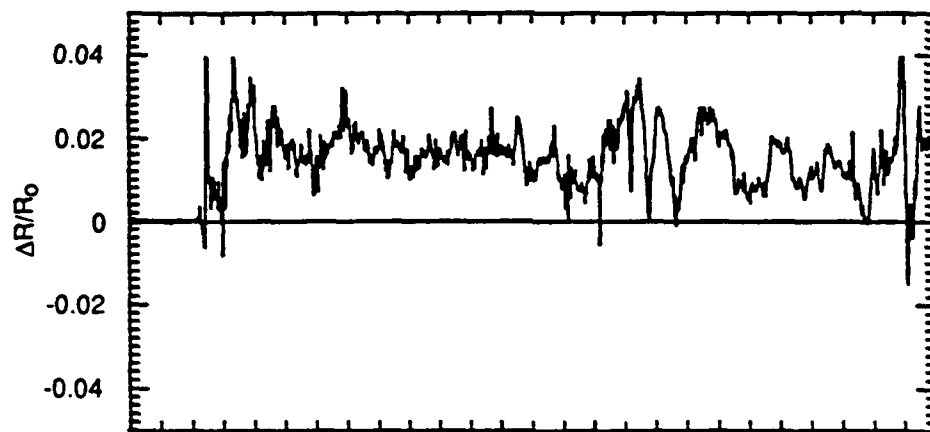
(a) Manganin
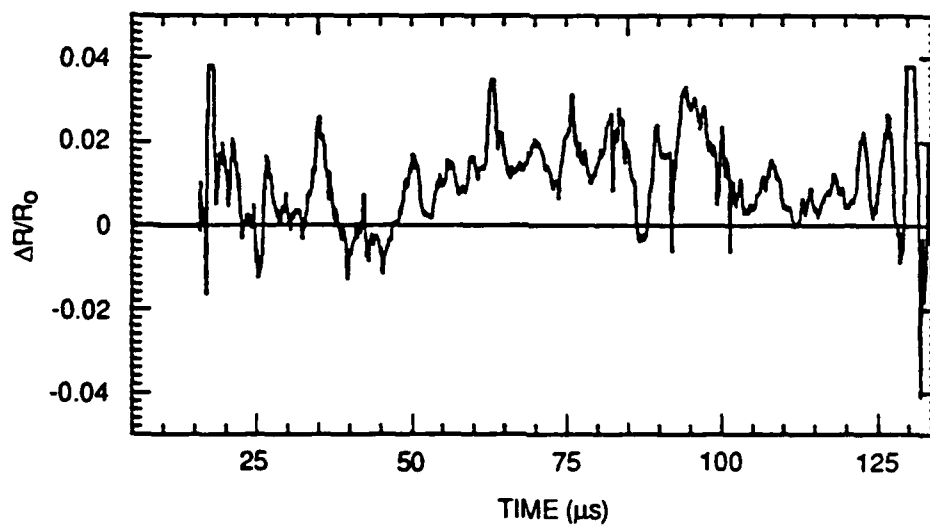
(b) Constantan 1

(c) Constantan 2

RA-7422-51A

Figure 17.   Resistance histories from FP-2.

23
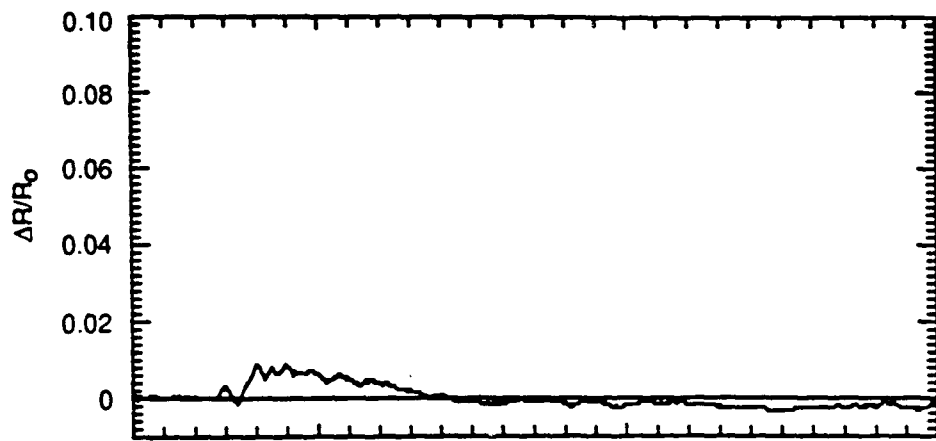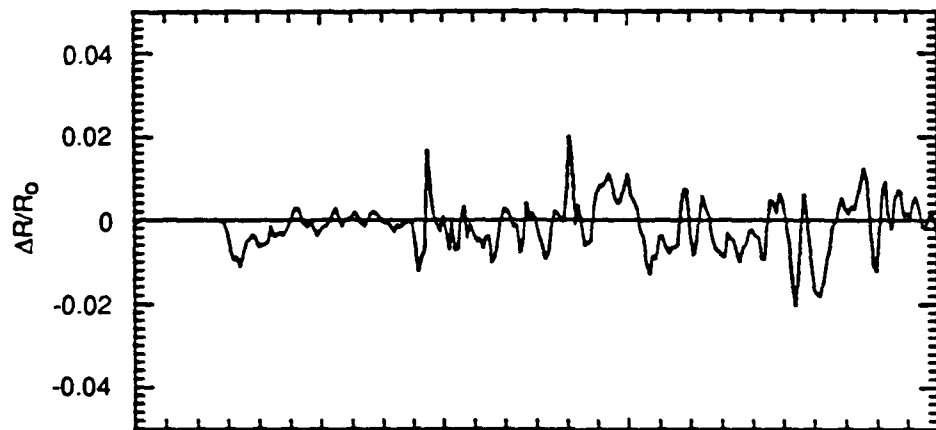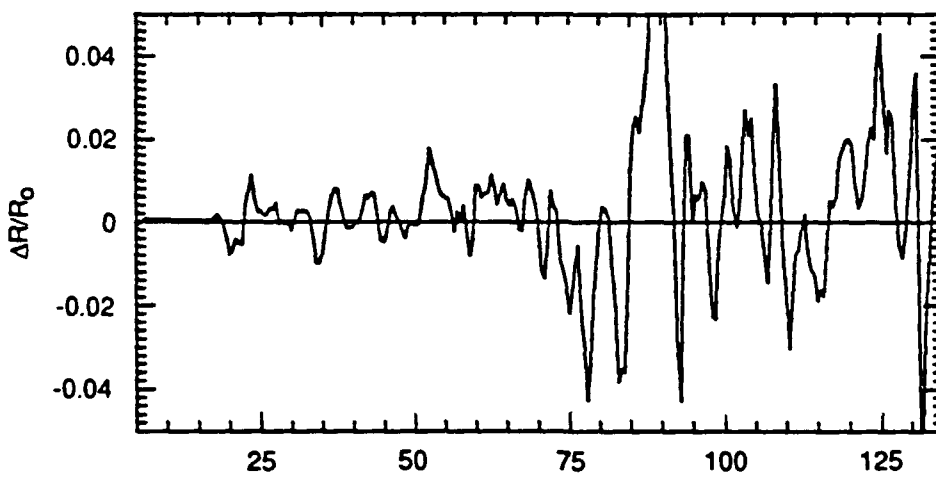
Figure 18. Resistance histories from FP-4.

R-7422-52A

24
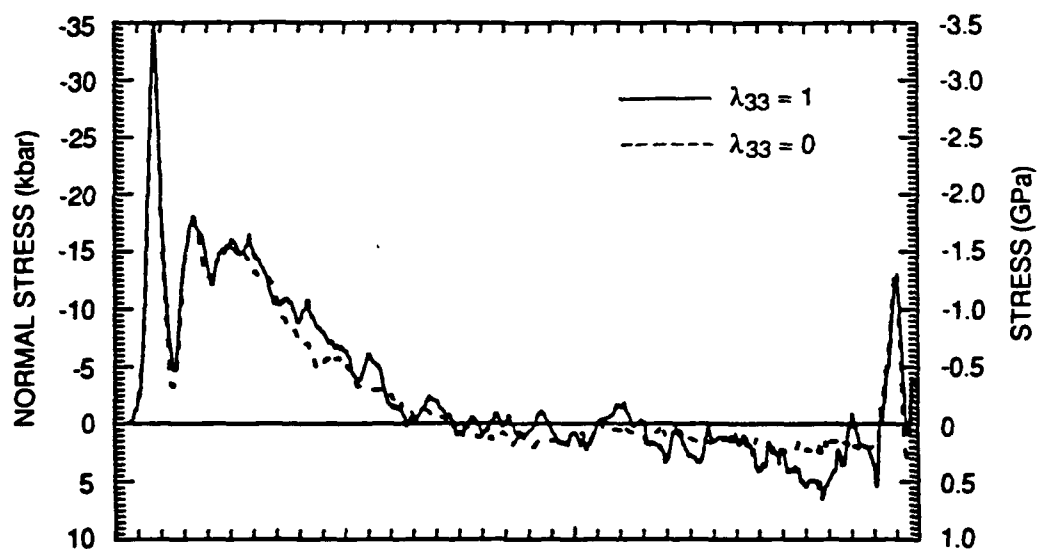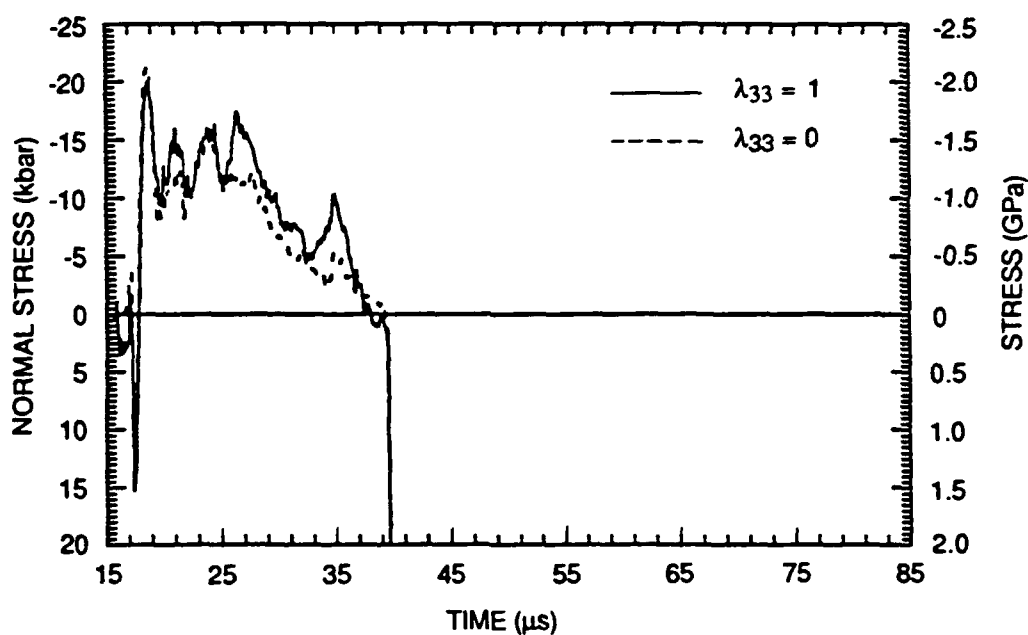
Figure 19.   Normal stresses in FP-1 and FP-2.

R-7422-53A

25
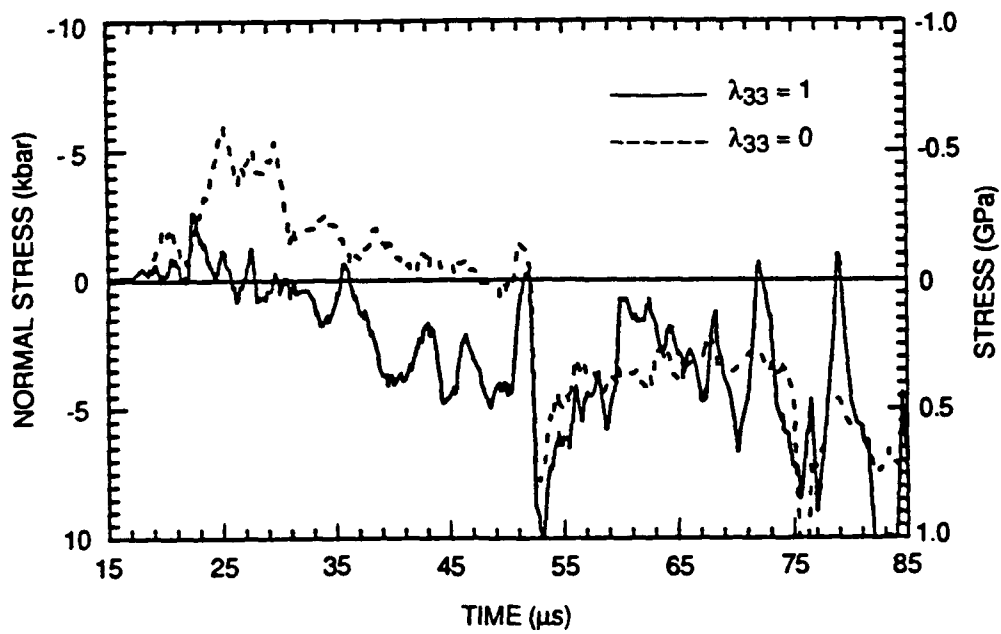
Figure 20.   Normal stress in FP-4.
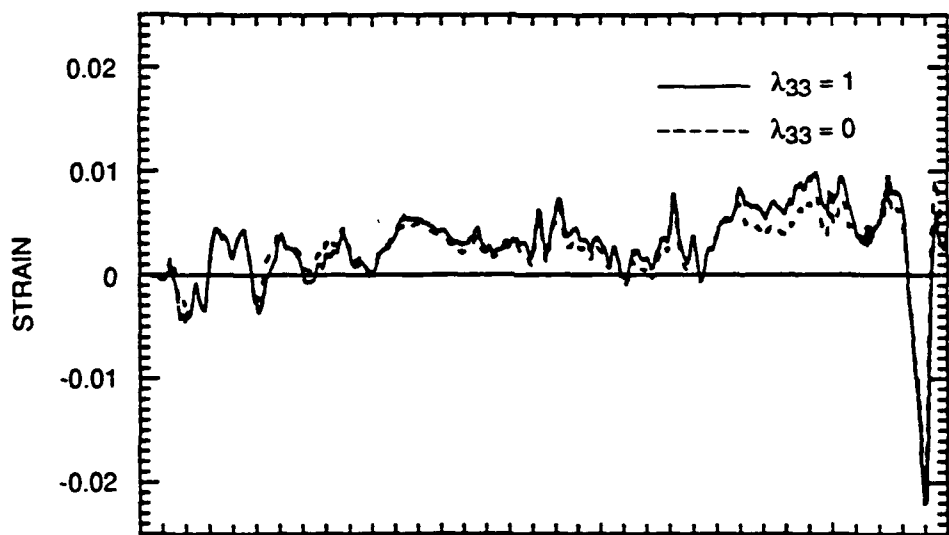
R-7422-54A

(a) Longitudinal strain
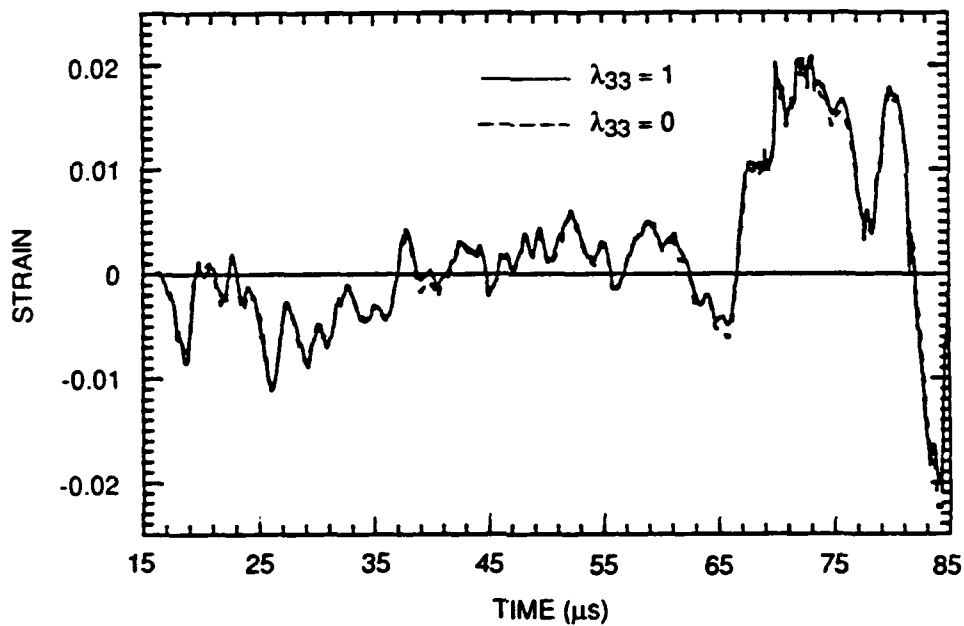
(b) Transverse strain

R-7422-55A

Figure 21.   In-plane strains in FP-1.

27
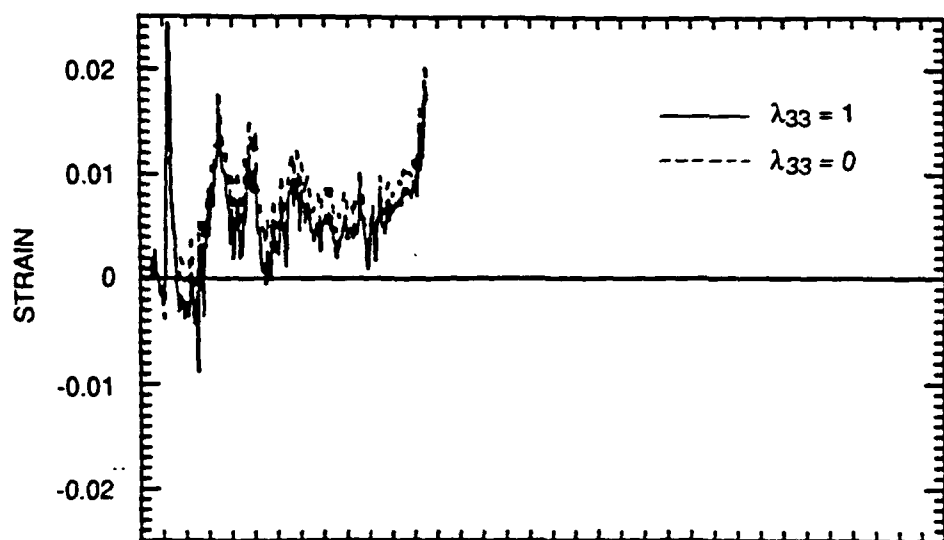
(a) Longitudinal strain
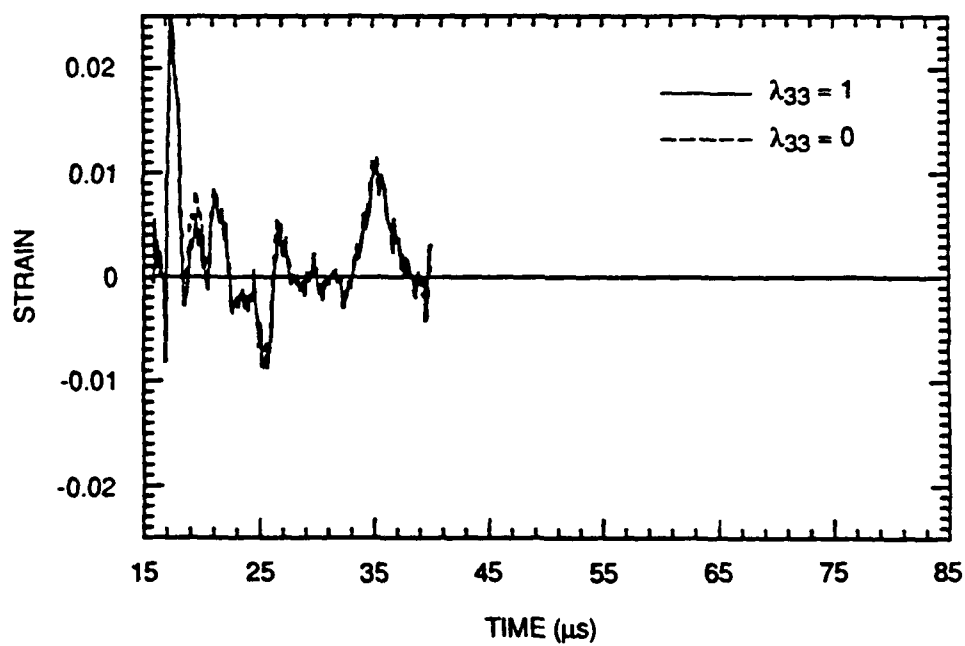
(b) Transverse strain

R-7422-56A

Figure 22.   In-plane strains in FP-2.

28
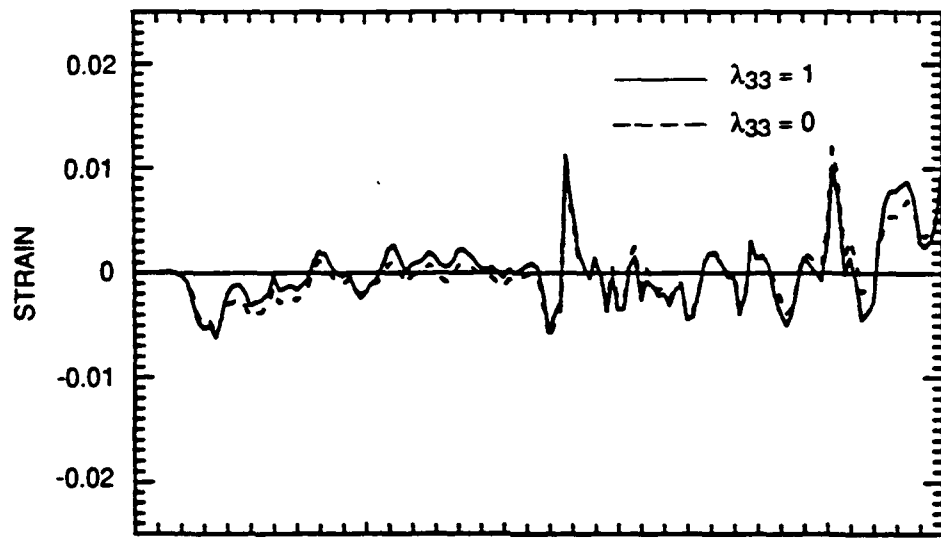
(a) Longitudinal strain
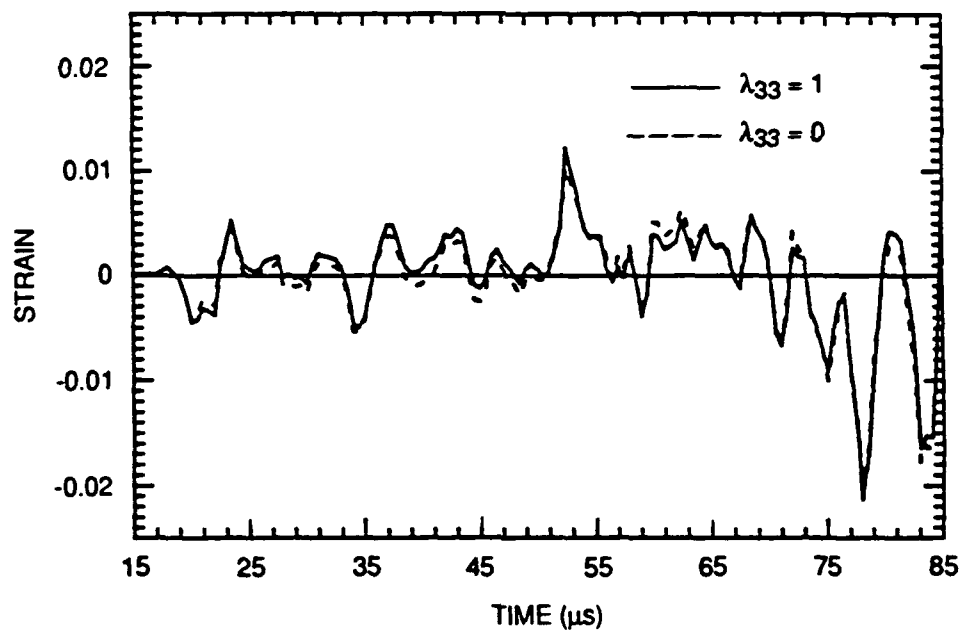
(b) Transverse strain

R-7422-57A

Figure 23.   In-plane strains in FP-4.

These two assumptions are approximate bounds on the actual coupling. In these analyses the piezoresistance hardening coefficient η for manganin was assumed to be a function of the plastic strain, as determined in shock-loading experiments (200 ns duration).[4] See Appendix A for the material properties and piezoresistance coefficients.

Several observations can be made from the data. The resolved late-time stresses in FP-1 [Figure 19(a)] and the early-time stresses in FP-4 [Figure 20] appear to support the assumption of zero coupling of transverse strain. That is, the dashed curves in the figures ($\lambda_{33} = 0$) are more physically plausible because we do not expect the stress at 2.54 cm to become negative after 30 μs and we do expect a peak stress of about 4 kbar (0.4 GPa) at 5.08 cm. For both FP-1 and FP-2, in which the stress produces a large resistance change in the manganin, the dependence of the computed stress on the transverse strain coupling assumption is small because the flatpack limits the transverse strains sufficiently. In the case of FP-4 this is not true, and it suggests that a ytterbium element (more sensitive to stress) would have been a better choice for the 5.08-cm range.

Figure 19 shows that the stresses in FP-1 and FP-2 (up to the time of failure of FP-2) are very nearly the same, which is consistent with the symmetry of the experiment. The peak stress in FP-4 (Figure 20) is much lower than those in FP-1 and FP-2, which is consistent with the rapid decay of the blast wave with radius. Figures 21 and 22 show that during the time of interest both the longitudinal and transverse strains in FP-1 are about half those in FP-2, suggesting that the FP-1 design is the better of the two. (FP-1 also survived much longer.)

One more analysis was performed with the data from FP-1. In this analysis, the piezoresistance hardening coefficient η for manganin was assumed to be zero, which is consistent with data from quasistatic tests.[1] Figure 24 shows that this assumption raises the resolved stress in the flatpack at late time to about 2 kbar (0.2 GPa). This result suggests that η lies between the values determined from static experiments[1] and gas-gun experiments.[3]

30

$\lambda_{33} = 0, \eta = 0$
$\lambda_{33} = 0, \eta \neq 0$
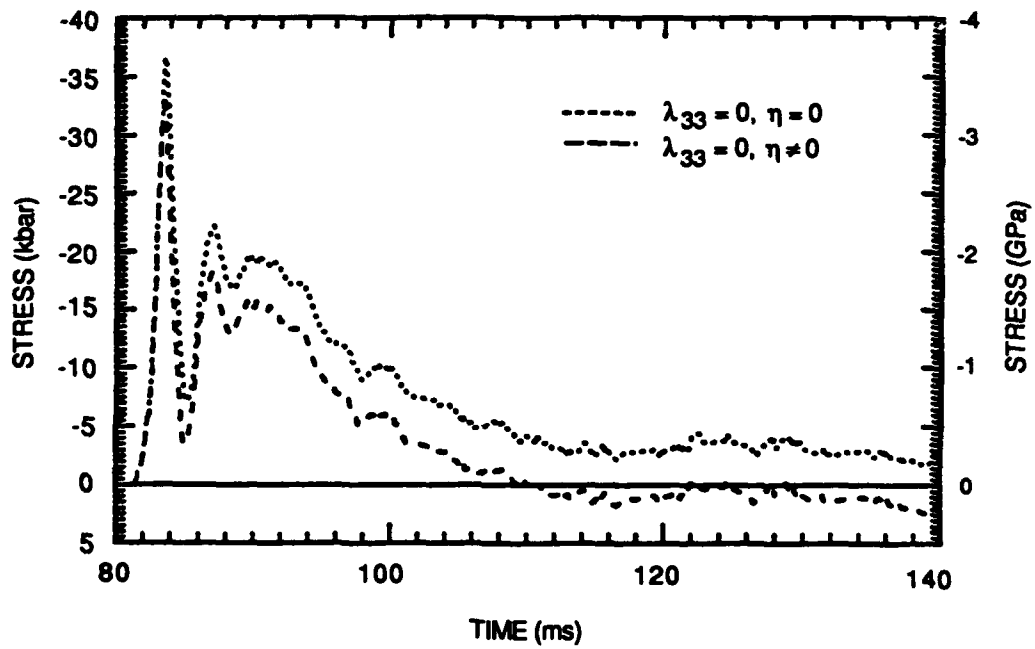
RM-7422-59B

Figure 24.   Normal stress in FP-1.

31

SECTION 5

PLATE-IMPACT EXPERIMENT

The objective of the plate-impact test was to demonstrate the performance of the flatpack gage and the PIEZOR algorithm under conditions for which the applied loading is known. Symmetric plate-impact experiments provide a known value of incident stress if the flyer and target density, the flyer velocity, and the shock velocity are measured ($\sigma = \frac{1}{2} \rho cv$). Uniaxial strain loading is maintained until relief waves from the perimeter of the flyer and target arrive at a measurement location. Although an ideal loading for a blast-pressure gage would be a known high-pressure shock wave in a gas, plate-impact experiments use solid or liquid media. Solid flyers and targets are by far easier to use. Thus, our approach was to place gages on the front of a steel target, cover them with a PMMA buffer plate, and impact this assembly with a PMMA flyer.

The design of the test is shown in Figure 25. The 25.4-mm-thick flyer plate produces a pulse duration of about 20 μs. The 25.4-mm-thick buffer plate delays the arrival of the rarefaction from the upstream face of the flyer at the gage plane by another 20 μs. The thickness of the steel target plate is such that the rarefaction from the rear of the target arrives at the gage plane at about the same time. The 300-mm-diameter of the flyer and target was selected to allow uniaxial strain conditions to maintain for about 30 μs (longer than the incident pulse duration). Two flatpack gages (FP-1 and FP-4) and two Kapton-covered element clusters (FP-2 and FP-3) were mounted on the steel target plate. Shallow channels were machined into the surface of the PMMA buffer plate to accommodate the gages. These were filled with Epon 815 epoxy when the plates were bonded together. The measured impact velocity was 44.7 m/s. The measured tilt was 9 μs from top to bottom.

One-, two-, and three-dimensional pretest computations were performed (see Appendix F). These predicted that the stress inside the flatpacks would be only slightly perturbed from the reflected stress pulse at the steel target face. More specifically, the registration of stress into the flatpack was predicted to be one-to-one, and the oscillations in the stress caused by the motion of the cover plate were predicted to be about ±0.2 kbar (20 MPa). For the measured impact velocity, the predicted reflected stress was 1.35 kbar (135 MPa).

As shown in Figure 26,* the resistance histories from the ytterbium elements inside the flatpacks were very different from those mounted directly on the steel plate, and neither set matched the predictions. First, the bare (Kapton covered) element records indicate a very much more rounded wave front than expected, although the pulse duration (about 17.4 μs) and the arrival time of the second rarefaction are about as predicted. The elements inside the flatpacks indicate a much lower equilibrium level and a large overshoot. In Figure 27, these resistance histories are converted to stress using the assumption of uniaxial strain and element properties based on Gupta's results for foils** (see Appendix A). This interpretation indicates that the equilibrium stress level inside the flatpacks was about half of that at the steel target face.

---

*Zero time in the plots corresponds to first sense of impact (9-μs tilt).

**The ytterbium elements are vapor-deposited rather than foils, so the properties may be different.

32

Honeycomb — PMMA — Flatpack — Steel

102 mm

300 mm

6 mm

25 mm

102 mm

25 mm

25 mm

FP-1 (Steel Case)

(Steel Case) FP-4

25 mm

50 mm

FP-2 (Kapton Only)

(Kapton Only) FP-3
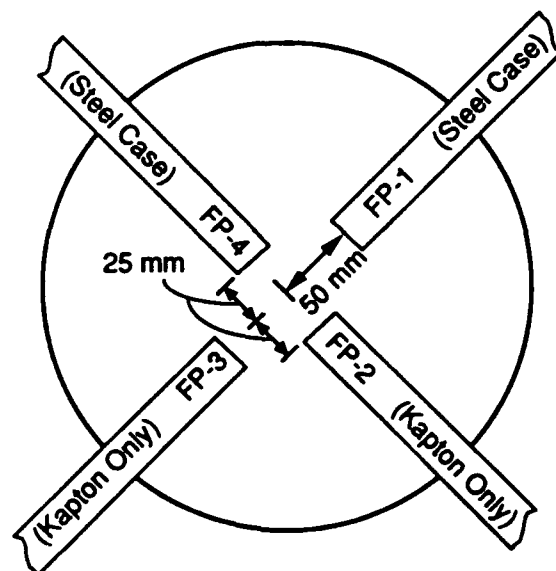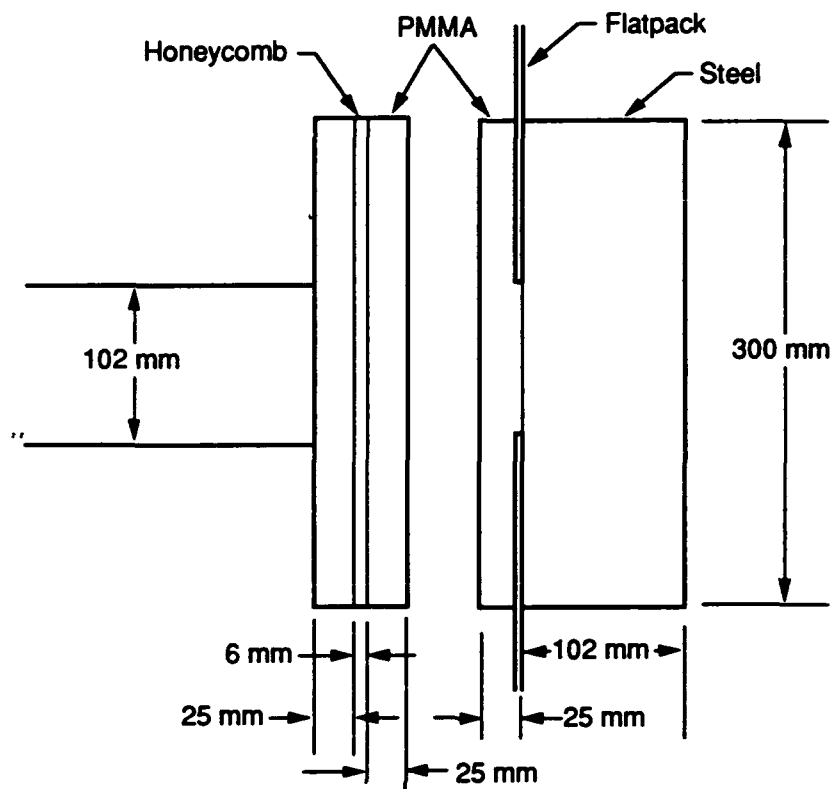
RM-7422-60

Figure 25.   Plate-impact test design.

33
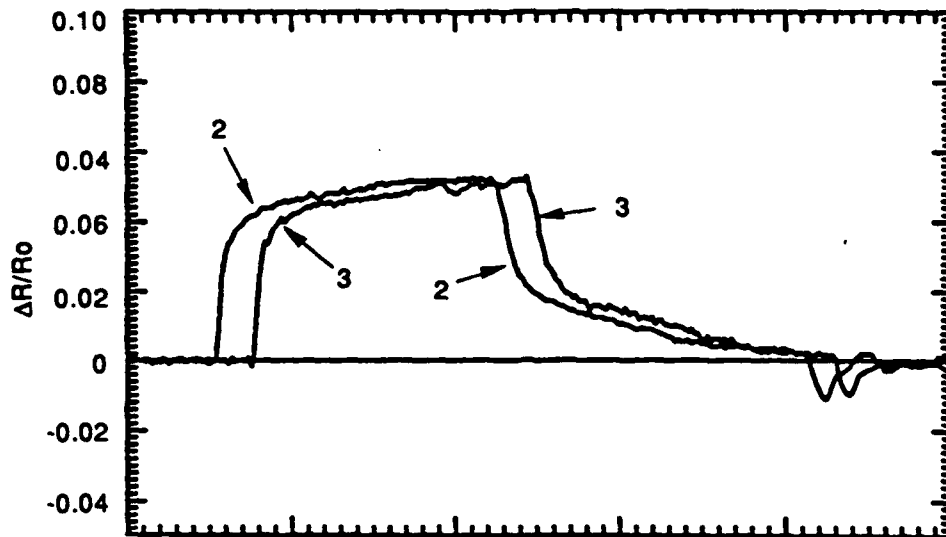
(a) Kapton covered elements (FP-2 & FP-3)
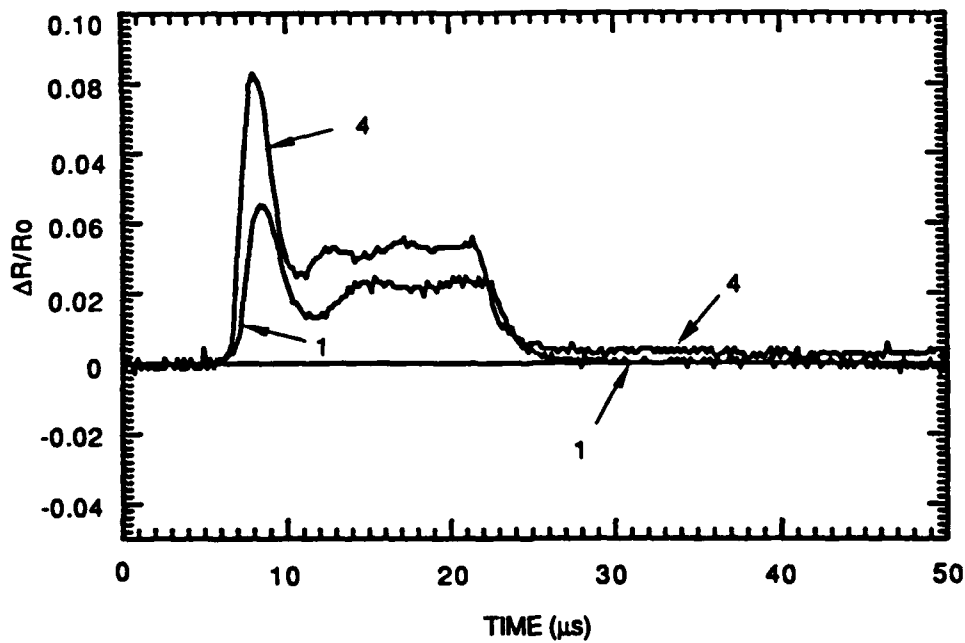
(b) Flatpack gages (FP-1 & FP-4)

RM-7422-61

Figure 26.   Ytterbium element resistance histories.

34
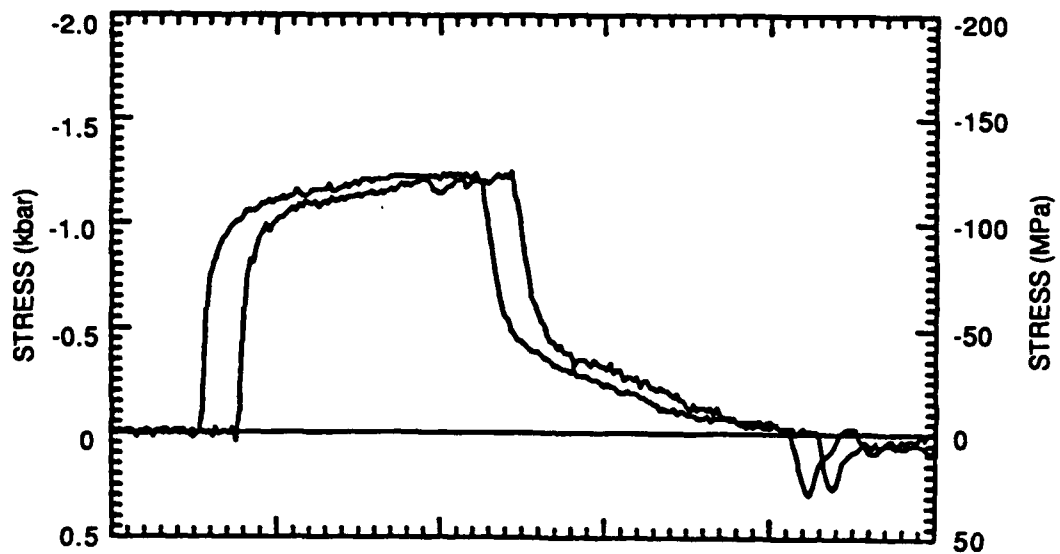
(a) Kapton-covered elements
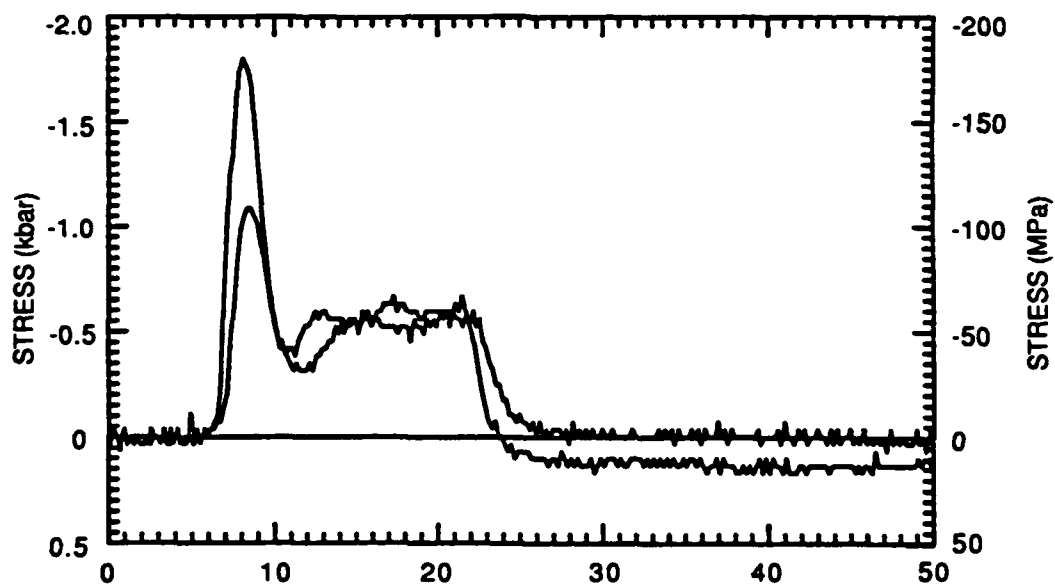
(b) Flatpack gages

RM-7422-62

Figure 27.   Stresses computed for uniaxial strain conditions.

35

The measured tilt was 9 μs (top to bottom). Tilt may be the reason for non-simulaneity of the signals from the four gages, but tilt does not account for the nature of the records.

The constantan element records are shown in Figures 28 through 31. For the bare gages, these signals look suspiciously like electromagnetically induced signals because during the uniaxial strain phase (before about 30 μs) the constantan output resembles the time-derivative of the ytterbium output (except for the 2.5-μs-late time-of-arrival for the FP-3 ytterbium element, which cannot be explained). The large excursions in the records from the bare constantan elements at about 45 μs coincide with the arrival of the rarefaction from the rear of the target. The constantan elements inside the flatpacks indicated relatively small strains with some oscillations during the uniaxial strain phase. In contrast to the bare elements, the flatpack case mitigated the late-time strains.

The data from flatpacks FP-1 and FP-4 were interpreted with PIEZOR three ways. First, the transverse strain coupling (λ_{33}) was assumed to be zero and the piezoresistance strain-hardening coefficient (η) was set to zero. Second, $\lambda_{33} = 1$ with $\eta = 0$. Third, $\lambda_{33} = 0$ with η a function of the plastic strain (see Appendix A). These interpretations are shown in Figures 32 and 33. None of these interpretations brings the flatpack stresses into agreement with the free-field. The data from FP-2 and FP-3 were not analyzed with PIEZOR because the measured strains are zero during the uniaxial strain phase (for which the stress is known).

We do not fully understand these results. It may be that the compliance of the flatpack is much greater than assumed in the pretest calculation. That is, because of this compliance, the full stress in the PMMA buffer was not transmitted to the sensing region of the flatpack. Also, in our calculation we assumed that the PMMA and epoxy remained elastic for this loading (see Appendix F for details). Plastic response, especially inside the flatpack, may be a source of lower compliance. A set of posttest calculations would likely provide a much better understanding of this test. However, these calculations could not be included in the current contract.

36
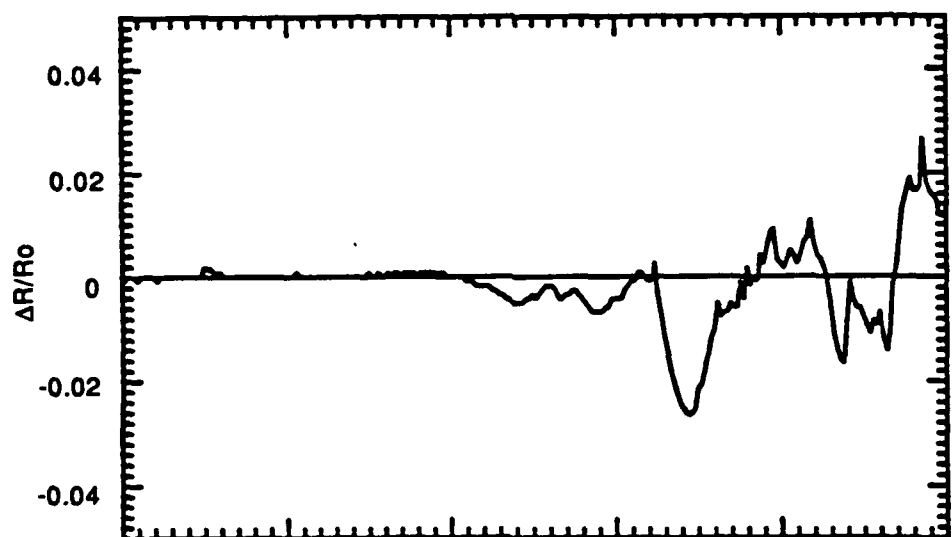
(a) Parallel to ytterbium grid
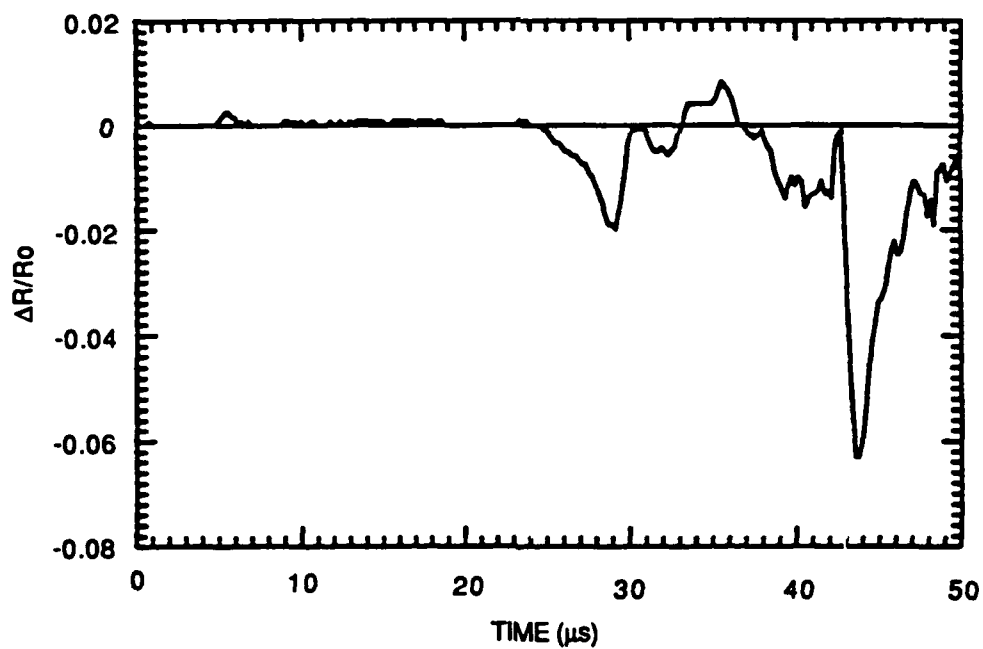
(b) Orthogonal to ytterbium grid

RM-7422-63

Figure 28.   Constantan element resistance histories for FP-2 (Kapton-covered).

37
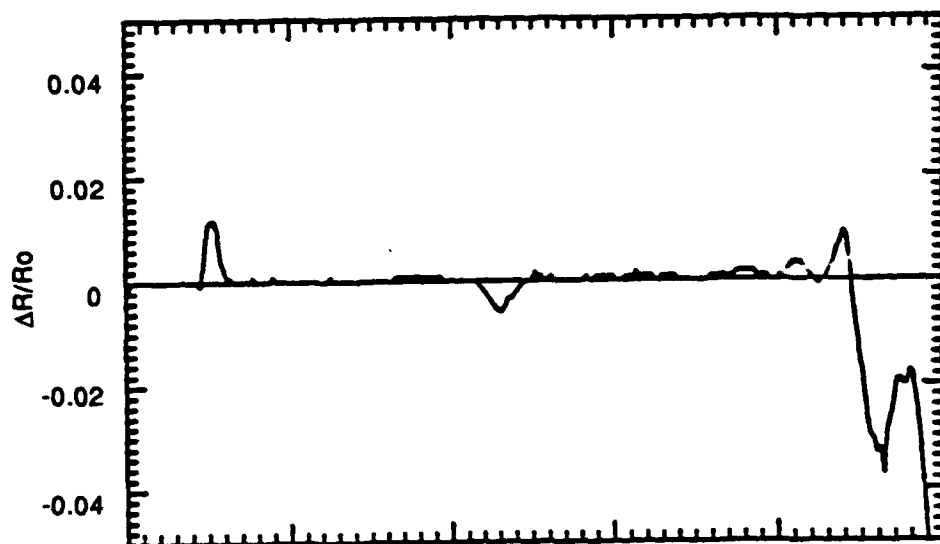
(a) Parallel to ytterbium grid
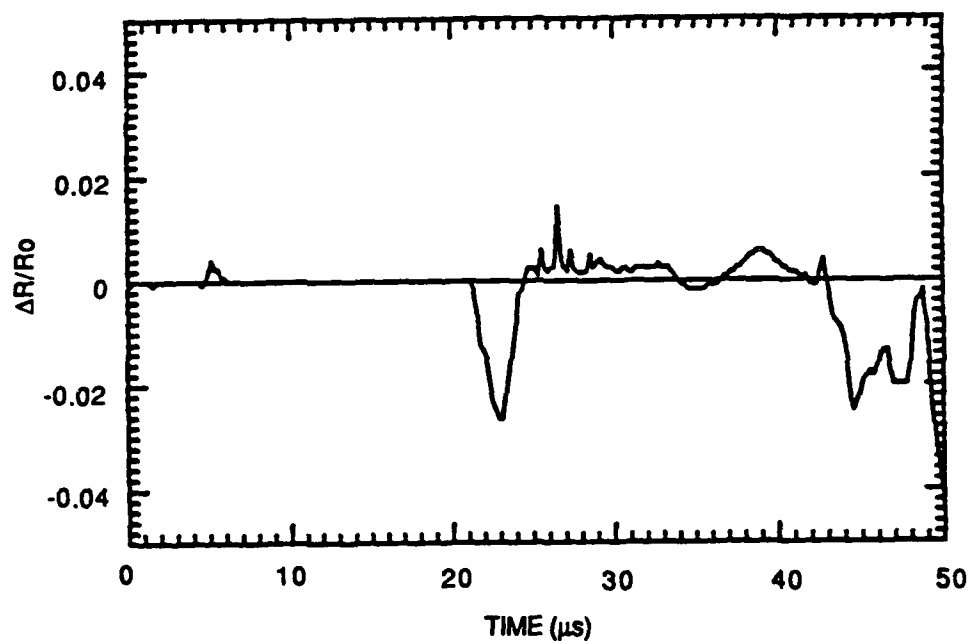
(b) Orthogonal to ytterbium grid

RM-7422-64

Figure 29. Constantan element resistance histories for FP-3 (Kapton-covered).

38
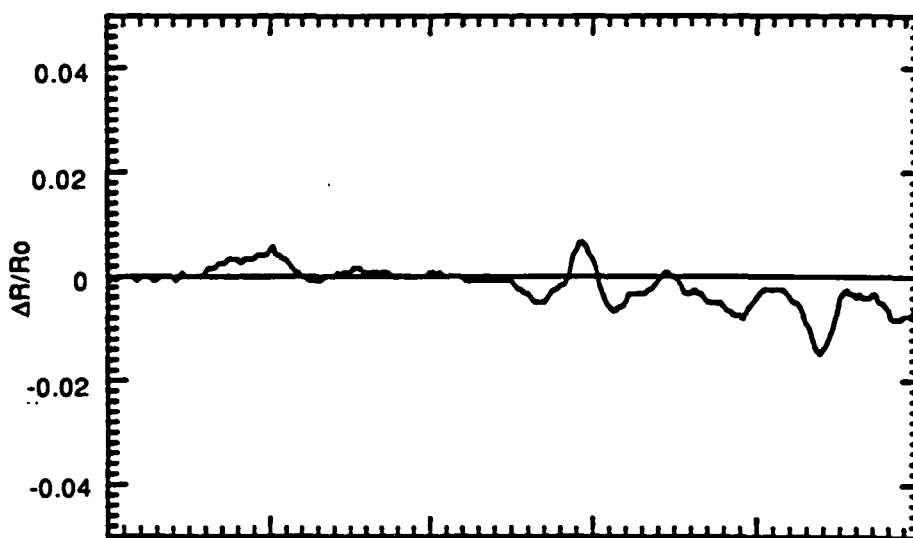
(a) Parallel to ytterbium grid
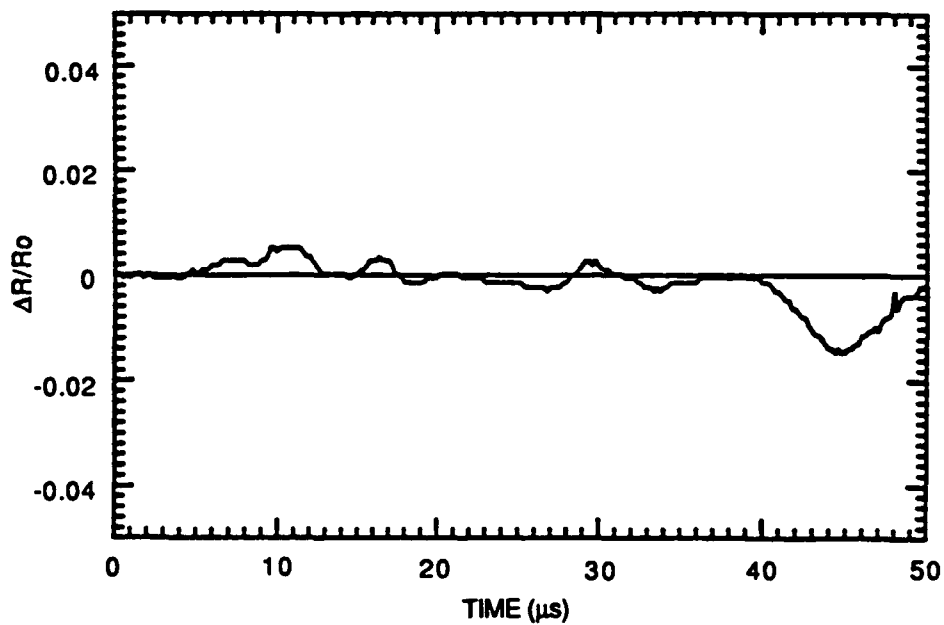
(b) Orthogonal to ytterbium grid

RM-7422-65

Figure 30. Constantan element resistance histories for FP-1 (flatpack gage).

39
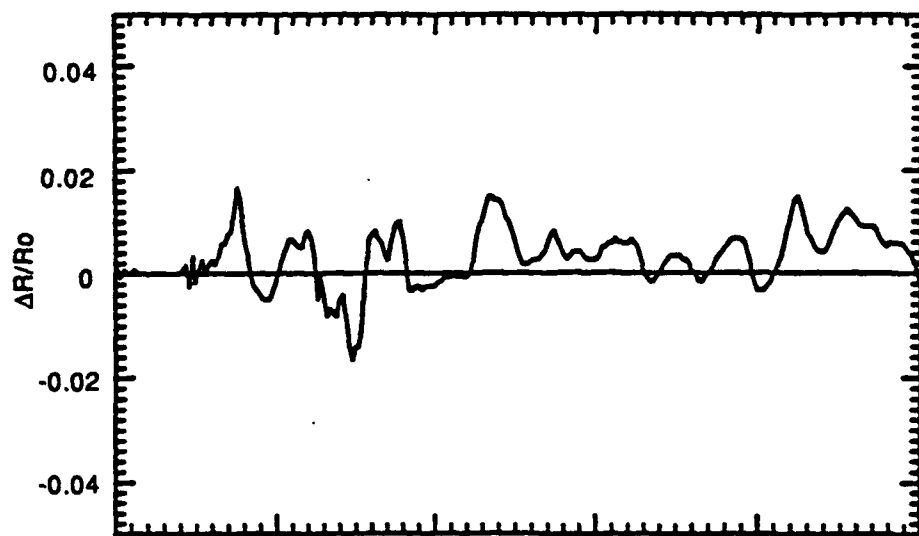
(a) Parallel to ytterbium grid
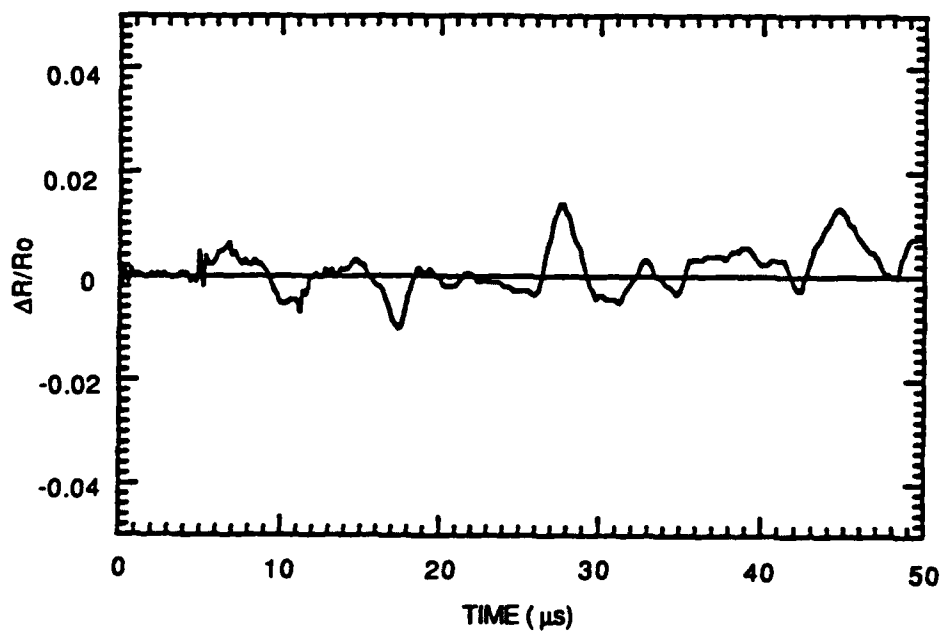
(b) Orthogonal to ytterbium grid

RM-7422-66

Figure 31. Constantan element resistance histories for FP-4 (flatpack gage).
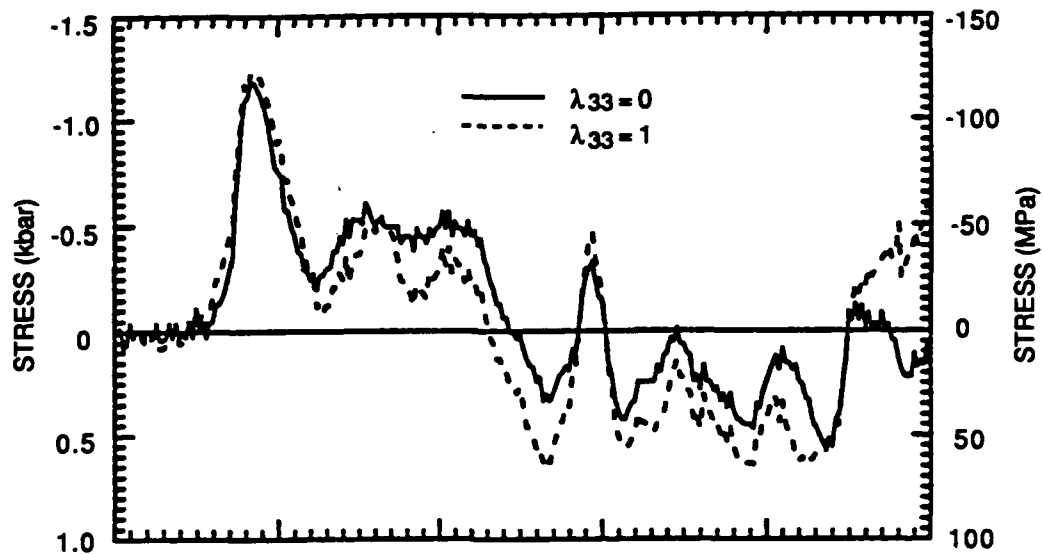
40

(a) Effect of transverse strain coupling with $\eta = 0$.
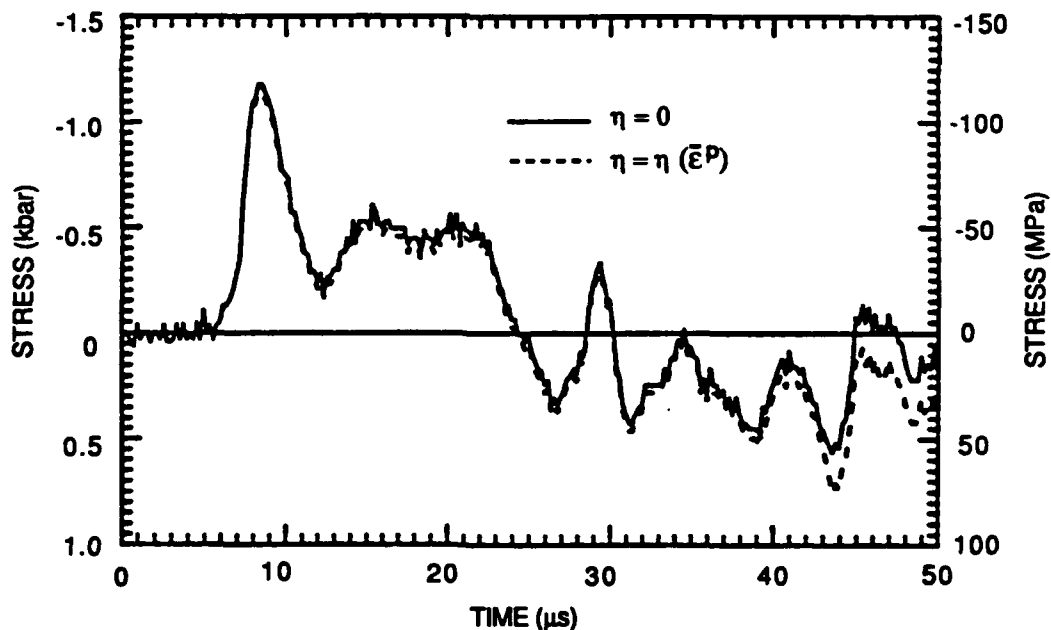
(b) Effect of plastic strain with $\lambda_{33} = 0$.

RM-7422-67

Figure 32. PIEZOR interpretation of FP-1 records.
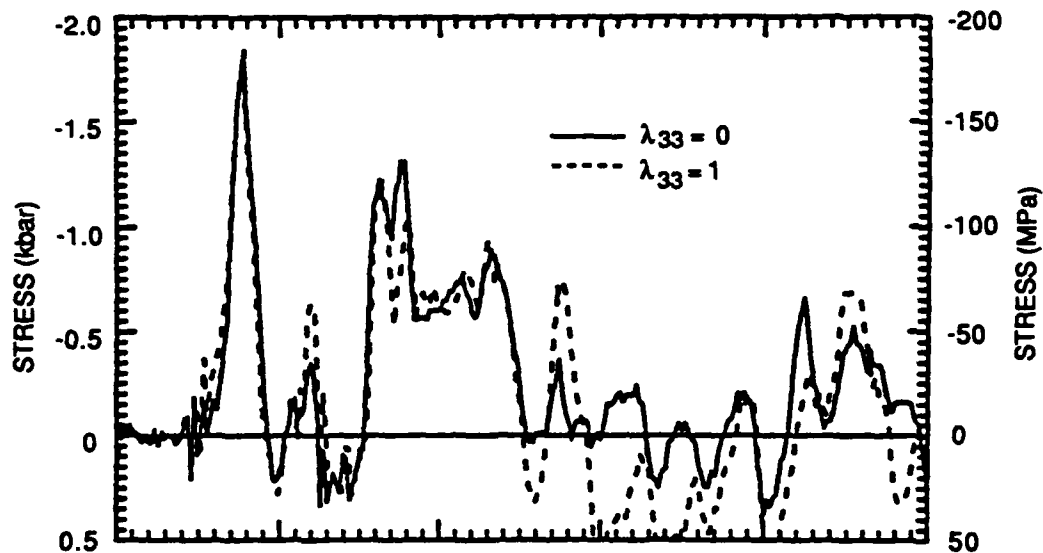
41

(a) Effect of transverse strain coupling with $\eta = 0$.
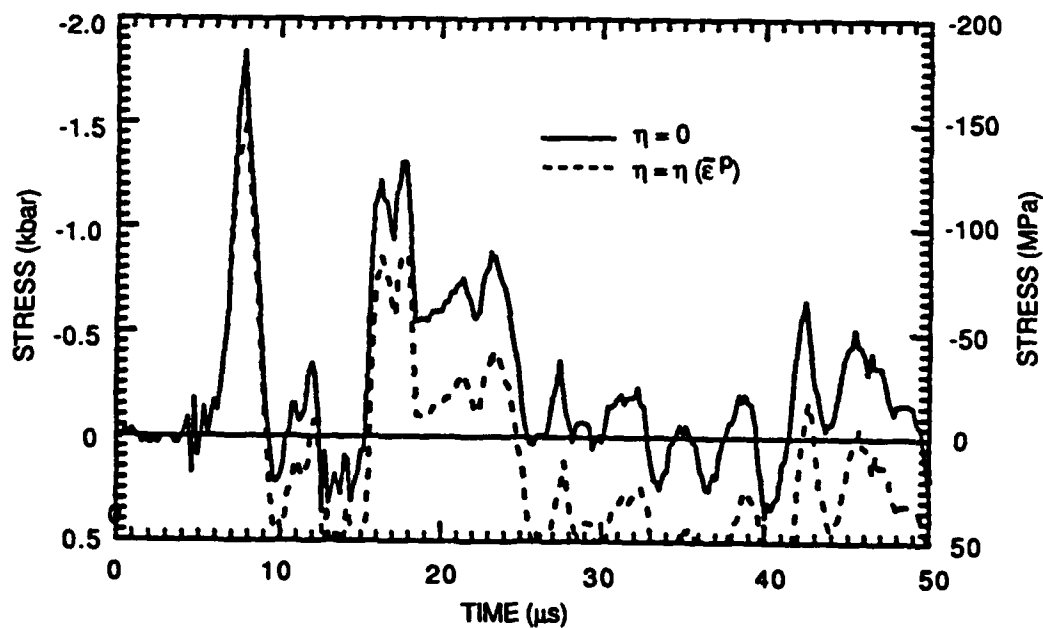
(b) Effect of plastic strain with $\lambda_{33} = 0$.

RM-7422-68

Figure 33. PIEZOR interpretation of FP-4 records.

42

SECTION 6

CONCLUSIONS AND RECOMMENDATIONS

A flatpack stress gage containing piezoresistance foil elements is very well suited for measuring blast pressure loads on the surface of an armored vehicle because it can be attached to the target with no penetrations (by welding or bonding with epoxy) and it presents a very-low-profile obstacle to blast waves. However, at the beginning of this project, the usefulness of flatpack gages for this application was limited primarily because large in-plane strains in the elements would significantly perturb the element output and prevent it from being properly interpreted.

In this project we accomplished two major developments to make flatpacks usable for this application. First, the flatpack design was improved by using a very-high-strength steel case, incorporating three piezoresistance elements in a single gage, confining the piezoresistance elements in a shallow cavity to mitigate strains, and reducing the size of the gage so that all the elements fit within a 5-mm radius. Second, an analytical procedure was derived and a computer code was written to interpret resistance histories from the piezoresistance elements under nonuniaxial strain conditions based on the constitutive and piezoresistance properties of the elements. With these developments, the flatpack gage is now a usable tool for many blast-load measurement problems.

Further improvements could be made. First, transverse strain coupling into foil grid-type elements may be insignificant. This possibility should be studied further (with computations) because it would allow one of the elements to be eliminated. Second, the mechanical and piezoresistance properties of the commercially available elements should be measured. Third, the response time (natural period) of the flatpack gage is probably adequate for most explosive load situations, but additional design changes (such as mica insulation and a titanium cover) may improve this response time. Finally, only a few measurements of close-in blast pressures have been made with the current flatpack gage design, and although the results are good, further use of the gage (and comparisons with calculations and other measurements) would further substantiate its capabilities.

REFERENCES

1. D. Y. Chen, Y. M. Gupta, and M H. Miles, "Quasistatic Experiments to Determine Material Constants for the Piezoresistance Foils Used in Shock Wave Experiments," *J. Appl. Phys.* **55**(11) (1 June 1984).

2. S. C. Gupta and Y. M. Gupta, "Piezoresistance Response of Longitudinally and Laterally Oriented Ytterbium Foils Subjected to Impact and Quasistatic Loading," *J. Appl. Phys.* **57**(7) (1 April 1985).

3. Y. M. Gupta and S. C. Gupta, "Incorporation of Strain Hardening in Piezoresistance Analysis: Application to Ytterbium Foils in a PMMA Matrix," *J. Appl. Phys.* **61**(2) (15 January 1987).

4. S. C. Gupta and Y. M. Gupta, "Experimental Measurements and Analysis of the Loading and Unloading Response of Longitudinal and Lateral Manganin Gauges Shocked to 90 kbar," *J. Appl. Phys.* **62**(7) (1 October 1987).

5. H. J. Sutherland, "Acoustical Determination of the Shear Relaxation Functions for PMMA and Epon 828-Z," *J. Appl. Phys.* **49**(7) (July 1978).

6. Y. M. Ito and Y. Muki, "Numerical Simulation of Piezoresistance Gage Response," DNA-TR-87-130 (September 1990).

7. L. Seaman, "Plasticity Analysis for Isotropic Material," SRI International, Poulter Laboratory Technical Report PLTR-003-79 (December 1979).

8. J. Drotleff, FMC Corporation, San Jose, CA (personal communication, May 1990).

9. S. Mullin, Southwest Research Institute, San Antonio, TX (personal communication, May 1990).

10. Micro-Measurements, "Catalog 500, Part B—Strain Gage Technical Data."

11. S. P. Timoshenko and J. N. Goodier, "Theory of Elasticity," McGraw-Hill Book Co., Third Edition, 1970, p. 23.

12. J. Hallquist and D. Bensonr, "DYNA3D User's Manual (Nonlinear Dynamic Analysis of Structures in Three Dimensions)," Lawrence Livermore National Laboratory, Report UCID-19592, Rev. 2 (March 1986).

13. J. Hallquist, "NIKE2D—A Vectorized, Duplicit, Finite Deformation, Finite Element Code for Analyzing the Static and Dynamic Response of 2-D Solids," Lawrence Livermore National Laboratory, Report UCID-19677 (February 1983).

APPENDIX A

PIEZORESISTANCE MATERIAL MODELS

The material models for ytterbium, manganin, and constantan used in this project are based on the publications of Gupta and associates.[1-4] This Appendix compares model predictions with test data. Table A-1 lists the values for the constitutive and piezoresistance parameters used in PIEZOR. Tensile stresses and strains are positive-throughout.

Figure A-1 shows stress-strain curves and resistance change for static uniaxial tension tests. The odd nature of the $\frac{\Delta R}{R_0}$ versus ϵ_1 curve exhibited by ytterbium [Figure A-1(b)] arises because of ytterbium's very high stress sensitivity and its low strength. During the elastic phase of the tensile test the resistance change is

$$\frac{\Delta R}{R_0} = [(\alpha + 2\beta) E + (1 + 2v)] \epsilon_1 \qquad (A-1)$$

where the first term represents the effect of the axial stress and the second term accounts for the strains. Using the values for α, β, E and v in Table A-1, the first term in the brackets has a value -5.05 and the second term 1.73. Thus, the slope of the $\frac{\Delta R}{R_0}$ versus ϵ_1 curve is -3.32. In contrast, for large plastic strains the stress is limited to about 1 kbar [Figure A-1(a)] and the ytterbium is approximately incompressible. Thus, ignoring elastic strains

$$\frac{\Delta R}{R_0} = (\alpha + 2\beta) (1 \text{ kbar}) + (1 + 2 \times \frac{1}{2}) \epsilon_1 \qquad (A-2)$$

Now the stress term has a value of about -0.04 and the strain coefficient is 2. The same effects occur in the response of manganin and constantan, but for these materials the stress sensitivity is overwhelmed by the strains so the slopes of their $\frac{\Delta R}{R_0}$ versus ϵ_1 curves approach 2 at much lower strains.

[1] D. Y. Chen, Y. M. Gupta, and M. H. Miles, "Quasistatic Experiments to Determine Material Constants for the Piezoresistance Foils Used in Shock Wave Experiments," *J. Appl. Phys.* 55(11) (1 June 1984).

[2] S. C. Gupta and Y. M. Gupta, "Piezoresistance Response of Longitudinally and Laterally Oriented Ytterbium Foils Subjected to Impact and Quasistatic Loading," *J. Appl. Phys.* 57(7) (1 April 1985).

[3] Y. M. Gupta and S. C. Gupta, "Incorporation of Strain Hardening in Piezoresistance Analysis: Application to Ytterbium Foils in a PMMA Matrix," *J. Appl. Phys.* 61(2) (15 January 1987).

[4] S. C. Gupta and Y. M. Gupta, "Experimental Measurements and Analysis of the Loading and Unloading Response of Longitudinal and Lateral Manganin Gauges Shocked to 90 kbar," *J. Appl. Phys.* 62(7) (1 October 1987).

Table A-1. Material Properties

	E (kbar) [GPa]	υ	σ_y (kbar) [GPa]	H* (kbar) [GPa]	α** (kbar^{-1}) [GPa^{-1}]	β (kbar^{-1}) [GPa^{-1}]	A	g
Constantan	1485 [148.5]	0.33	8.2 [0.82]	409 [40.9]	-0.49×10^{-4} [-0.49×10^{-3}]	1.89×10^{-4} [1.89×10^{-3}]	0	0
Manganin	876 [87.6]	0.374	2.3 [0.23]	24 [2.4]	-0.44×10^{-3} [-0.44×10^{-2}]	-0.31×10^{-3} [-0.31×10^{-2}]	0.0105	80
Ytterbium	120 [12.0]	0.365	0.49 [0.049]	212.5 (8.0×10^{-4}) [21.25] 122.2 (1.7×10^{-4}) [12.22] 53.85 (3.0×10^{-4}) [5.385] 18.75 (5.4×10^{-3}) [1.875] 9.091 (7.6×10^{-3}) [0.9091] 0.8772 (1.33×10^{-2}) [0.08772]	-0.788×10^{-2} [-0.788×10^{-1}]	-1.71×10^{-2} [-1.71×10^{-1}]	0.0425	80

*For ytterbium a multilinear stress-strain curve is used. The quantities in parentheses are the values of plastic strain at the beginning of each linear segment.

**For ytterbium the pressure dependence of α is -7.6×10^{-4} kbar^{-2} [-7.6×10^{-2} GPa^{-2}].
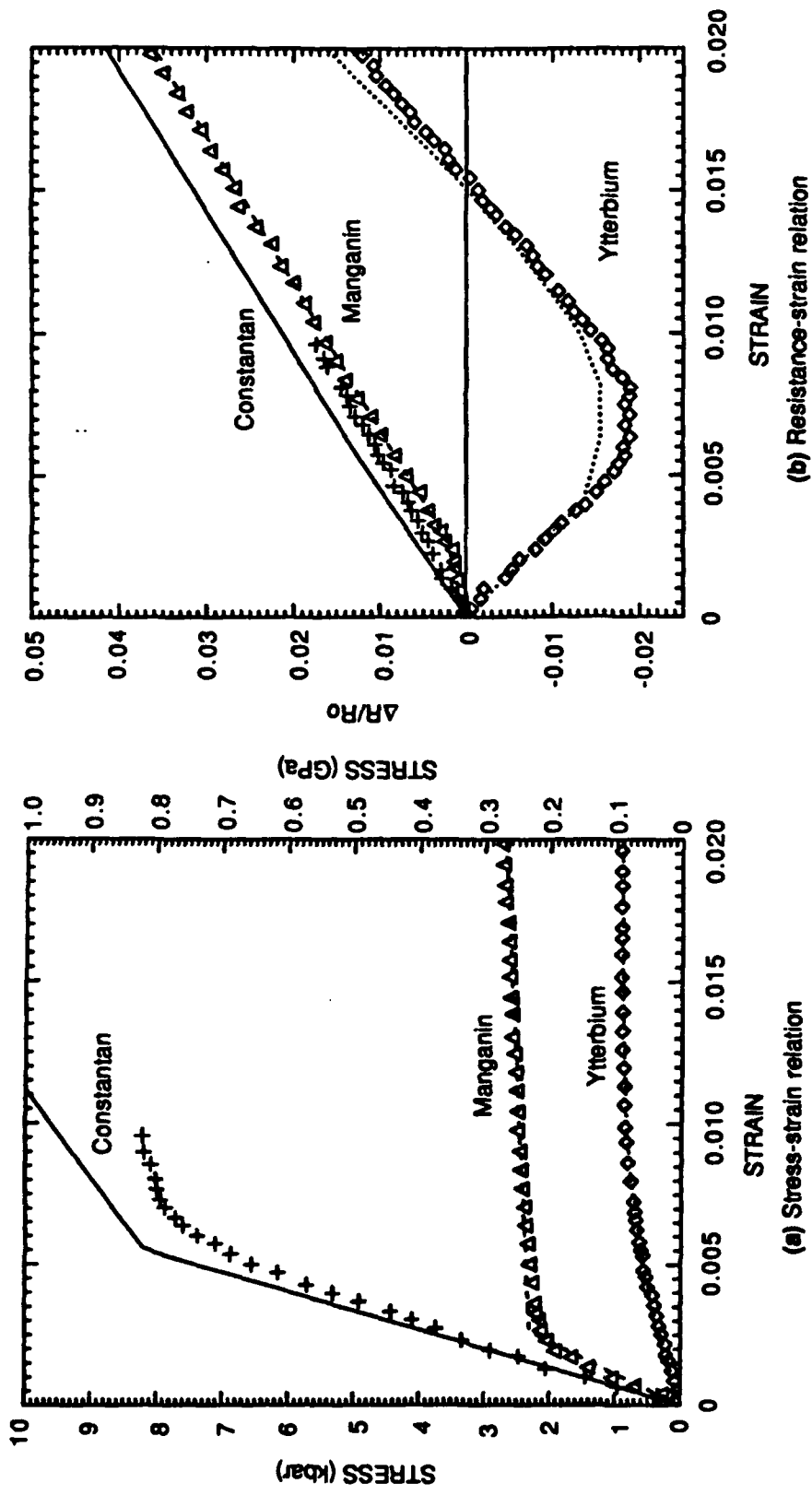
Figure A-1. Static uniaxial tension tests. Points are data from Reference 1. Curves are PIEZOR model prediction.

RM-7422-70

A-3

Figure A-2 shows resistance change versus *normal stress* for uniaxial strain compression. The PIEZOR program uses the ytterbium curve without the pressure-dependent coefficients terms, so it should be modified for use above 2 kbar (200 MPa).

Figure A-3 shows exponential fits to the piezoresistance strain-hardening coefficient (η) for shock wave loading. The fits for η could be improved for plastic strains less than 1%.

The coefficient η in equation (11) (Section 3) is defined as the sensitivity of the material's resistance to an increment of plastic strain. The determination of η in References 3 and 4, however, is based on the average sensitivity over a finite step in plastic strain. Put another way, equation (11) calls for a tangent value of the $\frac{\Delta R}{R_0}$ vs $\bar{\epsilon}^p$ curve, whereas References 3 and 4 give secant values. Tangent values were determined from the results presented in References 3 and 4 as follows.

First, we use the definitions for the secant values of the $\frac{\Delta R}{R_0}$ vs $\bar{\epsilon}^p$ curve (denoted η_s) and the tangent values (denoted η_t)

$$\frac{\Delta R}{R_0} = \eta_s \gamma_p \tag{A-3}$$

$$\frac{\Delta R}{R_0} = \int_0^{\gamma_p} \eta_t(\gamma_p) d\gamma_p \tag{A-4}$$

where $\gamma_p = \frac{\sqrt{3}}{2} \bar{\epsilon}^p$. Differentiating (A-4) and substituting from (A-3) gives

$$\eta_t(\gamma_p) = \frac{d}{d\gamma_p}\left[\frac{\Delta R}{R_0}(\gamma_p)\right] = \frac{d}{d\gamma_p}\left[\eta_s \gamma_p\right] = \eta_s' \gamma_p + \eta_s \tag{A-5}$$

Next, the $\frac{\Delta R}{R_0}$ vs γ_p curve is constructed from the results given in References 3 and 4 using (A-3), and this curve is fit with the form

$$\frac{\Delta R}{R_0} = A\left(1 - e^{-g\gamma_p}\right) \tag{A-6}$$

For this form, η_s and η_t are given by

$$\eta_s = \frac{A}{\gamma_p}\left(1 - e^{-g\gamma_p}\right) \tag{A-7}$$

and

$$\eta_t = A g e^{-g\gamma_p} \tag{A-8}$$

A-4
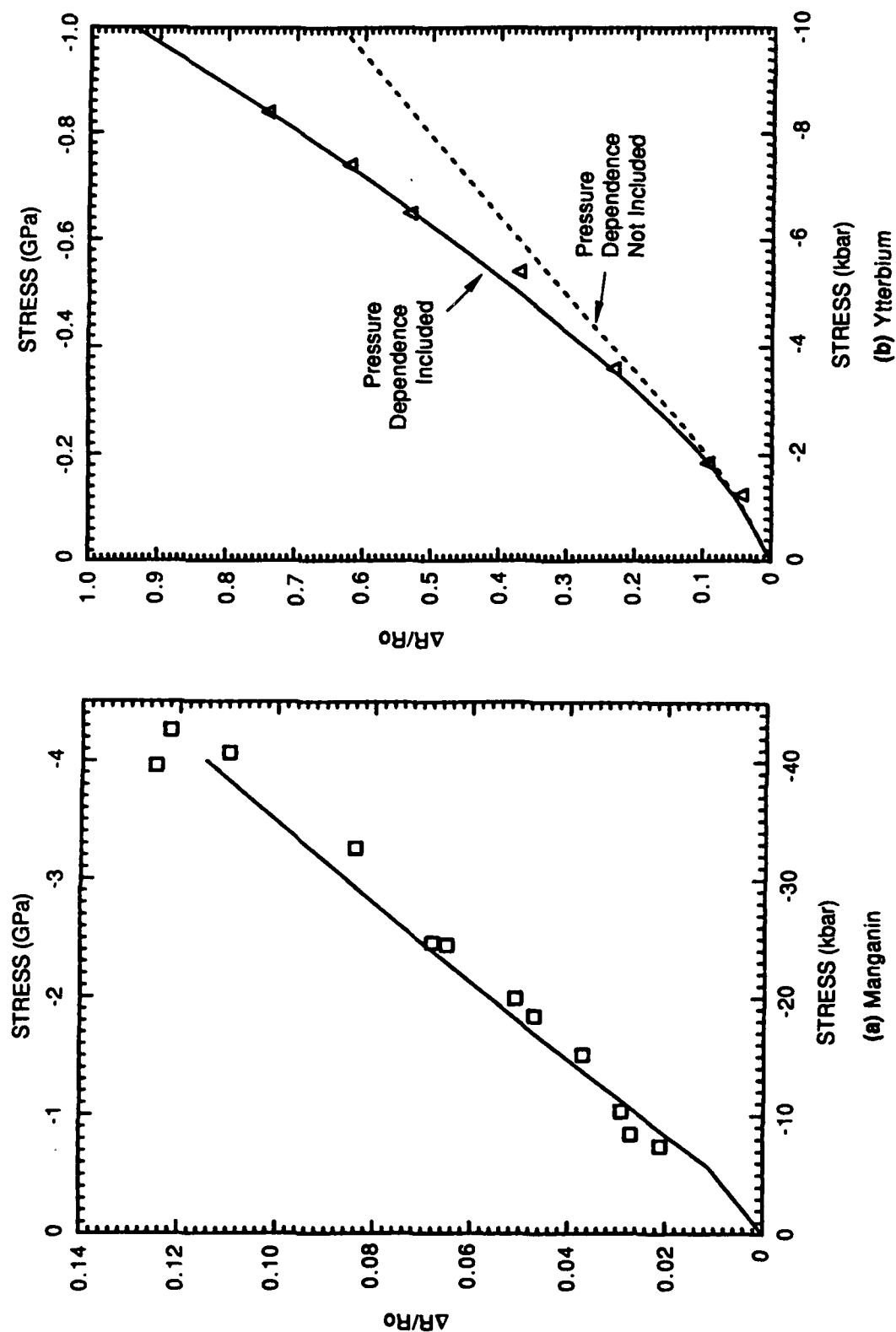
Figure A-2. Sensitivity of piezoresistance foils to uniaxial strain compression. Points are data from Reference 3 and 4. Curves are PIEZOR model predictions.

A-5

(a) Manganin

(b) Ytterbium
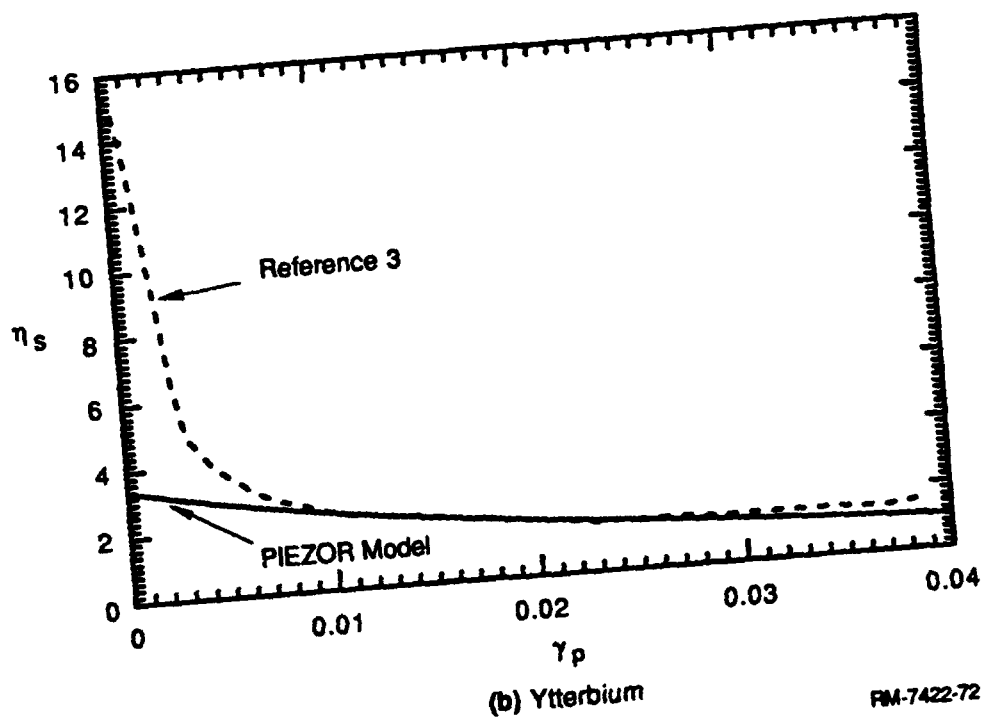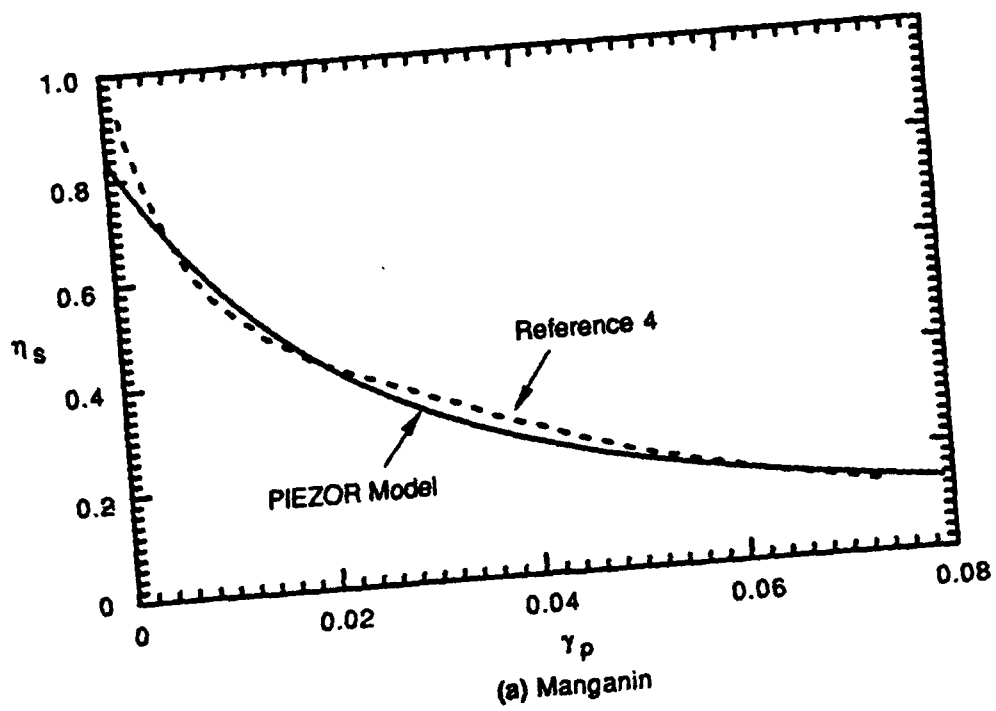
RM-7422-72

Figure A-3.   Piezoresistance strain-hardening coefficients.

APPENDIX B

PIEZOR COMPUTER PROGRAM

This Appendix contains a listing of the PIEZOR computer program and its associated subroutines. These are followed by a sample input set and a partial listing of output.

The first line of input is a title. Each element is described separately, beginning with a material name (MAT N). Table B-1 gives the definitions of the input parameters. The orientations of the elements are fixed; elements 1 and 2 are aligned in the x direction, and element 3 is aligned in the y direction.

Table B-1. PIEZOR Variable Definitions

MAT	Material name
MODELETA	$= 0$ for $\eta =$ constant
	$= 1$ for $\eta = Age^{-g}\sqrt{\frac{3}{2}\bar{\epsilon}^p}$
MODELH	$= 0$ for H = constant
	$= 1$ for H $(\bar{\epsilon}^p)$

EM	Elastic modulus
ANU	Poisson's ratio
Y_0	Yield stress
H	Hardening modulus (for MODELH = 0)

NH	Number of points for hardening curve (for MODELH = 1
EBARP, H	$\bar{\epsilon}^p$, H pairs for hardening curve

ALPHA	α
BETA	β
ETA1	η (for MODELETA = 0) or A (for MODELETA = 1)
ETA2	g (for MODELETA = 1)

LAMN (i,i)	λ_{ii}, i = 1,3

```
      PROGRAM PIEZOR3
C
C     ****    MODIFIED 6/14/91 TO ADD FEATURE OF H AS A FUNCTION OF EPSBARP
C
C     ----    FEBRUARY, 1991
C     PIEZOR3 CORRECTS PROBLEM WHERE SIGMABAR (SB) DOES NOT TRACK THE YIELD
C     ACCURATELY.  PIEZOR3 CALCULATES B MATRIX AND N,
C                        WHERE N = (H+3*G*SBOLD/SBN)/(H+3*G)
C     PROGRAM ITERATES UNTIL SBN CONVERGES.
C     PIEZOR3 USES SUBROUTINE MATRXM2
C     GIVEN 3 GAGE HISTORIES IN DR/R0 VS TIME, WHERE THE GAGES CONSIST
C     OF:
C        1.  A STRESS GAGE IN THE RADIAL DIRECTION
C        2.  A STRAIN GAGE IN THE RADIAL DIRECTION
C        3.  A STRAIN GAGE PERPENDICULAR TO THE STRESS GAGE
C                (IN THE CIRCUMFERENTIAL DIRECTION)
C     THIS PROGRAM CALCULATES THE NORMAL STRESS (SIGMAZ), RADIAL STRAIN,
C     & CIRCUMFERENTIAL STRAIN FOR THESE GAGE DATA.  OTHER QUANTITIES ALSO
C     CALCULATED ARE THE REMAINING STRESSES AND STRAINS FOR UP TO 3
C     MATERIALS TO COMPLETE THE SET OF STRESSES & STRAINS IN 3 DIRECTIONS.
C
C     UNITS:  OUTPUT CONSISTENT WITH INPUT UNITS
C
C     INPUT:
C        *  DATA FILE FOR STRESS GAGE
C        *  DATA FILES (2) FOR STRAIN GAGES
C        *  MATERIAL PROPERTIES FOR EACH GAGE:
C              AK      BULK MODULUS
C              G       SHEAR MODULUS
C              YIELD   YIELD STRESS
C              H       WORK HARDENING MODULUS
C              MODELH  INDICATOR FOR H
C                      = 0 FOR CONSTANT H
C                      = 1 FOR H AS A FUNCTION OF EPSBARP
C                          INPUT ARE PAIRS OF POINTS (EPSBARP,H).
C                          H IS CONSTANT WITHIN AN EPSBARP INTERVAL.
C        *  PIEZORESISTIVE CONSTANTS FOR EACH GAGE
C              ALPHA   PIEZORESISTIVE COEFFICIENT (1/Kbar)
C              BETA    PIEZORESISTIVE COEFFICIENT (1/Kbar)
C              MODELETA  INDICATOR FOR MODEL TO BE USED TO CALCULATE ETA, THE
C                          PLASTIC DEFORMATION COEFFICIENT
C                          = 0  FOR ETA=ETA1  (A CONSTANT)
C                          = 1  FOR ETA=ETA1*ETA2*EXP(-ETA2*SQRT(0.75)*EBP)
C              ETA1    CONSTANT TERM FOR ETA = CONSTANT;
C                      ONE OF 2 COEFFICIENTS FOR MODELETA=1
C              ETA2    2ND COEFFICIENT FOR MODELETA=1
C
C        *  DIAGONAL OF LAMBDA, THE COUPLING MATRIX FOR EACH GAGE
C              LAMBDA(1,1), LAMBDA(2,2), & LAMBDA(3,3)    (0 <= LAMBDA(3,3) <= 1)
C
C     OUTPUT:
C        *  FILE FOR006 FOR BATCH JOB
C              FOR EACH GAGE : S, EP, SB, SD, DEPD, EBP, Y, COND
C        *  FILE FOR008 - BINARY SCRATCH FILE FOR STRESS-STRAIN STATES
C        *  FILE FOR009 - HISTORIES FOR STRESSES, STRAINS, EFFECTIVE STRESS
C                        & EFFECTIVE PLASTIC STRAIN FOR EACH GAGE
C
C
C
C
```

```fortran
      PARAMETER (MAXNPT=10001)
      IMPLICIT REAL*8 (A-H,O-Z)
      INTEGER COND,CONDS
      REAL*8 LAM,LAMN
      REAL*4 TS(MAXNPT),RS(MAXNPT),RE1(MAXNPT),RE2(MAXNPT),TE1(MAXNPT)
     1   ,TE2(MAXNPT),DTS,DTE1,DTE2,TMIN,TMAX
      DIMENSION AM(3,3,3),AMM(3,3),R(3),LAM(3,3),
     1   AMS(3,3,3),PS(3,3),PM(1,3),QS(3,3),QM(1,3),QP(1,3),WS(3,3),
     2   SS(3,3),SS2(3,1),TST(3,3),TS2(3,1),ROR(3),THETA(3),GM(3,3,3),
     3   PROD(3,3),FM(3),FM2(3,1),OM(3,3),B(3,3)
      DIMENSION S(3,3),EP(3,3),SD(3,3),SB(3),EBP(3),DEBP(3),
     1   Y(3),SOLD(3,3),P(3),EPOLD(3,3),SBOLD(3),EBPOLD(3),YOLD(3),
     2   SDOLD(3,3),COND(3),FR(3),RT(3),DSD(3,3),ETA(3),SDN(3,3),
     3   DEPD(3,3),SBN(3),SBNL(3),AN(3)
      CHARACTER*80 TITLE
      CHARACTER*50 FILENAMEO,FILENAMEH
      CHARACTER*10 IDAT,MATNAM
      LOGICAL*1 LBATCH,LPC,LMATRX
      COMMON IDAT,TITLE,IOUT,LBATCH,FILENAMEO,FILENAMEH
C     LAMN(I,M) = LAMBDA DIAGONAL FOR MATERIAL M
      COMMON /MAT/ AK(3),G(3),Y0(3),H(3),ETA1(3),ETA2(3),ALPHA(3),
     1   BETA(3),MATNAM(3),LAMN(3,3),MODELETA(3),MODELH(3),NH(3),
     2   EPH(50,3),HH(50,3)

      EQUIVALENCE (FM(1),FM2(1,1))

      DATA MATNAM /'MATERIAL 1','MATERIAL 2','MATERIAL 3'/
      DATA DEGPRAD /57.295795/
      DATA THETA /2*0.,90./
      DATA TOLER /1.0E-5/

C
C     DEFINE ETA FOR MODELETA=1
      ETAJ(C1,C2,EBP)=C1*C2*EXP(-C2*SQRT(0.75)*EBP)
C
      DO M=1,3
        THETA(M)=THETA(M)/DEGPRAD
      ENDDO
C
C     READ INPUT DATA

      CALL INPUT(MAXNPT,TS,RS,DTS,NPTS,TE1,RE1,DTE1,NPTE1,TE2,RE2,DTE2,
     1   NPTE2,TMIN,TMAX)
C
C     OPEN SCRATCH FILE
C      OPEN (UNIT=8,FORM='UNFORMATTED',STATUS='SCRATCH')
      OPEN (UNIT=8,FORM='UNFORMATTED',STATUS='NEW')
C
C     INITIALIZE

      K=0
      KBEG1=1
      KBEG2=1
      NPT=0
      TIM=TMIN
      DTSNEW=0.
      DO M=1,3
        DO I=1,3
          S(I,M)=0.
```

B-4

```fortran
                EP(I,M)=0.
                SD(I,M)=0.
                SOLD(I,M)=0.
                SDOLD(I,M)=0.
                EPOLD(I,M)=0.
                DSD(I,M)=0.
                SDN(I,M)=0.
                DEPD(I,M)=0.
            ENDDO
            SB(M)=0.
            SBOLD(M)=0.
            EBP(M)=0.
            DEBP(M)=0.
            EBPOLD(M)=0.
            SBN(M)=0.
            SBNL(M)=0.
            Y(M)=Y0(M)
            YOLD(M)=Y0(M)
C           MATERIAL IS ASSUMED ELASTIC INITIALLY
C                 1 = ELASTIC
C                 2 = PLASTIC
C                 3 = CURRENT STEP IS ELASTIC, NEXT STEP PLASTIC
C                     (FRACTION OF NORMAL STEP SIZE FOR TREATMENT AT CORNER)
            COND(M)=1
        ENDDO

C
C       SET UP P* & Q*
        DO M=1,3
            PS(M,1)=ALPHA(M)
            PS(M,2)=1.
            PS(M,3)=-1.
            QS(M,1)=ALPHA(M)+2.*BETA(M)
            QS(M,2)=ALPHA(M)
            QS(M,3)=-1.
        ENDDO

C
C       SET UP ROTATION MATRIX OM & COUPLING MATRIX LAM
        DO M=1,3
            DO I=1,3
                DO J=1,3
                    LAM(I,J)=0.
                    OM(I,J)=0.
                    IF (J .EQ. I) THEN
                        LAM(I,J)=LAMN(I,M)
                        IF (I .EQ. 1) THEN
                            OM(I,J)=1.
                        ELSE
                            OM(I,J)=COS(THETA(M))**2
                        ENDIF
                    ENDIF
                ENDDO
            ENDDO
            OM(2,3)=SIN(THETA(M))**2
            OM(3,2)=SIN(THETA(M))**2
```

```
            CALL MATMPY(LAM,3,3,OM,3,PROD)
            DO I=1,3
               DO J=1,3
                  GM(I,J,M)=PROD(I,J)
               ENDDO
            ENDDO
         ENDDO

C        LOOP OVER GAGE DATA
20       K=K+1
         IF (K .GT. NPTS) GO TO 300
         IF (TS(K) .LT. TMIN-1.E-4*DTS) GO TO 20
         IF (TS(K) .GT. TMAX+1.E-4*DTS) GO TO 300
         IF (NPT .EQ. 0) THEN
            R(1)=RS(K)
            GO TO 25
         ENDIF
         R(1)=RS(K)-RS(K-1)
         DTSNEW=DTS
25       DO I=KBEG1,NPTE1
            IF (ABS(TE1(I)-TS(K)) .LE. DTE1/2.) THEN
               KBEG1=I
               IF (NPT .EQ. 0) THEN
                  R(2)=RE1(I)
               ELSE
                  R(2)=RE1(I)-RE1(I-1)
               ENDIF
               GO TO 30
            ENDIF
         ENDDO
30       DO I=KBEG2,NPTE2
            IF (ABS(TE2(I)-TS(K)) .LE. DTE2/2.) THEN
               KBEG2=I
               IF (NPT .EQ. 0) THEN
                  R(3)=RE2(I)
               ELSE
                  R(3)=RE2(I)-RE2(I-1)
               ENDIF
               GO TO 40
            ENDIF
         ENDDO
40       CONTINUE
C
C        PREPARE FOR ITERATION,  DEPD(I,M)=0. AS 1ST GUESS
42       ITER=0
         DO M=1,3
            DO I=1,3
                  DEPD(I,M)=0.
            ENDDO
            SBNL(M)=0.
            SBN(M)=0.
         ENDDO
C
C        ASSUME MATERIAL IS ELASTIC INITIALLY;  AN(M)=1 IF ELASTIC
         DO M=1,3
            COND(M)=1
            AN(M)=1.0
            FR(M)=0.
            RT(M)=0.
```

```
           ENDDO
           FRAC=1.0E+30
           NCORNER=0
           CONDS=0
           LMATRX=.FALSE.
           LPC=.FALSE.

C
C          CALCULATE ETA HERE

45         CONTINUE
           DO M=1,3
              IF (MODELETA(M) .EQ. 0) THEN
                    ETA(M)=ETA1(M)
              ELSE IF (MODELETA(M) .EQ. 1) THEN
                    ETA(M)=ETAJ(ETA1(M),ETA2(M),EBP(M))
              ELSE
                    WRITE (IOUT,9275) M,MODELETA(M)
9275                FORMAT(' *****    ERROR IN SELECTION OF MODEL FOR ETA --'
     1                ,' M ='I2,' MODELETA ='I2/
     2                '          ALLOWABLE MODELS ARE:'/
     3                '             0      ETA=CONSTANT                OR'
     4                /'            1      ETA=ETA1*ETA2*EXP(-ETA2*EBP)')
                    STOP
              ENDIF
           ENDDO
C
C          CALCULATE THE M & M* MATRICES FOR EACH MATERIAL

50         DO M=1,3
              CALL MATRXM2(M,AK(M),G(M),H(M),AN(M),AM)
              DO J=1,2
                 AMS(J,1,M)=AM(J,3,M)/AM(3,3,M)
                 AMS(J,2,M)=AM(J,1,M)-AM(J,3,M)*AM(3,1,M)/AM(3,3,M)
                 AMS(J,3,M)=AM(J,2,M)-AM(J,3,M)*AM(3,2,M)/AM(3,3,M)
              ENDDO
              AMS(3,1,M)=1./AM(3,3,M)
              AMS(3,2,M)=-AM(3,1,M)/AM(3,3,M)
              AMS(3,3,M)=-AM(3,2,M)/AM(3,3,M)
           ENDDO
C
C          CALCULATE W* & B

60         DO M=1,3
              DO I=1,3
                 QM(1,I)=QS(M,I)
                 PM(1,I)=PS(M,I)
                 DO J=1,3
                       AMM(I,J)=AMS(I,J,M)
                       PROD(I,J)=GM(I,J,M)
                 ENDDO
              ENDDO
              CALL MATMPY(PM,1,3,PROD,3,QP)
              CALL MATMPY(QM,1,3,AMM,3,PM)
              CALL MATMPY(PM,1,3,PROD,3,QM)
              DO J=1,3
                 WS(M,J)=QP(1,J)+QM(1,J)
              ENDDO
```

```fortran
            SS2(1,1)=(AN(M)-1.`*SDOLD(3,M)
            SS2(2,1)=0.
            SS2(3,1)=0.
            CALL MATMPY(AMM,3,3,SS2,1,TS2)
            DO I=1,3
                  IF (I .NE. 3` THEN
                    B(I,M)=(AN(M)-1.)*SDOLD(I,M)-TS2(I,1)
                  ELSE
                    B(I,M)=-TS2(I,1)
                  ENDIF
            ENDDO
         ENDDO
C
C      CALCULATE S*

       DO M=1,3
         DO I=1,3
                  QM(1,I)=QS(M I)
                  SS2(I,1)=B(I,M)
         ENDDO
         CALL MATMPY(QM,1,3,SS2,1,TS2(M,1))
         FM(M)=R(M) - SQRT(0.75)*ETA(M)*(EBP(M)-EBPOLD(M)) - TS2(M,1)
       ENDDO

       CALL SIMQ(WS,FM,3,IFLAG)
C
C      CALCULATE S & T MATRICES
C
       DO M=1,3
         DO I=1,3
                  DO J=1,3
                      PROD(I,J)=GM(I,J,M)
                      AMM(I,J)=AMS(I,J,M)
                  ENDDO
         ENDDO
         CALL MATMPY(PROD,3,3,FM2,1,SS2)
         CALL MATMPY(AMM,3,3,SS2,1,TS2)
         DO J=1,3
            SS(J,M)=SS2(J,1) ·
            TST(J,M)=TS2(J,1) + B(J,M)
         ENDDO
       ENDDO

C
C      COMPUTE STRESS DEVIATORS & STRAIN DEVIATOR INCREMENT

       DO M=1,3
         S(1,M)=SOLD(1,M)+TST(1,M)
         S(2,M)=SOLD(2,M)+TST(2,M)
         S(3,M)=SOLD(3,M)+SS(1,M)
         P(M)=(S(1,M)+S(2,M)+S(3,M))/3.

         DO I=1,3
            SD(I,M)=S(I,M)-P(M)
            DSD(I,M)=SD(I,M)-SDOLD(I,M)
         ENDDO
         SB(M)=SQRT(1.5*(SD(1,M)**2+SD(2,M)**2+SD(3,M)**2))
       ENDDO
```

```
C
C      TEST FOR YIELDING, SET MATERIAL CONDITIONS
C      IF 1ST POINT IS PLASTIC OR A CORNER, STOP CALCULATION
C      -----     MODIFIED TEST FOR PLASTIC CONDITION

       IF (LMATRX) GO TO 95

       DO 70 M=1,3
C         ELASTIC
          IF (SB(M) .LT. YOLD(M)) THEN
                COND(M)=1
C         PLASTIC
C          ELSE IF (SB(M) .GT. YOLD(M) .AND. ABS(SBOLD(M)-YOLD(M)) .LT.
C     1       1.E-4*YOLD(M)) THEN
          ELSE IF (SB(M) .GT. YOLD(M) .AND. SBOLD(M) .GT. YOLD(M)*0.9999)
     1      THEN

                COND(M)=2

C               STRAIN DEVIATOR INCREMENT
                DEPD(1,M)=2.*SS(2,M)/3.-(SS(3,M)+TST(3,M))/3.
                DEPD(2,M)=2.*SS(3,M)/3.-(TST(3,M)+SS(2,M))/3.
                DEPD(3,M)=2.*TST(3,M)/3.-(SS(2,M)+SS(3,M))/3.
                DO I=1,3
                   SDN(I,M)=SDOLD(I,M)+2.*G(M)*DEPD(I,M)
                ENDDO
                SBN(M)=SQRT(1.5*(SDN(1,M)**2+SDN(2,M)**2+SDN(3,M)**2))
                AN(M)=(H(M)+3.*G(M)*SBOLD(M)/SBN(M))/(H(M)+3.*G(M))
C         CORNER
          ELSE
                COND(M)=3
                NCORNER=NCORNER+1
          ENDIF
          IF (NPT .EQ. 0 .AND. COND(M) .GT. 1) GO TO 950
          CONDS=CONDS+COND(M)
70     CONTINUE

C
C      IF ONE OR MORE MATERIAL IS PLASTIC WHEN ANOTHER HAS REACHED A
C         CORNER, RECALCULATE M, M* AND W MATRICES WITH PLASTIC CONDITION
C         SO THAT THE CORNER CAN BE CALCULATED MORE ACCURATELY
C

       IF (CONDS .GE. 6 .AND. CONDS .LE. 8) THEN
          IF ((CONDS .LE. 7 .AND. NCORNER .EQ. 1) .OR.
     1           (CONDS .EQ. 8 .AND. NCORNER .EQ. 2)) THEN
             IF (.NOT. LPC) THEN
                   LPC=.TRUE.
                   CONDS=0
                   NCORNER=0
                   GO TO 50
             ENDIF
          ENDIF
       ENDIF

C      IF CORNER, CALCULATE FRACTION
       DO M=1,3
          IF (COND(M) .EQ. 3) THEN
```

```fortran
              C1=1.5*(DSD(1,M)**2+DSD(2,M)**2+DSD(3,M)**2)
              C2=3*(SDOLD(1,M)*DSD(1,M)+SDOLD(2,M)*DSD(2,M)+SDOLD(3,M)
     1          *DSD(3,M))
              C3=SBOLD(M)**2-YOLD(M)**2
              RAD=SQRT(C2**2-4.*C1*C3)
              IF (C3 .EQ. 0.) THEN
                COND(M)=2
                CONDS=CONDS-1
                NCORNER=NCORNER-1
                GO TO 72
              ENDIF
              RT(1)=(-C2+RAD)/(2.*C1)
              RT(2)=(-C2-RAD)/(2.*C1)
C             INSURE ONE OF ROOT MUST BE BETWEEN 0 AND 1
              DO I=1,2
                IF (ABS(RT(I)) .LT. 1.0E-5)  RT(I)=0.
                IF (ABS(RT(I)-1.0D0) .LT. 1.0E-5) RT(I)=1.0
              ENDDO
              IF ((RT(1) .LT. 0. .OR. RT(1) .GT. 1.) .AND. (RT(2) .LT.
     1          0. .OR. RT(2) .GT. 1.)) THEN
                  WRITE (IOUT,9055) M,COND(M),NPT,TIM,DTSNEW,RT(1),RT(2)
9055              FORMAT(//' ***** STOP -- ROOTS OUTSIDE RANGE (0,1) '/
     1                 ' M ='I2,' COND ='I2,' NPT ='I6,' TIM,DTSNEW ='
     2                  1P2E12.4,' RT(1),RT(2) ='2E15.6)
                  STOP '  ***  ROOTS OUTSIDE RANGE (0,1)'
              ENDIF
              DO I=1,2
                IF (RT(I) .GT. 0. .AND. RT(I) .LE. 1.) THEN
                  FR(M)=RT(I)
                  GO TO 72
                ENDIF
              ENDDO
          ENDIF
72        CONTINUE
          ENDDO

          GO TO (960,960,95,75,80,80,80,80,80) CONDS
C         ELASTIC/PLASTIC
75        LMATRX = .TRUE.
          GO TO 50

80        IF (NCORNER .EQ. 0) GO TO 75
C         CORNER(S)
          DO M=1,3
            IF (COND(M) .EQ. 3) FRAC=MIN(FR(M),FRAC)
          ENDDO

90        DTSNEW=DTSNEW*FRAC
          DO J=1,3
            ROR(J)=R(J)
            R(J)=FRAC*R(J)
          ENDDO
          LMATRX = .TRUE.
          GO TO 50


C
C     MAKE CORRECTION TO STAY ON YIELD SURFACE
C
95        CONTINUE
```

```fortran
C
C       COMPUTE STRAIN DEVIATORS AND YIELD

        DO M=1,3
           EP(1,M)=EPOLD(1,M)+SS(2,M)
           EP(2,M)=EPOLD(2,M)+SS(3,M)
           EP(3,M)=EPOLD(3,M)+TST(3,M)
           IF (COND(M) .EQ. 2) THEN
                   DEPD(1,M)=2.*SS(2,M)/3.-(SS(3,M)+TST(3,M))/3.
                   DEPD(2,M)=2.*SS(3,M)/3.-(TST(3,M)+SS(2,M))/3.
                   DEPD(3,M)=2.*TST(3,M)/3.-(SS(2,M)+SS(3,M))/3.
                   DO I=1,3
                      SDN(I,M)=SDOLD(I,M)+2.*G(M)*DEPD(I,M)
                   ENDDO
                   SBNL(M)=SBN(M)
                   SBN(M)=SQRT(1.5*(SDN(1,M)**2+SDN(2,M)**2+SDN(3,M)**2))
                   AN(M)=(H(M)+3.*G(M)*SBOLD(M)/SBN(M))/(H(M)+3.*G(M))
                   DEBP(M)=(SBN(M)-SBOLD(M))/(H(M)+3.*G(M))
           ELSE
                   DEBP(M)=0.
           ENDIF
           EBP(M)=EBPOLD(M)+DEBP(M)
           Y(M)=YOLD(M)+H(M)*DEBP(M)
        ENDDO


C
C       TEST FOR CONVERGENCE   (SBN)
C
        DO M=1,3
           DELSBN=SBN(M)-SBNL(M)
           IF (ABS(DELSBN) .GT. MAX(ABS(TOLER*SBN(M)),0.D0)) GO TO 120
        ENDDO
        GO TO 150

120     MLAST=M
        IF (ITER .LE. 20) THEN
           ITER=ITER+1
           DO M=1,MLAST
                   SBNL(M)=SBN(M)
           ENDDO
           GO TO 45
        ELSE
           WRITE (IOUT,9050) NPT,K,TIM,TOLER,(M,ETA(M),
     1           SBNL(M),SBN(M), M=1,MLAST)
9050       FORMAT(' *****  STOP: ITER>20, NPT,K =' 2I5,' TIM ='1PE11.3,
     1        ' TOLER ='E10.3/('    M ='I3,' ETA ='1PE11.3,
     2        ' SBNL,SBN ='2E13.5))
           STOP '  ITERATION EXCEEDED 20'
        ENDIF


C
C
C       UPDATE STRESS AND STRAIN STATES

150     CONTINUE
        NPT=NPT+1
        TIM=TIM+DTSNEW
        DO M=1,3
```

```fortran
                 DO J=1,3
                     SOLD(J,M)=S(J,M)
                     SDOLD(J,M)=SD(J,M)
                     EPOLD(J,M)=EP(J,M)
                 ENDDO
                 SBOLD(M)=SB(M)
                 EBPOLD(M)=EBP(M)
                 IF (COND(M) .EQ. 2) YOLD(M)=SB(M)
C                CALCULATE H
                 CALL STRNHARD(M,NH(M),EPH(1,M),HH(1,M),MODELH(M),EBP(M),H(M))
             ENDDO


C
C        WRITE STRESSES & STRAINS TO BINARY FILE FOR008

200      WRITE (8) NPT,TIM,((S(I,M),I=1,3),(SD(I,M),I=1,3),SB(M),Y(M),
     1    P(M),(SS(I,M),I=1,3),(TST(I,M),I=1,3),(EP(I,M),I=1,3),
     2    (DEPD(I,M),I=1,3),EBP(M),COND(M), M=1,3)
C        CHECK TO SEE IF TIME STEP ADJUSTMENT HAS BEEN MADE

         IF (NCORNER .EQ. 0) THEN
C            GO TO NEXT TIME STEP
             GO TO 20
         ELSE
C            RESET TIME STEP AND DR/R0
             DTSNEW=DTS*(1.-FRAC)
             DO J=1,3
                     R(J)=ROR(J)*(1.-FRAC)
             ENDDO
             GO TO 42
         ENDIF


C
C        WRITE OUTPUT TO FOR006 (BATCH)

300      CONTINUE
         DO 340 MT=1,3
             REWIND (8)
320          READ (8,END=340) NPT,TIM,((S(I,M),I=1,3),(SD(I,M),I=1,3),SB(M),
     1        Y(M),P(M),(SS(I,M),I=1,3),(TST(I,M),I=1,3),(EP(I,M),I=1,3),
     2        (DEPD(I,M),I=1,3),EBP(M),COND(M), M=1,3)
             IF (NPT .EQ. 1) WRITE (IOUT,1110) TITLE, MT,MATNAM(MT)
1110         FORMAT(1H1,/1X,A79//30X,'MATERIAL ',I1,' = 'A10
     1              //'    I        TIME        S[3]       EPS[1]       EPS[2]'
     2              '        S[1]        S[2]       EPS[3]            P'
     3              '        SBAR       YIELD C  EPSBARP'/)
             WRITE (IOUT,1115) NPT,TIM,S(3,MT),EP(1,MT),EP(2,MT),S(1,MT),
     1        S(2,MT),EP(3,MT),P(MT),SB(MT),Y(MT),COND(MT),EBP(MT)
1115         FORMAT(I6,1P8E11.3,2E10.3,I2,E10.3)
             GO TO 320
340      CONTINUE


C
C        WRITE STRESS-STRAIN HISTORIES TO FOR009 FOR POST PROCESSING

         OPEN (UNIT=9,STATUS='NEW',RECL=300)
         WRITE (9,1120) IDAT,TITLE
1120     FORMAT(1X,A10,A69)
         WRITE (9,1130) (M,MATNAM(M), M=1,3)
```

```
1130   FORMAT(3(I5,'=',A10))
       WRITE (9,1135)
1135   FORMAT(1X,'TIME,  (S1(M),S2(M),S3(M),EPS1(M),EPS2(M),EPS3(M),',
      1  'EBP(M),SBAR(M), M=1,3)')

       REWIND (8)
350    READ (8,END=370) NPT,TIM,((S(I,M),I=1,3),(SD(I,M),I=1,3),SB(M),
      1  Y(M),P(M),(SS(I,M),I=1,3),(TST(I,M),I=1,3),(EP(I,M),I=1,3),
      2  (DEPD(I,M),I=1,3),EBP(M),COND(M), M=1,3)
       WRITE (9,1125) TIM, ((S(J,M),J=1,3),(EP(J,M),J=1,3),EBP(M),SB(M),
      1   M=1,3)
1125   FORMAT(1P25E12.4)
       GO TO 350
370    CONTINUE
       CLOSE (9)
       CLOSE (8)
       CLOSE (IOUT)
       GO TO 990
910    WRITE (IOUT,9020) FILENAMEH
9020   FORMAT(' ~***  ERROR IN OPENING OUTPUT FILE ',A50)
       GO TO 990
950    WRITE (IOUT,9057) NPT,M,COND(M)
9057   FORMAT(' ****  ERROR EXIT -- NPT ='I2,' MATERIAL ='I2,' COND ='I2)
       GO TO 990
960    WRITE (IOUT,9030) CONDS
9030   FORMAT(' ****  ERROR EXIT -- COND(1)+COND(2)+COND(3) ='I2)
990    STOP
       END
```

```
      SUBROUTINE INPUT(MAXNPT,TS,RS,DTS,NPT,TE1,RE1,DTE1,NPTE1,TE2,RE2,
     1  DTE2,NPTE2,TMIN,TMAX)
C
C     READS STRESS VS TIME, STRAINS VS TIME, & MATERIAL PROPERTIES
C
      IMPLICIT REAL*8 (A-H,O-Z)
      REAL*4 TS(MAXNPT),RS(MAXNPT),RE1(MAXNPT),RE2(MAXNPT),TE1(MAXNPT),
     1  TE2(MAXNPT),DTS,DTE1,DTE2,TSHIFT,VSHIFT,TOA,TMIN,TMAX
      REAL*8 LAMN
      DIMENSION E(2),ANU(2)
      CHARACTER*50 FILENAME,FILENAMEO,FILENAMEH
      CHARACTER*80 TITLES,TITLE1,TITLE
      CHARACTER*40 NAME
      CHARACTER*10 IDAT,A1,A2,A3,A4,MATNAM
      LOGICAL*1 LBATCH
      COMMON IDAT,TITLE,IOUT,LBATCH,FILENAMEO,FILENAMEH
C     LAMN(I,M) = LAMBDA DIAGONAL FOR MATERIAL M
      COMMON /MAT/ AK(3),G(3),Y0(3),H(3),ETA1(3),ETA2(3),ALPHA(3),
     1  BETA(3),MATNAM(3),LAMN(3,3),MODELETA(3),MODELH(3),NH(3),
     2  EPH(50,3),HH(50,3)
C
C     FOR BATCH JOBS, MATERIAL PROPERTIES AND FILENAMES OF GAGE DATA
C        ARE READ FROM FOR005, GAGE DATA FROM FOR001
C
      CALL DATE(IDAT)
      IN=5
      IOUT=6
C
C     WRITE DATE

      WRITE (IOUT,1100) IDAT
1100  FORMAT(1H1,'      DATE ='A10,30X,'BATCH JOB')
C
C     READ MATERIAL PROPERTIES
C        ***    MATERIAL 1 = MATERIAL OF STRESS GAGE
C        ***    MATERIAL 2 = MATERIAL OF STRAIN GAGE 1
C        ***    MATERIAL 3 = MATERIAL OF STRAIN GAGE 2

      READ (IN,1025) TITLE
1025  FORMAT(A80)
      WRITE (IOUT,1110) TITLE
1110  FORMAT(1X,A79)

C
C     MODELH   =  0  FOR CONSTANT H
C              =  1  FOR H AS A FUNCTION OF EPSBARP
C                    (input as points; H is constant in an interval of EPSBARP)
C
      DO MAT=1,3
         READ (IN,1028) A1,MATNAM(MAT),A2,MODELETA(MAT),A3,MODELH(MAT)
1028     FORMAT(2A10,2(A10,I10))
         WRITE (IOUT,1028) A1,MATNAM(MAT),A2,MODELETA(MAT),A3,
     1          MODELH(MAT)
        READ (IN,1030) A1,E(MAT),A2,ANU(MAT),A3,Y0(MAT),A4,H(MAT)
        WRITE (IOUT,1035) A1,E(MAT),A2,ANU(MAT),A3,Y0(MAT),A4,H(MAT)
C       READ (IN,1030) A1,AK(MAT),A2,G(MAT),A3,Y0(MAT),A4,H(MAT)
1030    FORMAT(4(A10,E10.3))
C       WRITE (IOUT,1035) A1,AK(MAT),A2,G(MAT),A3,Y0(MAT),A4,H(MAT)
         IF (MODELH(MAT) .EQ. 1) THEN
```

```
                  READ (IN,1033) A1,NH(MAT)
1033              FORMAT(A10,I10)
                  WRITE (IOUT,1033) A1,NH(MAT)
                  READ (IN,1050) A1,(EPH(I,MAT),HH(I,MAT), I=1,NH(MAT))
1050              FORMAT(A10,6E10.3/(8E10.3))
                  WRITE (IOUT,1055) A1,(EPH(I,MAT),HH(I,MAT), I=1,NH(MAT))
1055              FORMAT(A10,1P6E10.3/(1P8E10.3))
               ENDIF
1035        FORMAT(4(A10,1PE10.3))
C           INITIALIZE H
            IF (MODELH(MAT) .EQ. 1) H(MAT)=HH(1,MAT)
            READ (IN,1030) A1,ALPHA(MAT),A2,BETA(MAT),A3,ETA1(MAT),
     1          A4,ETA2(MAT)
            WRITE (IOUT,1035) A1,ALPHA(MAT),A2,BETA(MAT),A3,ETA1(MAT),
     1          A4,ETA2(MAT)
          AK(MAT)=E(MAT)/(3.*(1.-2*ANU(MAT)))
          G(MAT)=E(MAT)/(2.*(1.+ANU(MAT)))
          WRITE (IOUT,1040) AK(MAT),G(MAT)
1040        FORMAT(10X,'AK ='1PE12.4,'   G ='E12.4)
            READ (IN,1030) A1,LAMN(1,MAT),A2,LAMN(2,MAT),A3,LAMN(3,MAT)
            WRITE (IOUT,1035) A1,LAMN(1,MAT),A2,LAMN(2,MAT),A3,LAMN(3,MAT)
          ENDDO

C
C     BATCH INPUT USES FREE-FIELD FORMAT FOR READING GAGE DATA
C
      CALL READB(IN,IOUT,FILENAME,TITLES,NPT,DTS,TS,RS,TSHIFT,TOA)
      WRITE (IOUT,1110) FILENAME
      CALL READB(IN,IOUT,FILENAME,TITLE1,NPTE1,DTE1,TE1,RE1,TSHIFT,TOA)
      IF (DTE1 .NE. DTS) THEN
        WRITE (IOUT,9900) DTE1,DTS
9900      FORMAT('  ***** DTE1 & DTS ARE NOT THE SAME...DTE1 ='1PE11.3,
     1      '  DTS ='E11.3/'    >>>>>  STOP IN SUBROUTINE INPUT')
        STOP
      ENDIF
      WRITE (IOUT,1110) FILENAME
      CALL READB(IN,IOUT,FILENAME,TITLE1,NPTE2,DTE2,TE2,RE2,TSHIFT,TOA)
      IF (DTE2 .NE. DTS) THEN
        WRITE (IOUT,9905) DTE2,DTS
9905      FORMAT('  ***** DTE2 & DTS ARE NOT THE SAME...DTE2 ='1PE11.3,
     1      '  DTS ='E11.3/'    >>>>>  STOP IN SUBROUTINE INPUT')
        STOP
      ENDIF
      WRITE (IOUT,1110) FILENAME

C
C     SETUP DATA
C
200   K=0
      TMIN=MAX(TS(1),TE1(1))
      TMIN=MAX(TMIN,TE2(1))
      IF (ABS(TMIN-TS(1)) .LE. 1.E-4*DTS) THEN
        TMIN=TS(1)
        GO TO 210
      ELSE IF (ABS(TMIN-TE1(1)) .LE. 1.E-4*DTE1) THEN
        TMIN=TE1(1)
        GO TO 210
      ELSE IF (ABS(TMIN-TE2(1)) .LE. 1.E-4*DTE2) THEN
        TMIN=TE2(1)
```

```
      ENDIF
210   TMAX=MIN(TS(NPT),TE1(NPTE1))
      TMAX=MIN(TMAX,TE2(NPTE2))
      DO I=1,NPTE1
         IF (ABS(TE1(I)-TMAX) .LE. DTE1/2.) GO TO 220
      ENDDO
220   NPTE1=I
      DO I=1,NPTE2
         IF (ABS(TE2(I)-TMAX) .LE. DTE2/2.) GO TO 230
      ENDDO
230   NPTE2=I
      RETURN
900   WRITE (IOUT,9910) FILENAME
9910  FORMAT(' ***** ERROR IN OPENING FOR001, FILE 'A50)
      GO TO 990
910   WRITE (IOUT,9920) FILENAMEO
9920  FORMAT(' ***** ERROR IN OPENING FILE :'A50)
990   STOP
      END
```

```fortran
      SUBROUTINE READB(IN,IOUT,FILENAME,TITLE,NPT,DT,T,A,TSHIFT,TOA)
C
C     READ DATA FROM FOR001 WITH FREE-FIELD FORMAT
C     WRITE ERROR MESSAGE TO UNIT 'IOUT'
C
      IMPLICIT REAL*4 (A-H,O-Z)
      CHARACTER FILENAME*50, TITLE*80
      DIMENSION T(1),A(1)
C
      READ (IN,1010) FILENAME
1010  FORMAT(A50)
      OPEN (UNIT=1,FILE=FILENAME,STATUS='OLD',ERR=900)
      CALL RDFLATPK(1,TITLE,NPT,DT,T,A,TSHIFT,TOA)
      CLOSE (UNIT=1)
      RETURN
900   WRITE (IOUT,1100) FILENAME
1100  FORMAT(' *****  ERROR IN OPENING FILE :'A50
     1      /'               >>>>> STOP IN SUBROUTINE READB')
      STOP
      END
```

```
      SUBROUTINE RDFLATPK(IN,TITLE,NPT,DT,T,A,TSHIFT,TOA)
C
C     READ DATA WRITTEN IN FREE-FIELD FORMAT FROM FILE 'IN'
C        1. title
C        2. npt, dt, tshift, toa;   (DATA WILL BE SHIFTED BY T(1))
C        3. (a(i), i=1,npt)         (FREE-FIELD)
C
      IMPLICIT REAL*4 (A-H,O-Z)
      DIMENSION T(1),A(1)
      CHARACTER*80 TITLE
      TSHIFT=0.
      TOA=0.
      READ (IN,1030) TITLE
1030  FORMAT(A80)
      READ (IN,*) NPT, DT, TSHIFT, TOA
      READ (IN,*)  (A(I),I=1,NPT)
      DO I=1,NPT
        T(I)=(I-1)*DT + TSHIFT
      ENDDO
      RETURN
      END
```

```
      SUBROUTINE MATMPY(A,N,M,B,L,C)
C
C     MULTIPLIES MATRICES A BY B AND STORES IN C
C     A IS n X m
C     B IS m X l
C     C IS n X l
C
      IMPLICIT REAL*8 (A-H,O-Z)
      DIMENSION A(N,1),B(M,1),C(N,1)
      DO 10 I=1,N
        DO 10 J=1,L
          C(I,J)=0.
          DO 10 K=1,M
10        C(I,J)=C(I,J)+A(I,K)*B(K,J)
      RETURN
      END
```

```fortran
      SUBROUTINE MATRXM2(M,AK,G,H,AN,AM)
C
C     CALCULATE THE ELEMENTS OF M --  FOR PIEZOR3
C     NEW DEFINITION OF M MATRIX
C
      IMPLICIT REAL*8 (A-H,O-Z)
      DIMENSION AM(3,3,1)
      INTEGER COND

      AKP=AK+4.*G*AN/3.
      AKM=AK-2.*G*AN/3.
      DO I=1,3
        DO J=1,3
          IF (J .EQ. I) THEN
                AM(I,J,M) = AKP
          ELSE
                AM(I,J,M) = AKM
          ENDIF
        ENDDO
      ENDDO
      RETURN
      END
```

```fortran
      SUBROUTINE SIMQ(A,B,N,KS)
      IMPLICIT REAL*8 (A-H,O-Z)
      DIMENSION A(1),B(1)
C         FORWARD SOLUTION
      TOL=0.0
      KS=0
      JJ=-N
      DO 65 J=1,N
      JY=J+1
      JJ=JJ+N+1
      BIGA=0.
      IT=JJ-J
      DO 30 I=J,N
C         SEARCH FOR MAXIMUM COEFFICIENT IN COLUMN
      IJ=IT+I
      IF (ABS(BIGA)-ABS(A(IJ))) 20,30,30
   20 BIGA=A(IJ)
      IMAX=I
   30 CONTINUE
C         TEST FOR PIVOT LESS THAN TOLERANCE (SINGULAR MATRIX)
      IF (ABS(BIGA)-TOL) 35,35,40
   35 KS=1
      RETURN
C         INTERCHANGE ROWS IF NECESSARY
   40 I1=J+N*(J-2)
      IT=IMAX-J
      DO 50 K=J,N
      I1=I1+N
      I2=I1+IT
      SAVE=A(I1)
      A(I1)=A(I2)
      A(I2)=SAVE
C         DIVIDE EQUATION BY LEADING COEFFICIENT
   50 A(I1)=A(I1)/BIGA
      SAVE=B(IMAX)
      B(IMAX)=B(J)
      B(J)=SAVE/BIGA
C         ELIMINATE NEXT VARIABLE
      IF (J-N) 55,70,55
   55 IQS=N*(J-1)
      DO 65 IX=JY,N
      IXJ=IQS+IX
      IT=J-IX
      DO 60 JX=JY,N
      IXJX=N*(JX-1)+IX
      JJX=IXJX+IT
   60 A(IXJX)=A(IXJX)-(A(IXJ)*A(JJX))
   65 B(IX)=B(IX)-(B(J)*A(IXJ))
C         BACK SOLUTION
   70 NY=N-1
      IT=N*N
      DO 80 J=1,NY
      IA=IT-J
      IB=N-J
      IC=N
      DO 80 K=1,J
      B(IB)=B(IB)-A(IA)*B(IC)
      IA=IA-N
   80 IC=IC-1
```

```
RETURN
END
```

```fortran
      SUBROUTINE STRNHARD(M,NH,EPH,HH,MODELH,EBP,H)
C
C     CALCULATE H BASED ON MODELH
C
C     MODELH  =  0     FOR H = CONSTANT (INPUT)
C                1     FOR H AS A FUNCTION OF EPSBARP (TABLE OF INPUT VALUES)
C                      (H IS CONSTANT IN EACH EPSBARP INTERVAL)
C
      IMPLICIT REAL*8 (A-H,O-Z)
      DIMENSION EPH(50),HH(50)
      IF (MODELH .EQ. 0) RETURN
      IF (MODELH .EQ. 1) THEN
        DO I=1,NH
          IF (EBP .LE. 0.) RETURN
          IF (EBP .LE. EPH(I)) THEN
                H = HH(I)
                GO TO 100
          ENDIF
        ENDDO
        IF (EBP .GT. EPH(NH)) H=HH(NH)
      ENDIF
100   RETURN
      END
```

```
PLAS CELL - 3A - ETA(M) NOT 0,STRNHARDENING (NIKE DATA OF 6-91) ***PIEZOR3
MAT 1 = YTTERBIUM  MODELETA=        0 MODELH =        1
EM  =      120.0     ANU =        0.365  Y0Y =         0.49 HY =         0.
NH =              6
EBARP,H = 8.000E-04 2.125E+02 1.700E-03 1.2222E+2 3.000E-03 5.3846E+1
5.400E-03 1.875E+01 7.600E-03 9.0909E+0 1.330E-02 8.7719E-1
ALPHAY = -7.88E-03 BETAY =  -1.71E-02 ETA1Y =       1.13 ETA2Y =       0.
LAMN(1,1)          1. LAMN(2,2)         1. LAMN(3,3)        1.
MAT 2 = CONSTANTAN MODELETA=        0
EM  =     1484.4181 ANU =         0.33  Y0C =         8.2 HC =       409.
ALPHAC = -0.49E-04 BETAC =   1.89E-04 ETA1C =       0.0
LAMN(1,1)          1. LAMN(2,2)         1. LAMN(3,3)        1.
MAT 3 = CONSTANTAN MODELETA=        0
EM  =     1484.4181 ANU =         0.33  Y0C =         8.2 HC =       409.
ALPHAC = -0.49E-04 BETAC =   1.89E-04 ETA1C =       0.0
LAMN(1,1)          1. LAMN(2,2)         1. LAMN(3,3)        1.
YBPZ1.RES
C1PZ1.RES
C2PZ1.RES


YTTERBIUM CELL FOR PIEZOR TEST DR1/R0
    51      2.0000E-02      0.0000E+00      0.0000E+00
     0.0000E+00    2.0664E-02    4.1323E-02    6.5196E-02    9.2118E-02    1.2103E-01
     1.5244E-01    1.8552E-01    2.1967E-01    2.5490E-01    2.9013E-01    2.9228E-01
     2.9487E-01    2.9776E-01    3.0088E-01    3.0415E-01    3.0752E-01    3.1096E-01
     3.1444E-01    3.1795E-01    3.2147E-01    3.2609E-01    3.3071E-01    3.3533E-01
     3.3996E-01    3.4460E-01    3.4924E-01    3.5388E-01    3.5854E-01    3.6319E-01
     3.6785E-01    3.7252E-01    3.7719E-01    3.8187E-01    3.8656E-01    3.8986E-01
     3.9066E-01    3.9128E-01    3.9173E-01    3.9205E-01    3.9226E-01    3.8755E-01
     3.8284E-01    3.7813E-01    3.7344E-01    3.6874E-01    3.6405E-01    3.5937E-01
     3.5469E-01    3.5002E-01    3.4536E-01


CONSTANTAN CELL 1 FOR PIEZOR TEST DR1/R0
    51      2.0000E-02      0.0000E+00      0.0000E+00
     0.0000E+00    1.8270E-04    3.6546E-04    5.4803E-04    7.3067E-04    9.1319E-04
     1.0959E-03    1.2784E-03    1.4607E-03    1.6430E-03    1.8254E-03    3.8374E-03
     5.8483E-03    7.8579E-03    9.8663E-03    1.1864E-02    1.3856E-02    1.5844E-02
     1.7828E-02    1.9810E-02    2.1788E-02    1.9788E-02    1.7787E-02    1.5785E-02
     1.3781E-02    1.1776E-02    9.7702E-03    7.7629E-03    5.7544E-03    3.7446E-03
     1.7336E-03   -2.7880E-04   -2.2923E-03   -4.3070E-03   -6.2970E-03   -8.2017E-03
    -1.0117E-02   -1.2042E-02   -1.3976E-02   -1.5919E-02   -1.7869E-02   -1.5844E-02
    -1.3821E-02   -1.1799E-02   -9.7779E-03   -7.7582E-03   -5.7400E-03   -3.7232E-03
    -1.7074E-03    3.0706E-04    2.3202E-03


CONSTANTAN CELL 2 FOR PIEZOR TEST DR1/R0
    51      2.0000E-02      0.0000E+00      0.0000E+00
     0.0000E+00    1.8270E-04    3.6546E-04    5.4803E-04    7.3067E-04    9.1319E-04
     1.0959E-03    1.2784E-03    1.4607E-03    1.6430E-03    1.8254E-03    1.4155E-03
     1.0048E-03    5.9364E-04    1.8152E-04    2.1342E-05   -8.8538E-05   -1.9901E-04
    -3.1034E-04   -4.2254E-04   -5.3608E-04   -1.1747E-04    2.9986E-04    7.1637E-04
     1.1318E-03    1.5467E-03    1.9609E-03    2.3739E-03    2.7865E-03    3.1982E-03
     3.6091E-03    4.0189E-03    4.4282E-03    4.8367E-03    5.1757E-03    5.2616E-03
     5.3434E-03    5.4224E-03    5.4995E-03    5.5750E-03    5.6488E-03    5.2474E-03
     4.8449E-03    4.4418E-03    4.0381E-03    3.6327E-03    3.2272E-03    2.8206E-03
     2.4131E-03    2.0049E-03    1.5958E-03
```

```
1 DATE -15-JUL-91                                    BATCH JOB
PLAS CELL - 3A - ETA(M) NOT 0, STRNHARDENING (NIKE DATA OF 6-91) ***PIEZOR3
MAT 1 - YTTERBIUM MODELETA-     0 MODELH -     1
EM  -    1.200E+02 ANU -    3.650E-01 YOY -    4.900E-01 HY  -    0.000E+00
NH  -         6
EBARP,H - 8.000E-04 2.125E+02 1.700E-03 1.222E+02 3.000E-03 5.385E+01
5.400E-03 1.875E+01 7.600E-03 9.091E+00 1.330E-02 8.772E-01
ALPHAY -7.880E-03 BETAY -  -1.710E-02 ETA1Y -  1.130E+00 ETA2Y -  0.000E+00
AK  -    1.4815E+02  G -    4.3956E+01
LAMN(1,1) 1.000E+00 LAMN(2,2) 1.000E+00 LAMN(3,3) 1.000E+00
MAT 2 - CONSTANTAN MODELETA-      0
EM  -    1.484E+03 ANU -    3.300E-01 YOC -    8.200E+00 HC  -    4.090E+02
ALPHAC --4.900E-05 BETAC -  1.890E-04 ETA1C -  0.000E+00         0.000E+00
AK  -    1.4553E+03  G -    5.5805E+02
LAMN(1,1) 1.000E+00 LAMN(2,2) 1.000E+00 LAMN(3,3) 1.000E+00
MAT 3 - CONSTANTAN MODELETA-      0
EM  -    1.484E+03 ANU -    3.300E-01 YOC -    8.200E+00 HC  -    4.090E+02
ALPHAC --4.900E-05 BETAC -  1.890E-04 ETA1C -  0.000E+00         0.000E+00
AK  -    1.4553E+03  G -    5.5805E+02
LAMN(1,1) 1.000E+00 LAMN(2,2) 1.000E+00 LAMN(3,3) 1.000E+00
YBPZ1.RES
C1PZ1.RES
C2PZ1.RES
```

SAMPLE OUTPUT DATA

```
1 PLAS CELL - 3A - ETA(M) NOT 0,STRNHARDENING (NIKE DATA OF 6-91) ***PIEZOR3

                    MATERIAL 1 - YTTERBIUM
```

I	TIME	S(3)	EPS(1)	EPS(2)	EPS(3)	S(1)	S(2)	EPS[3]	P	SBAR	YIELD C	EPSBARP
1	0.000E+00	0.000E+00	0.000E+00	0.000E+00	0.000E+00	0.000E+00	0.000E+00	0.000E+00	0.000E+00	0.000E+00	4.900E-01	0.000E+00
2	2.000E-02	-4.988E-01	1.700E-07	1.700E-07	-2.412E-03	-2.867E-01	-2.867E-01	-2.412E-03	-3.574E-01	2.121E-01	4.900E-01	0.000E+00
3	4.000E-02	-9.974E-01	4.021E-07	4.021E-07	-4.825E-03	-5.732E-01	-5.732E-01	-4.825E-03	-7.146E-01	4.242E-01	4.900E-01	0.000E+00
4	4.548E-02	-1.154E+00	-4.194E-06	-4.194E-06	-5.578E-03	-6.643E-01	-6.643E-01	-5.578E-03	-8.276E-01	4.900E-01	4.900E-01	0.000E+00
5	6.000E-02	-1.498E+00	5.998E-08	5.998E-08	-7.449E-03	-9.063E-01	-9.063E-01	-7.449E-03	-1.104E+00	5.917E-01	5.917E-01	4.788E-04
6	8.000E-02	-2.031E+00	-7.540E-06	-7.540E-06	-1.033E-02	-1.283E+00	-1.283E+00	-1.033E-02	-1.532E+00	7.475E-01	7.475E-01	1.212E-03
7	1.000E-01	-2.563E+00	-1.520E-05	-1.520E-05	-1.334E-02	-1.689E+00	-1.689E+00	-1.334E-02	-1.980E+00	8.744E-01	8.744E-01	2.250E-03
8	1.200E-01	-3.086E+00	-2.036E-05	-2.036E-05	-1.649E-02	-2.131E+00	-2.131E+00	-1.649E-02	-2.449E+00	9.547E-01	9.547E-01	3.741E-03
9	1.400E-01	-3.587E+00	-2.096E-05	-2.096E-05	-1.972E-02	-2.597E+00	-2.597E+00	-1.972E-02	-2.927E+00	9.900E-01	9.547E-01	5.623E-03
10	1.600E-01	-4.088E+00	-2.143E-05	-2.143E-05	-2.301E-02	-3.079E+00	-3.079E+00	-2.301E-02	-3.415E+00	1.009E+00	1.009E+00	7.677E-03
11	1.800E-01	-4.587E+00	-2.165E-05	-2.165E-05	-2.637E-02	-3.576E+00	-3.576E+00	-2.637E-02	-3.913E+00	1.011E+00	1.011E+00	9.903E-03
12	2.000E-01	-5.086E+00	-2.181E-05	-2.181E-05	-2.973E-02	-4.074E+00	-4.074E+00	-2.973E-02	-4.411E+00	1.013E+00	1.013E+00	1.213E-02
13	2.200E-01	-5.086E+00	9.771E-04	-2.286E-05	-3.074E-02	-4.036E+00	-4.036E+00	-3.074E-02	-4.412E+00	1.013E+00	1.013E+00	1.314E-02
14	2.400E-01	-5.087E+00	1.975E-03	-2.455E-05	-3.176E-02	-4.008E+00	-4.008E+00	-3.176E-02	-4.416E+00	1.014E+00	1.014E+00	1.420E-02
15	2.600E-01	-5.087E+00	2.973E-03	-2.661E-05	-3.279E-02	-3.985E+00	-3.985E+00	-3.279E-02	-4.421E+00	1.015E+00	1.015E+00	1.529E-02
16	2.800E-01	-5.088E+00	3.970E-03	-2.932E-05	-3.382E-02	-3.968E+00	-3.968E+00	-3.382E-02	-4.427E+00	1.016E+00	1.016E+00	1.639E-02
17	2.833E-01	-4.959E+00	4.166E-03	2.079E-05	-3.386E-02	-4.001E+00	-4.001E+00	-3.386E-02	-4.395E+00	8.682E-01	1.016E+00	1.639E-02
18	3.000E-01	-5.109E+00	4.960E-03	-3.714E-05	-3.500E-02	-3.980E+00	-3.980E+00	-3.500E-02	-4.457E+00	1.013E+00	1.016E+00	1.639E-02
19	3.003E-01	-5.112E+00	4.976E-03	-3.790E-05	-3.503E-02	-3.979E+00	-3.979E+00	-3.503E-02	-4.458E+00	1.016E+00	1.016E+00	1.639E-02
20	3.200E-01	-5.113E+00	5.954E-03	-4.294E-05	-3.604E-02	-3.969E+00	-3.969E+00	-3.604E-02	-4.464E+00	1.017E+00	1.017E+00	1.750E-02
21	3.400E-01	-5.113E+00	6.947E-03	-4.884E-05	-3.706E-02	-3.961E+00	-3.961E+00	-3.706E-02	-4.469E+00	1.018E+00	1.018E+00	1.863E-02
22	3.600E-01	-5.113E+00	7.939E-03	-5.554E-05	-3.808E-02	-3.954E+00	-3.954E+00	-3.808E-02	-4.474E+00	1.019E+00	1.019E+00	1.977E-02
23	3.800E-01	-5.113E+00	8.931E-03	-6.297E-05	-3.910E-02	-3.949E+00	-3.949E+00	-3.910E-02	-4.479E+00	1.020E+00	1.020E+00	2.091E-02
24	4.000E-01	-5.113E+00	9.921E-03	-7.133E-05	-4.011E-02	-3.944E+00	-3.944E+00	-4.011E-02	-4.483E+00	1.021E+00	1.021E+00	2.204E-02
25	4.200E-01	-5.113E+00	8.929E-03	-6.470E-05	-3.955E-02	-4.081E+00	-4.081E+00	-3.955E-02	-4.546E+00	9.071E-01	1.021E+00	2.204E-02
26	4.400E-01	-5.114E+00	7.937E-03	-5.880E-05	-3.842E-02	-4.219E+00	-4.219E+00	-3.842E-02	-4.608E+00	7.946E-01	1.021E+00	2.204E-02
27	4.600E-01	-5.114E+00	6.944E-03	-5.341E-05	-3.785E-02	-4.356E+00	-4.356E+00	-3.785E-02	-4.671E+00	6.845E-01	1.021E+00	2.204E-02
28	4.800E-01	-5.115E+00	5.949E-03	-4.880E-05	-3.729E-02	-4.494E+00	-4.494E+00	-3.729E-02	-4.734E+00	5.784E-01	1.021E+00	2.204E-02
29	5.000E-01	-5.116E+00	4.954E-03	-4.460E-05	-3.672E-02	-4.632E+00	-4.632E+00	-3.729E-02	-4.797E+00	4.789E-01	1.021E+00	2.204E-02
30	5.200E-01	-5.116E+00	3.959E-03	-4.082E-05	-3.672E-02	-4.770E+00	-4.770E+00	-3.672E-02	-4.860E+00	3.913E-01	1.021E+00	2.204E-02

B-25

INTENTIONALLY LEFT BLANK.

APPENDIX C

EXPLOSIVE BLAST CALCULATIONS

The L2D two-dimensional finite-difference code* was used to perform two calculations to help in understanding our preliminary experiments, Tests 2 and 3 (see Appendix D) and to help design later experiments. The mesh layout for these calculations is shown in Figure C-1. The steel was modeled as elastic perfectly plastic with a flow stress of 10 kbar (1 GPa). A planar interface was prescribed within the steel target at the 1.27-cm depth, corresponding to the location of the epoxy layer in Test 2. In the first calculation, no slip was allowed at the interface; in the second calculation, the interface was allowed to slip without friction. These conditions bound the in-plane properties of the epoxy layer; however, the effect of the finite thickness of the epoxy on stresses and displacements in the axial direction were not modeled in the calculations. The no-slip interface calculation also represents the geometry of Test 3 with the omission of the steel and epoxy strips comprising the flatpack gages.

Figures C-2 through C-4 show the normal stresses and in-plane strains calculated at the surface and at the interface for the no-slip condition. Except for the peaks, the calculated surface and interface stresses at r = 2.54 cm are very much alike, suggesting that a gage placed at a non-slipping interface 1.27-cm below the loaded surface should provide a reasonably accurate measurement of the surface load. These calculated stresses also resemble the manganin element records from those tests in that the pulse duration is about 25 μs and the peak stress at the surface is greater than at the interface. However, both calculated peaks are considerably lower than the (approximate) measurements.

The calculated stresses at r = 5.08 cm are also similar to each other, and the ~1.5 kbar magnitude is consistent with the interpretation of the manganin and strain-gage records.

The strains from the no-slip calculation, shown in Figures C-3 and C-4, are very different from the strain gage records. First, the overall levels of strain are about an order of magnitude lower than those indicated by the strain gages. Second, the large oscillations in the measurements are not predicted in the calculations.

Figure C-5 shows that allowing frictionless sliding at the interface has little effect on the predicted stresses at the interface. Figures C-6 and C-7 show that the sliding interface condition does change the sense of the strains at the interface (strains in the cylinder at the interface boundary), but the strain levels are unchanged and bear little resemblance to the strain-gage records.

The probable cause for the general lack of resemblance between the calculated and measured strains is that the finite thickness of the epoxy layer was not included in the calculation.
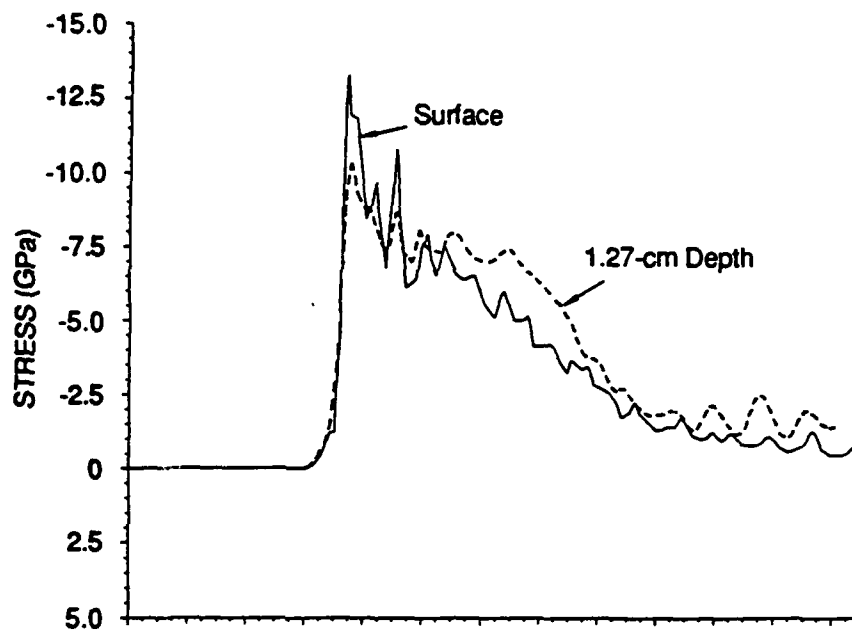

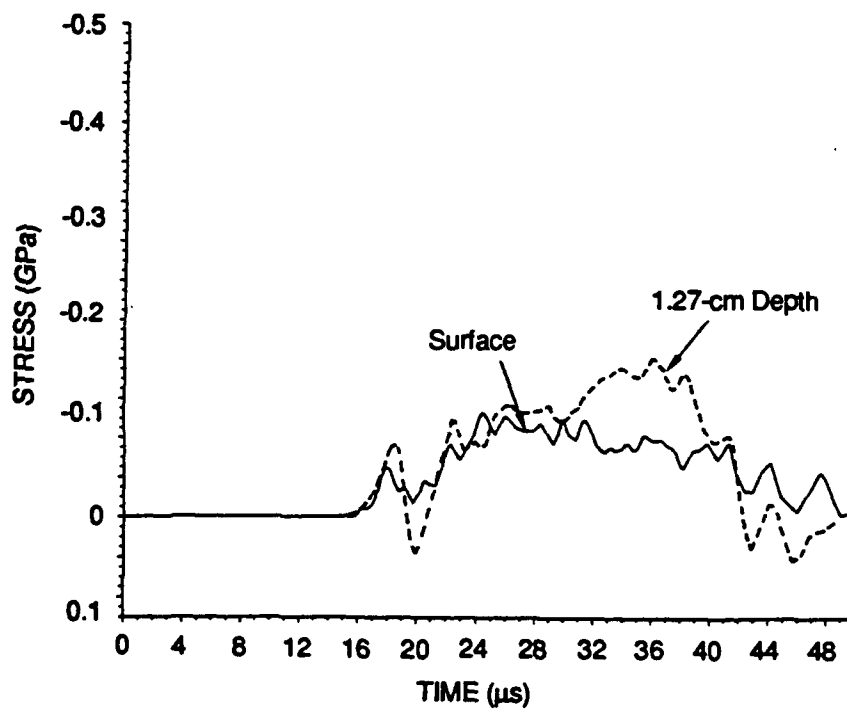*T. Cooper, "Users Manual for SWE2D," Swedish Detonic Research Foundation, Report DS 1982:14 (1982).
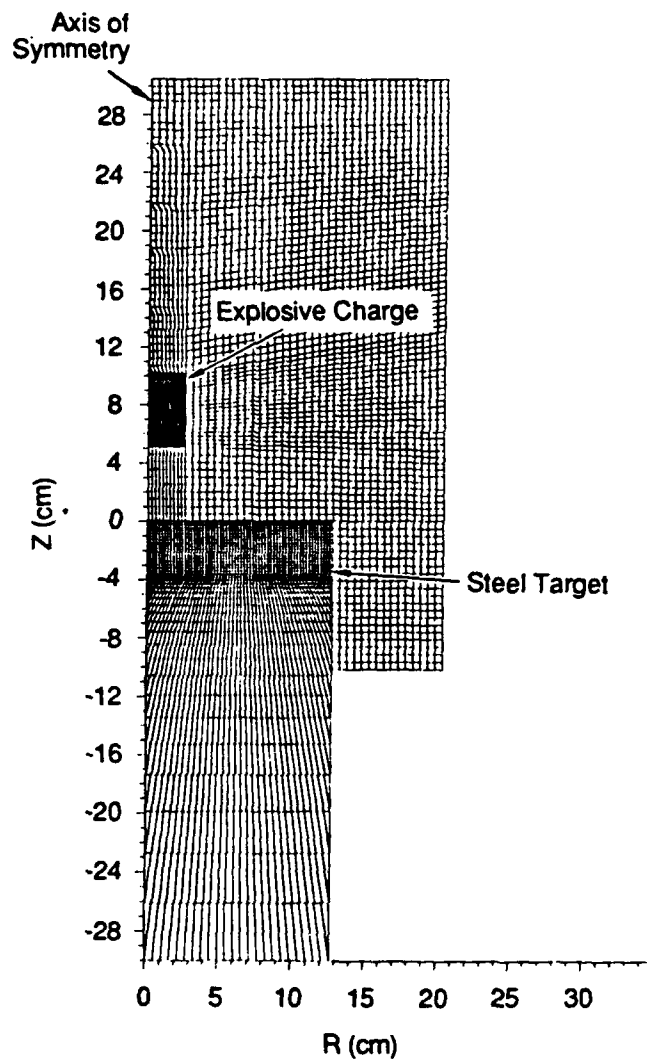
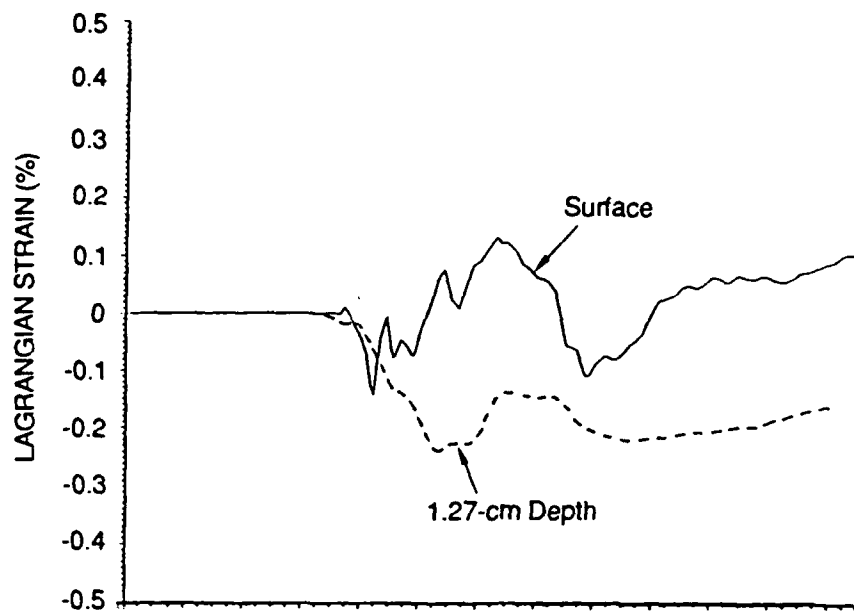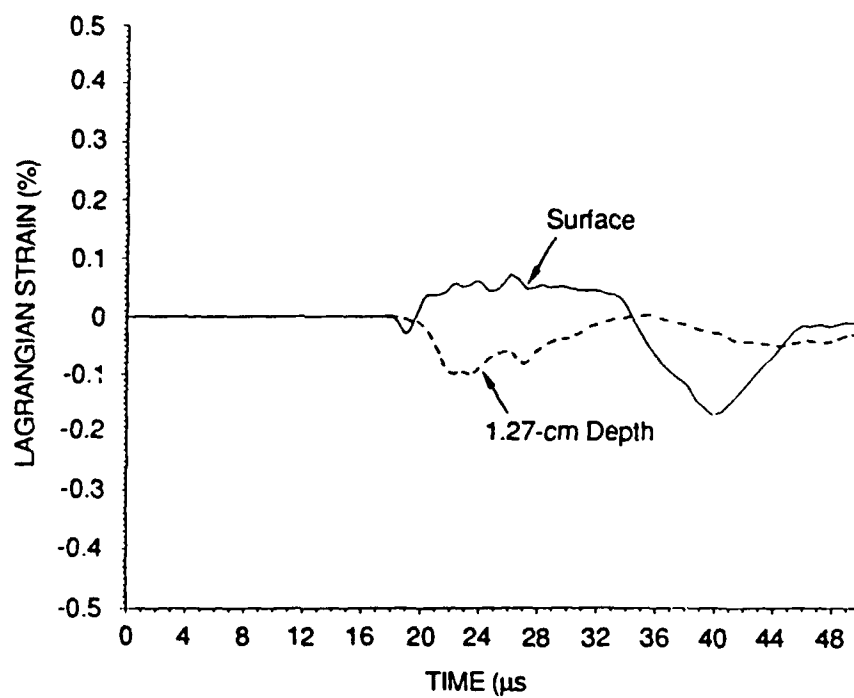Figure C-1. Initial mesh in finite-difference calculations of Tests 2 and 3.

Figure C-2.   Calculated normal stresses with no slip at the interface.
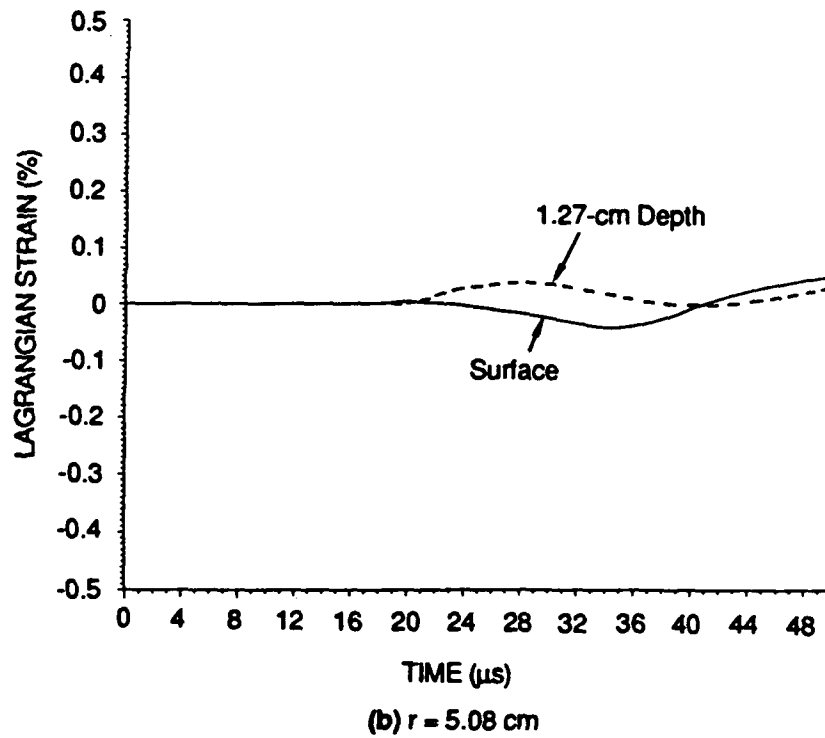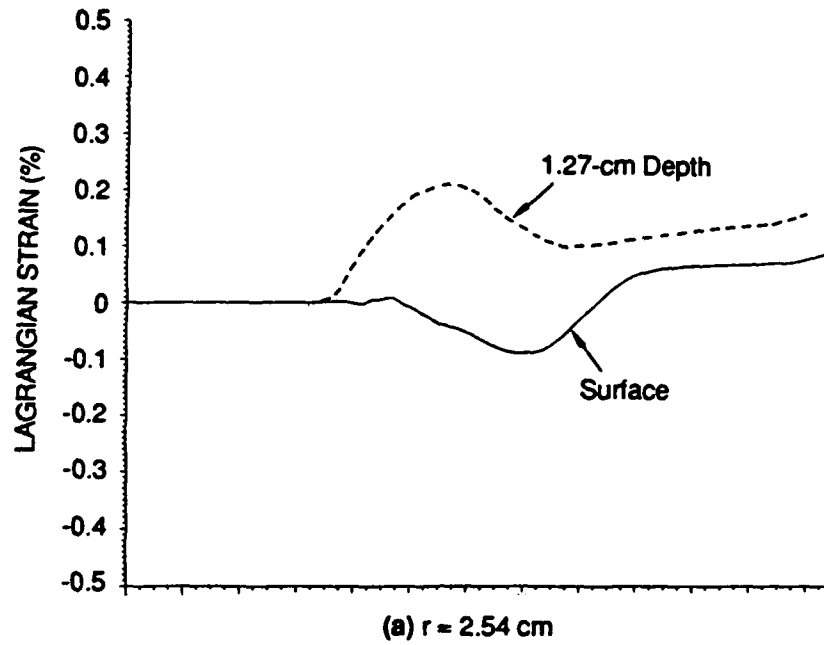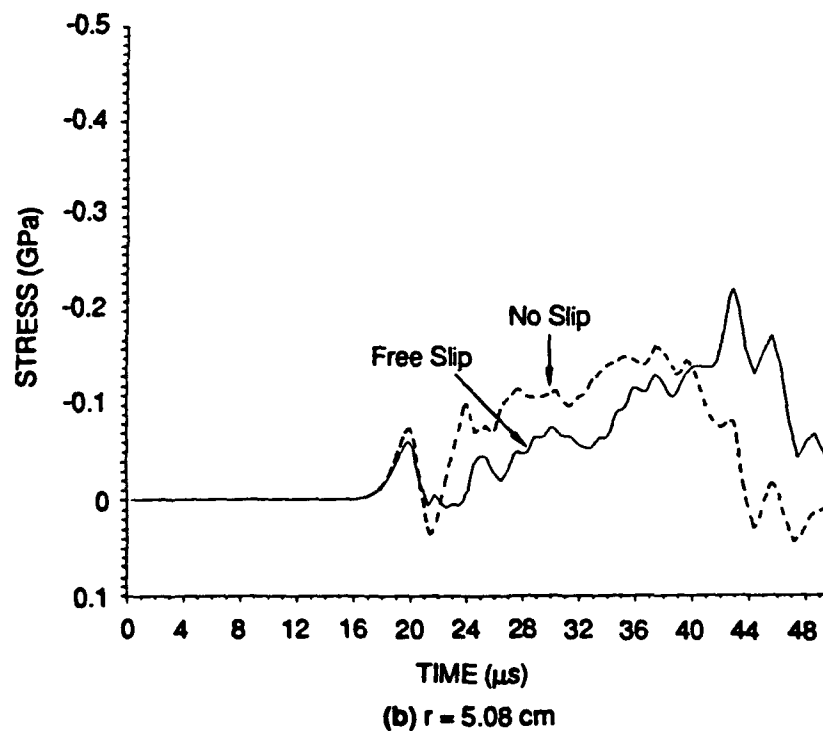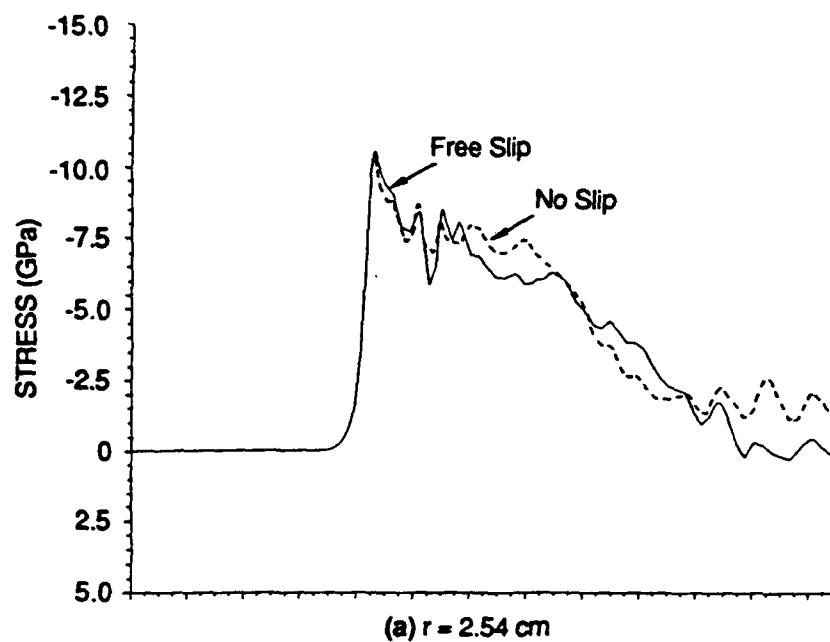
(a) r = 2.54 cm

(b) r = 5.08 cm

RA-7422-22

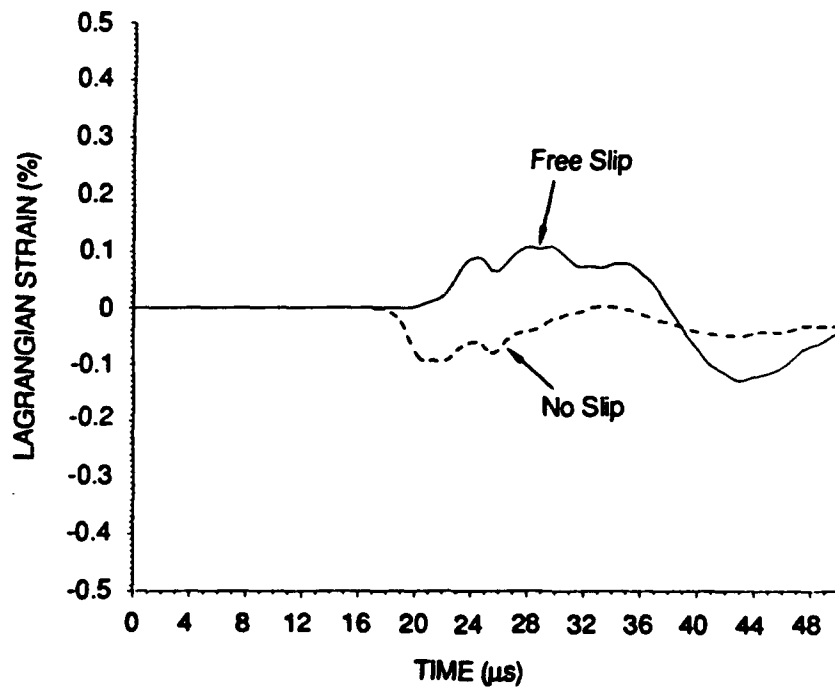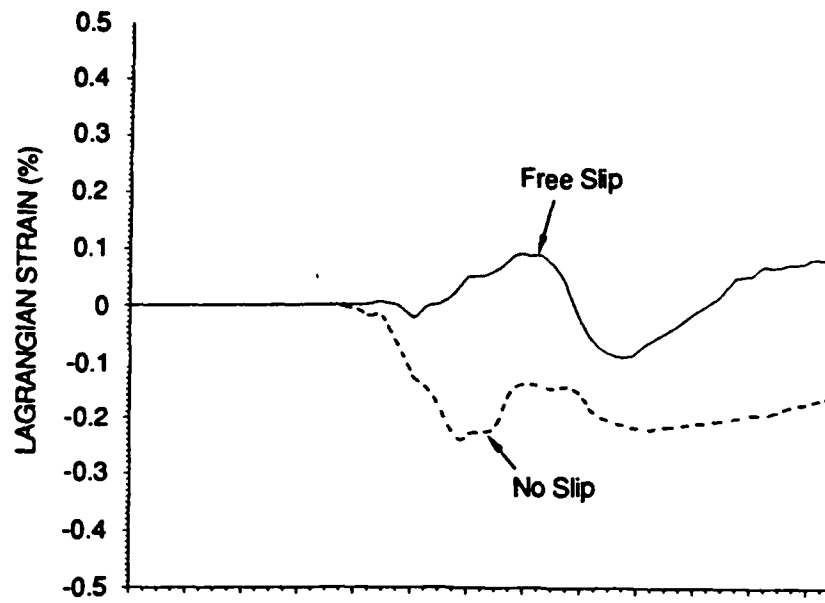Figure C-3. Calculated radial strains with no slip at the interface.

Figure C-4. Calculated circumferential strains with no slip at the interface.

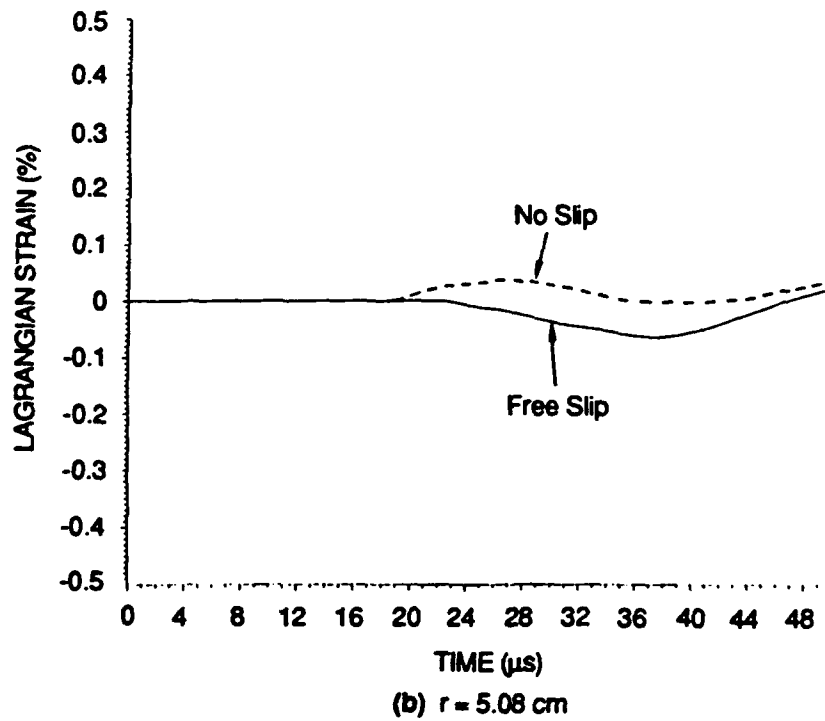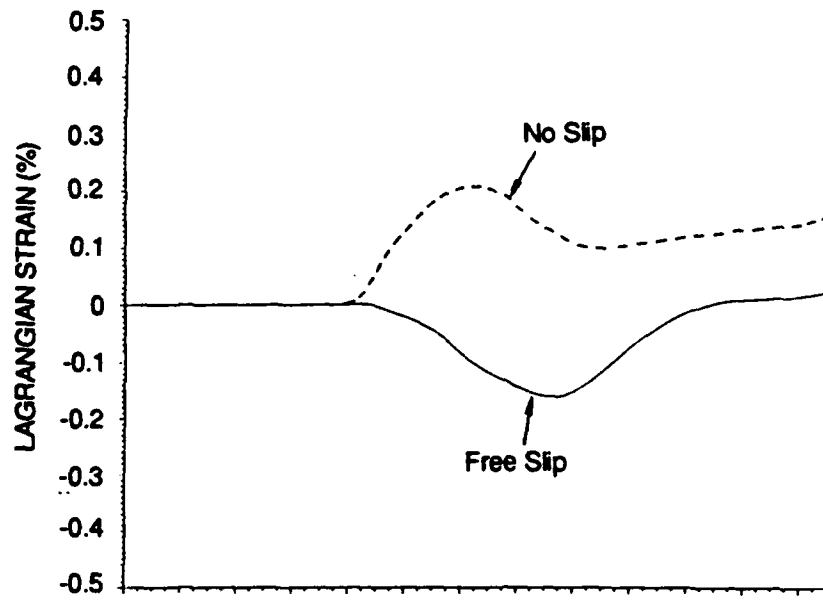Figure C-5. Calculated normal stresses at the interface (1.27-cm depth).

RA-7422-24

Figure C-6.   Calculated radial strains at the interface (1.27-cm depth).

Figure C-7. Calculated circumferential strains at the interface (1.27-cm depth).

APPENDIX D

PRELIMINARY EXPERIMENTS

The design of the flatpack evolved during the project, as directed by developmental experiments and design calculations. The developmental experiments are described in this Appendix. The steel case of the initial flatpack design (used in Tests 3 through 5) was simply two flat strips, without a cavity in the base. The Kapton/element sandwich was bonded to the base, and the cover and base were welded together. The lack of lateral confinement for the elements in this design led to measured in-plane strains as large as 4%. Larger elements (~6-mm square) were also used initially, limiting the spatial resolution of the gage. Further modifications intended to increase the frequency response of the flatpack were attempted with partial success in Test 6. These are described in Section 4.
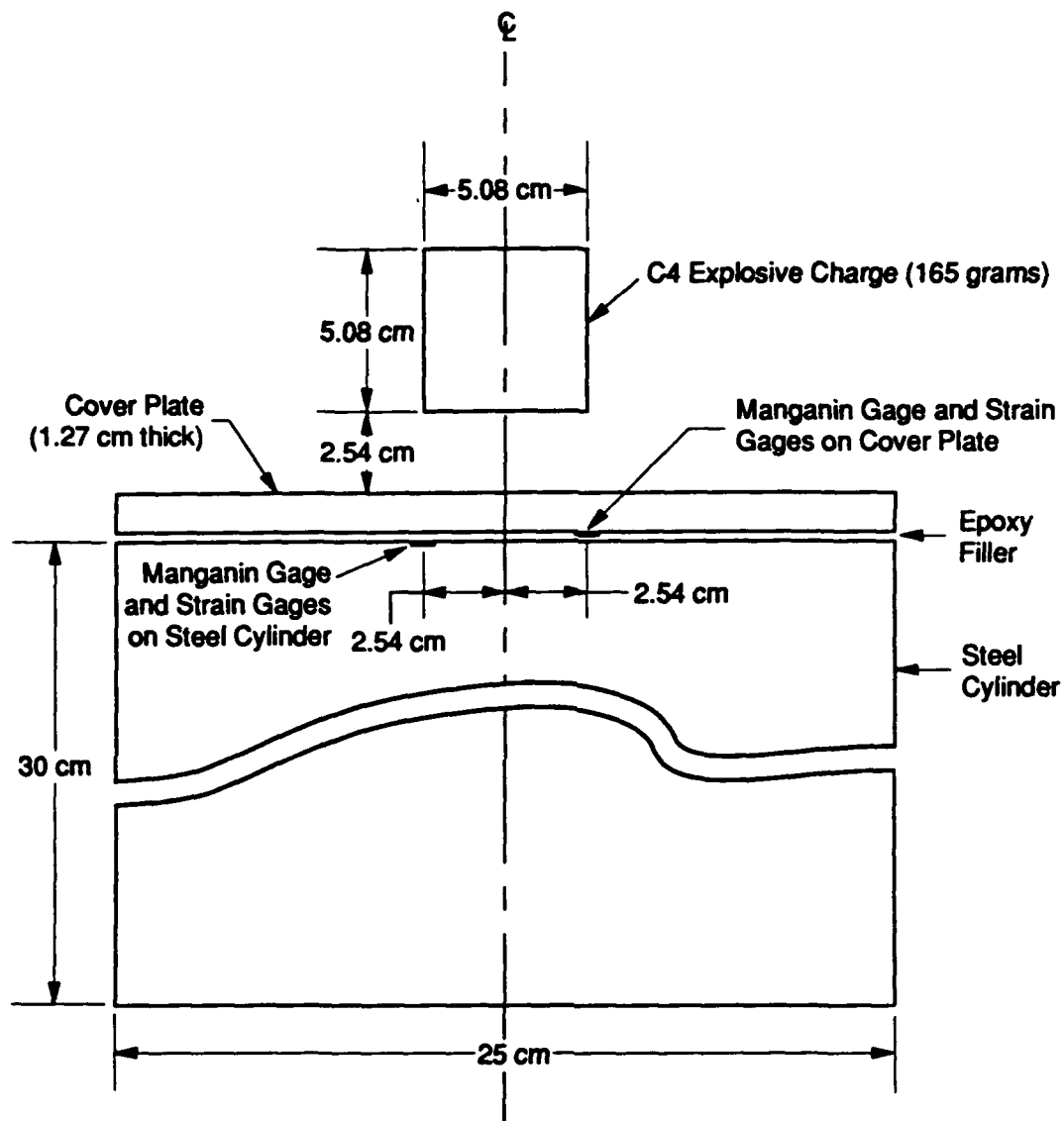
TEST 1

Figure D-1 shows a sketch of the hardware we used in our first experiment. The 4340 alloy steel (R_c 38) cover plate was 1.27 cm thick. We placed two sets of manganin elements and strain-gage elements between the steel cover plate and the steel cylinder to measure axial stress and radial and circumferential strain. One set of gages was bonded to the cover plate and one set was bonded to the cylinder, both located at a 2.54-cm radius. The space between the plate and cylinder was filled with 0.33 mm of epoxy. The explosive charge was a 5.08-cm-diameter, 5.08-cm-tall cylinder of C4, at a standoff distance of 2.54 cm. The charge was initiated at the center of the top surface.

In this experiment, large deformations were produced in both the plate and the cylinder, and the stress and strain gage elements were severely deformed. A 5-cm-diameter depression was made in both the plate and the cylinder. The depression on the top of the plate was about 0.07-cm deep, and the depression on the top of the cylinder was about 0.03-cm deep. The stress and strain elements on the plate were destroyed shortly after the arrival of the stress wave and provided no useful records. The gages on the cylinder survived, but the strain records went off-scale of the oscilloscopes. Manganin gage records were obtained, but were severely perturbed by the local strain.

TESTS 2 AND 3

The configurations for Tests 2 and 3 are shown in Figures D-2 and D-3, respecively. The objective of the tests was to obtain approximate measurements of the normal stresses and in-plane strains in these geometries to guide the design of future gage packages. In both tests, manganin and constantan elements were used. In Test 2 the gage elements were placed between the cylinder and the cover plate (Figure D-1); in Test 3 the elements were packaged in flatpacks, which were cemented to the top of the target cylinder (Figure D-3). The target cylinder and cover plate were made of 4340 alloy steel heat treated to a hardness of R_c37 and ground flat and parallel. In both tests the explosive charge was a 5.08-cm-diameter, 5.08-cm-tall cylinder of C4 explosive (165 grams), placed over the center of the target with a 5.08-cm standoff.
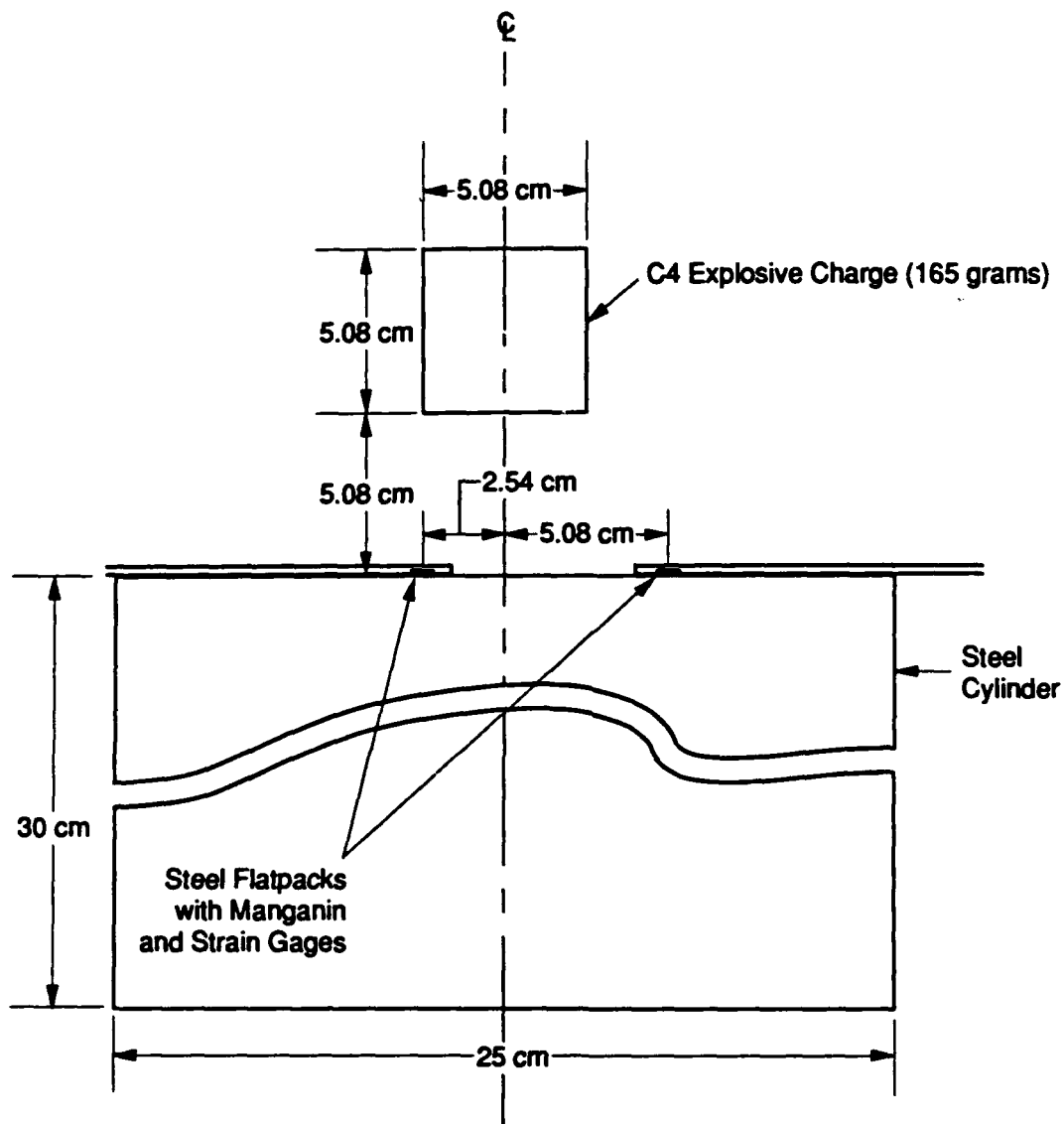
Figure D-1. Configuration for Test 1.
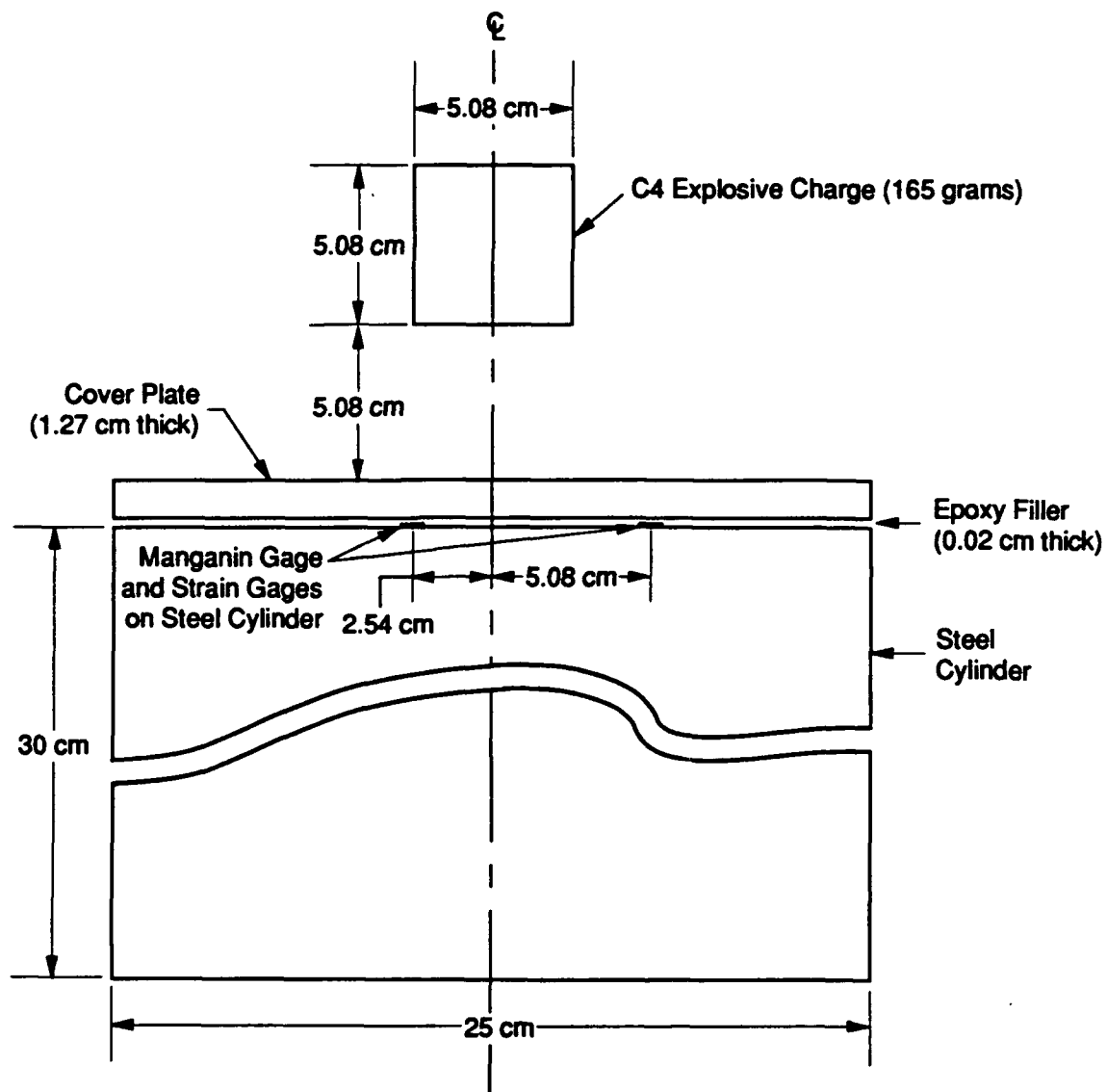
RM-7422-15A

Figure D-2. Configuration for Test 2.

RM-7422-15C

Figure D-3.   Configuration for Test 3.

RM-7422-15D

The manganin elements were Micromeasurements VM-SS-210AW-048 stress gages whose active grid dimensions are approximately 5.3 by 6.3 mm. The constantan elements were Micromeasurements CEA-06-250UT-350 strain gages, whose active grid dimensions are approximately 6.3 by 7.3 mm. In Test 2, sets of elements comprising one manganin stress gage and two strain gages were placed on the top surface of the steel cylinder (beneath the steel cover plate) at 2.54- and 5.08-cm radii. In each gage set, the gridlines of the stress gage and one of the strain gages were oriented in the radial direction; the gridlines of the other strain gage were oriented in the circumferential direction. The 1.27-cm-thick cover plate was bonded to the cylinder with a 0.2-mm-thick layer of Hysol epoxy. The flatpacks used in Test 3 were sandwiches comprising two pieces of 25-mm-wide by 1.2-mm-thick stainless steel with a 0.2-mm-thick by 12-mm-wide epoxy-filled cavity between them in which one stress gage and one strain gage were mounted side by side. The two flatpacks were bonded to the steel cylinder with epoxy, with the elements positioned at 2.54- and 5.08-cm radii and oriented in the radial direction.

The gage records are plotted in Figures D-4 through D-7. The solid curves are from Test 2; the dashed curves are from Test 3. The records from Test 3 have been shifted by 4 μs to match the times of arrival from Test 2. The left ordinate scale is resistance change; the right ordinate scale is approximate stress or strain. The latter are approximate because they do not account for the effects of in-plane strain on the manganin elements or the effects of normal stress on the constantan (strain gage) elements.

Figure D-4 shows that the manganin element records from the 2.54-cm radius in the two tests are very similar in shape and duration, but the initial peak registered in the flatpack at the top surface of the target was not registered under the 1.27-cm-thick cover plate. (This difference is qualitatively consistent with the computational results described below.) There is also a small amount of hysteresis in both elements; only slight additional resistance change occurred after the time shown in the plot. In general, these records are encouraging: the elements survived and provided clean records and there do not appear to have been large perturbations from in-plane strains.

The manganin records from the 5.08-cm radius, shown in Figure D-5, suggest a much different environment. The negative sense of these records implies that the effects of in-plane strain overwhelmed the normal stress signals because it is unreasonable to expect tensile stresses at these locations (compressive stress is positive in these figures). This result suggests that elements made of ytterbium , which is much more sensitive to normal stress than manganin, could be required at this radius. Another observation is that the two signals in Figure D-5 are very similar in rise time and magnitude, showing differences primarily in frequency content. The record from Test 3 goes off scale due to gage or lead failure.

The constantan strain gage records are shown in Figures D-6 and D-7. Records from the elements oriented in the radial direction in Test 2 are not shown because both elements failed at the time of arrival of the first stress wave. All the other records indicate that strains of 1% or greater were registered at both locations and in both the radial and circumferential directions. This level of strain would perturb the signals from the manganin gages by the equivalent of a few kbar. The strain-gage records also contain a strong oscillatory component with a period of 3 to 5 μs. In Test 2 the oscillations could be associated with wave reverberations in the 1.27-cm-thick cover plate, but in Test 3 there is no obvious source because the cover plate was not used.

As a check on the consistency of the measurements, we can compare the manganin records from the 5.08-cm radius (Figure D-5), which were apparently produced primarily by strain, with the record from the radially oriented strain gage at the same location in Test 3 (Figure D-7). The strain of approximately -0.5% indicated by the strain gage at 30 μs would produce a resistance
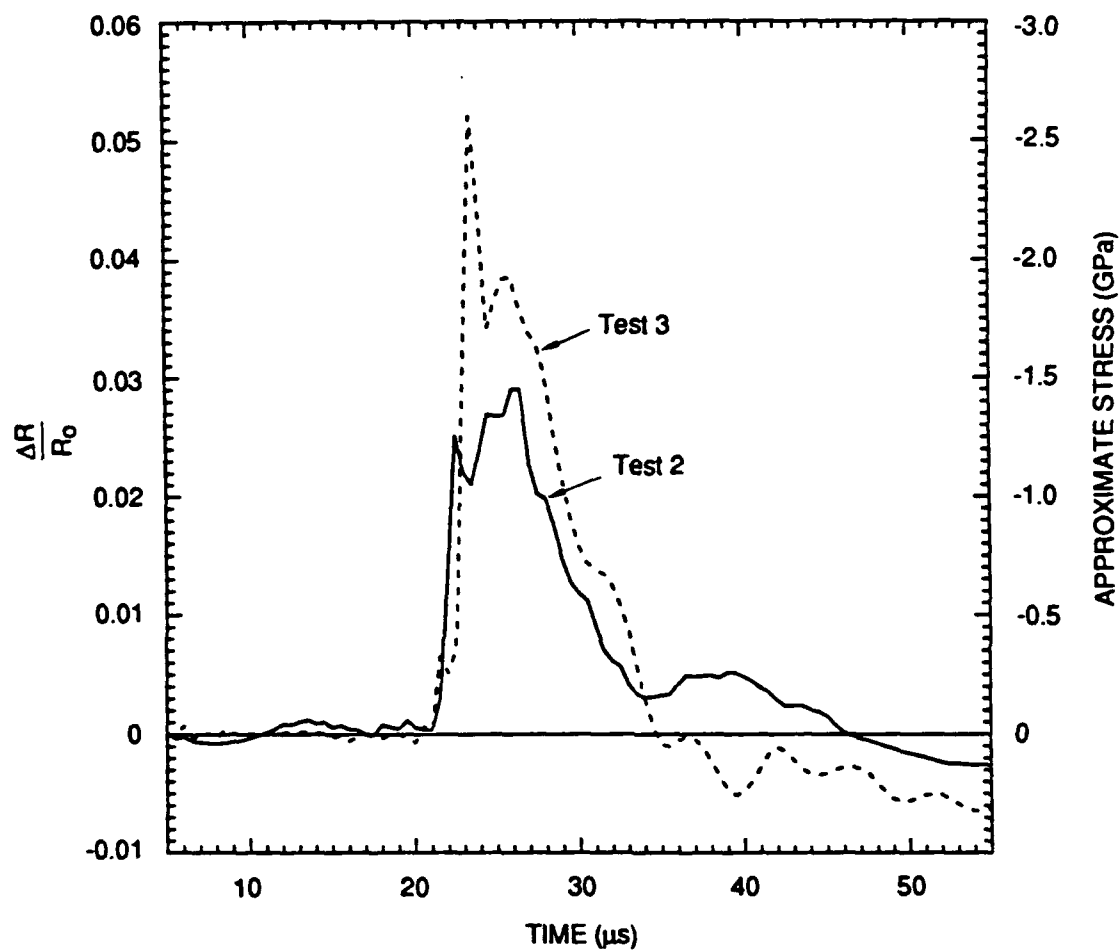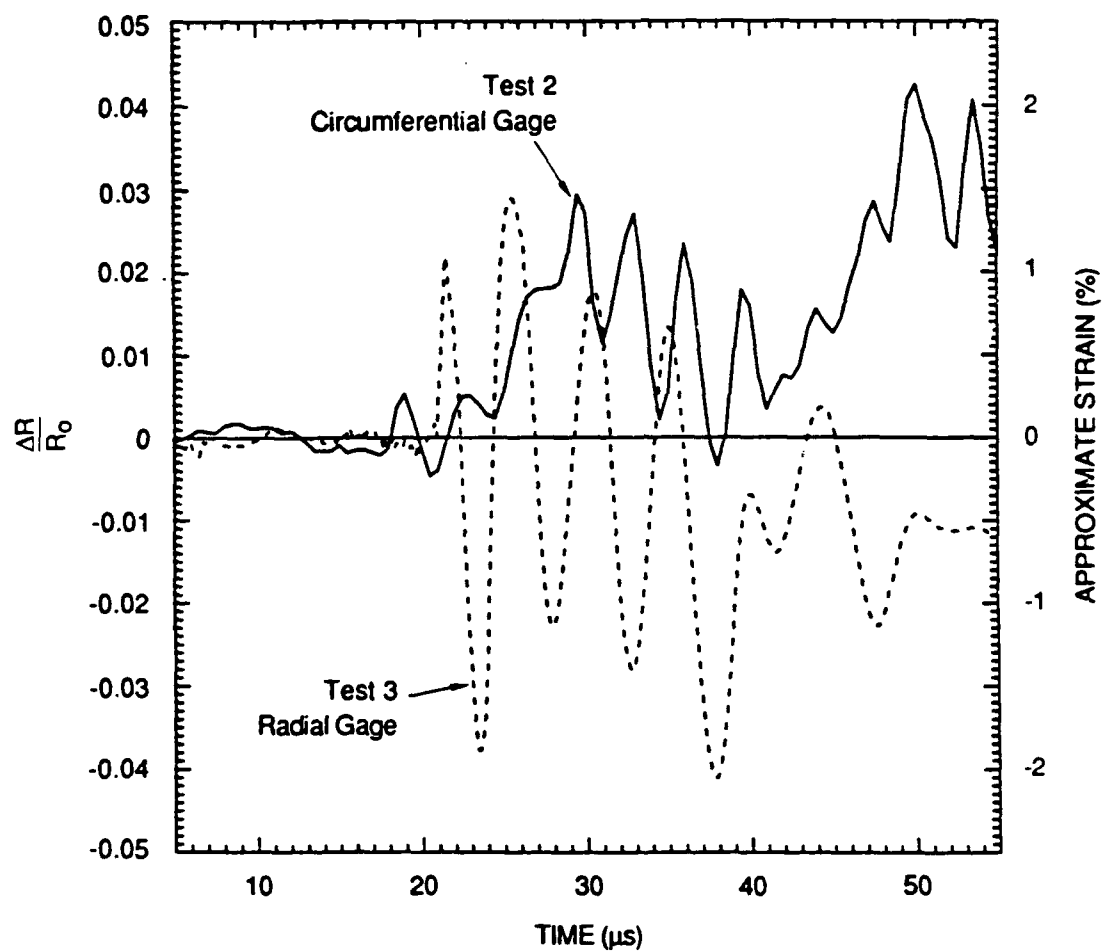
RA-7422-16A

Figure D-4. Manganin records at 2.54-cm radius in Tests 2 and 3.
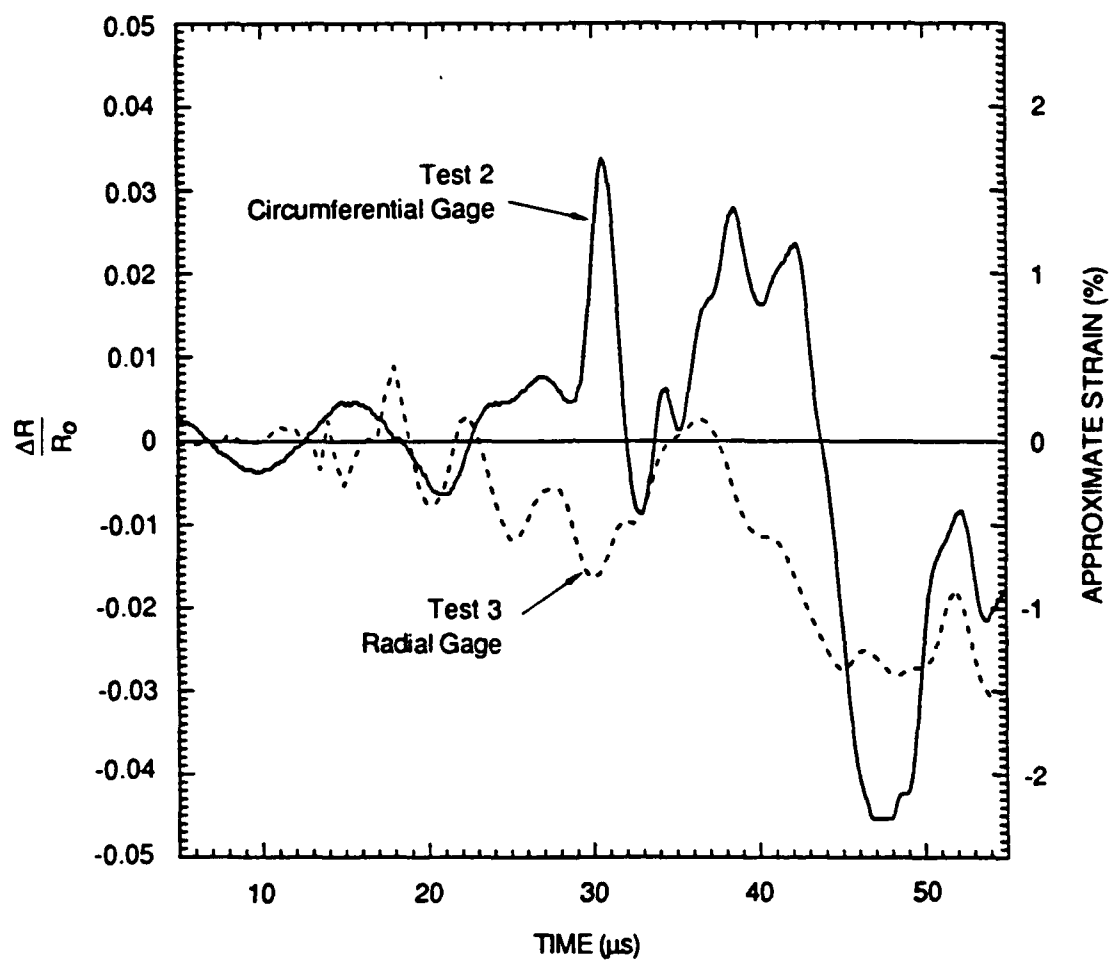
(Compressive stress is negative.)
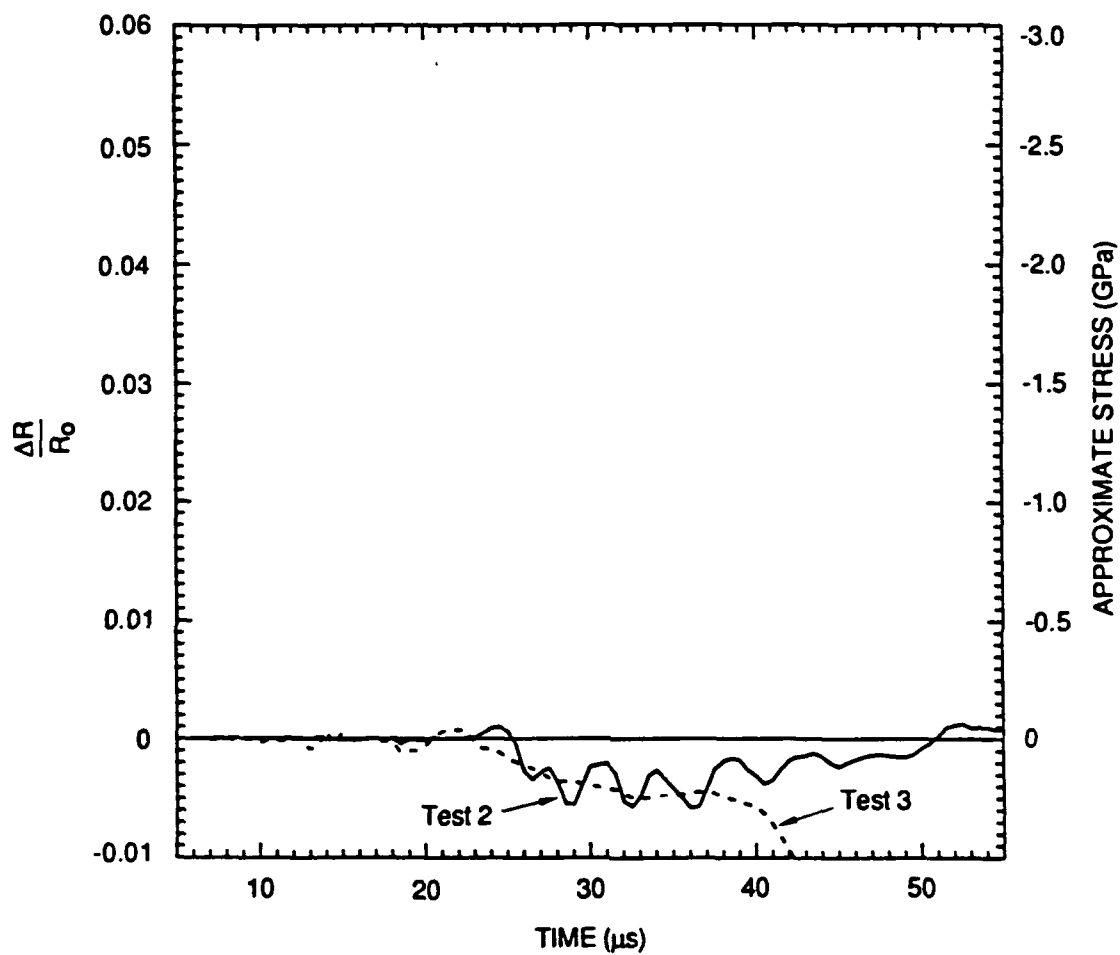
RA-7422-18A

Figure D-5. Manganin records at 5.08-cm radius in Tests 2 and 3.

(Compressive stress is negative.)

Figure D-6.   Strain-gage records at 2.54-cm radius in Tests 2 and 3.
(Tensile strain is positive.)

RA-7422-17

RA-7422-19

Figure D-7. Strain-gage records at 5.08-cm radius in Tests 2 and 3.
(Tensile strain is positive.)

change in the manganin elements of about -0.7%. The manganin records indicate a resistance change of about -0.4% at 30 μs, which leaves a difference of -0.3%. This difference corresponds to a stress of approximately 1.5 kbar (0.15 GPa), which is consistent with the calculated environment (see Appendix C).

The PIEZOR algorithm was used to interpret the measurements the two-element flatpack used in Test 3 even though the transverse strain was not measured. These measurements are shown in Figure D-8. For this exercise we *assumed* that the transverse strain was zero. (In fact, the transverse strain gages in Test 5 indicate that the transverse strain in the flatpack is comparable to the longitudinal strain, but the transverse strain may be very weakly coupled to the longitudinal elements.) As shown in Figure D-8, the stress history computed with this assumption is very oscillatory. The source of these oscillations could be reverberations in the flatpack,although one would then expect them to be more apparent in the manganin resistance history. The oscillations could also be an artifact of the assumption made in reducing the data that the transverse strain is zero, in which case the effect of the actual transverse strain could be to compensate for the oscillations introduced by the longitudinal strain.
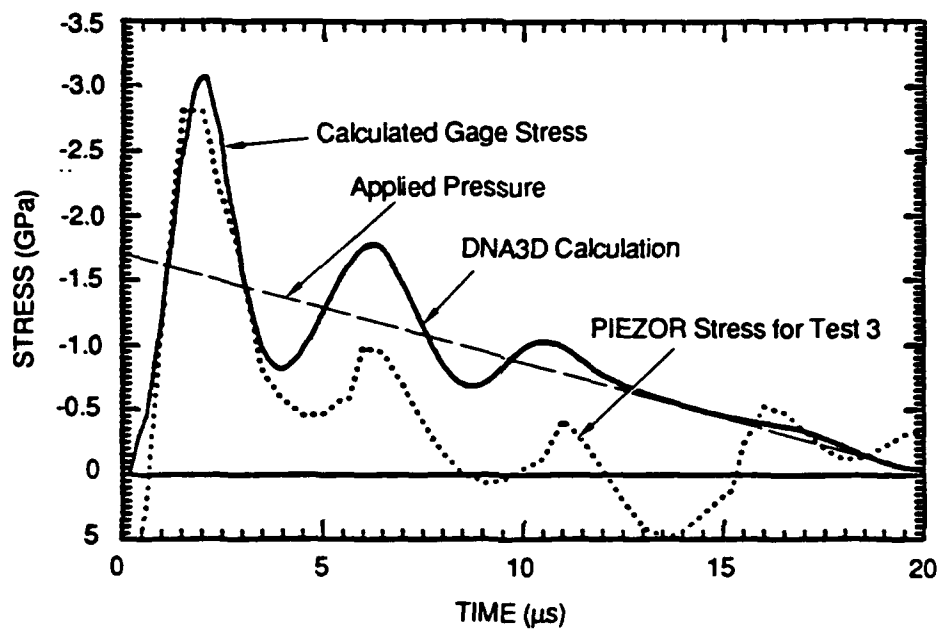
TEST 4

The purpose of Test 4 was to determine if the large-amplitude (±2%), high-frequency (200 - 300 kHz) oscillations in the strain-gage resistance histories in Tests 2 and 3 could have been produced artificially by the signal-conditioning equipment whose linear response is limited to about 100 kHz. As shown in Figure D-9, the configuration of Test 4 was identical to that of Test 3 except that only one flatpack gage was used. This gage was the same one used in Test 3 at the 2.54-cm radius. (It had survived Test 3 with only surface damage and small permanent resistance changes in the manganin and strain-gage elements.) Again the gage was placed at the 2.54-cm radius with the elements oriented in the radial direction. The strain-gage amplifier, identical to those used with the manganin gages in previous tests, has a linear frequency limit of greater than 1 MHz.

The unfiltered strain-gage record from Test 4 shown in Figure D-10(a) contains noise at a frequency of about 3 MHz in the first 10 μs. This record was filtered numerically at 500 kHz to obtain a more direct comparison with the strain record from Test 3. As shown in Figures D-10(b) and (c), the filtered strain gage record from Test 4 has a different character than the record obtained in Test 3. Unfortunately, not only is the frequency content different but the overall amplitude is also larger. Although a nonlinear filter applied to the Test 4 record might produce a closer match to the Test 3 record, we believe the element in Test 4 experienced a different strain environment, so the different response cannot be attributed solely to different signal conditioning. The mechanical properties of the flatpack may have been affected by its use in an earlier test. However, the Test 4 record clearly has significant frequency content at about 150 kHz and greater. Thus, the high-frequency signal conditioning for strain gages was used in subsequent experiments.

RESIDUAL DEFORMATION PROFILES

The purposes of measuring the deformed shapes of the steel targets are to help determine the strain environment that the gages experienced in the tests and to help determine the accuracy of the computational predictions presented in Appendix C. The deformation profiles were measured by traversing the surface of the test article along two orthogonal diameters with a dial indicator mounted in the head of a milling machine. The four elevation measurements taken at each radius were then averaged. For Test 2 we measured the shapes of the top surface of the plate, the bottom
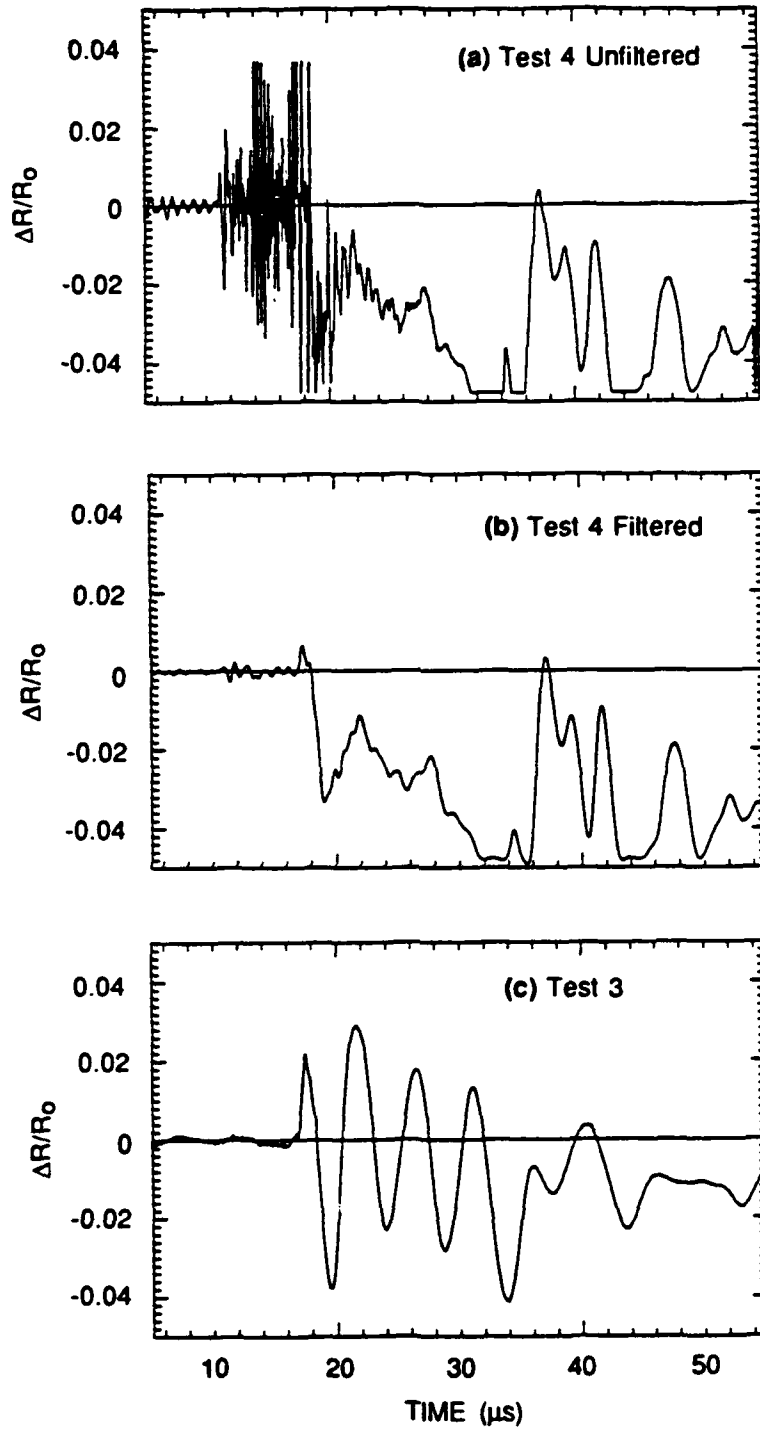
RA-7422-47C

Figure D-8. PIEZOR interpretation of Test 3 flatpack records for zero
transverse strain.

D-11
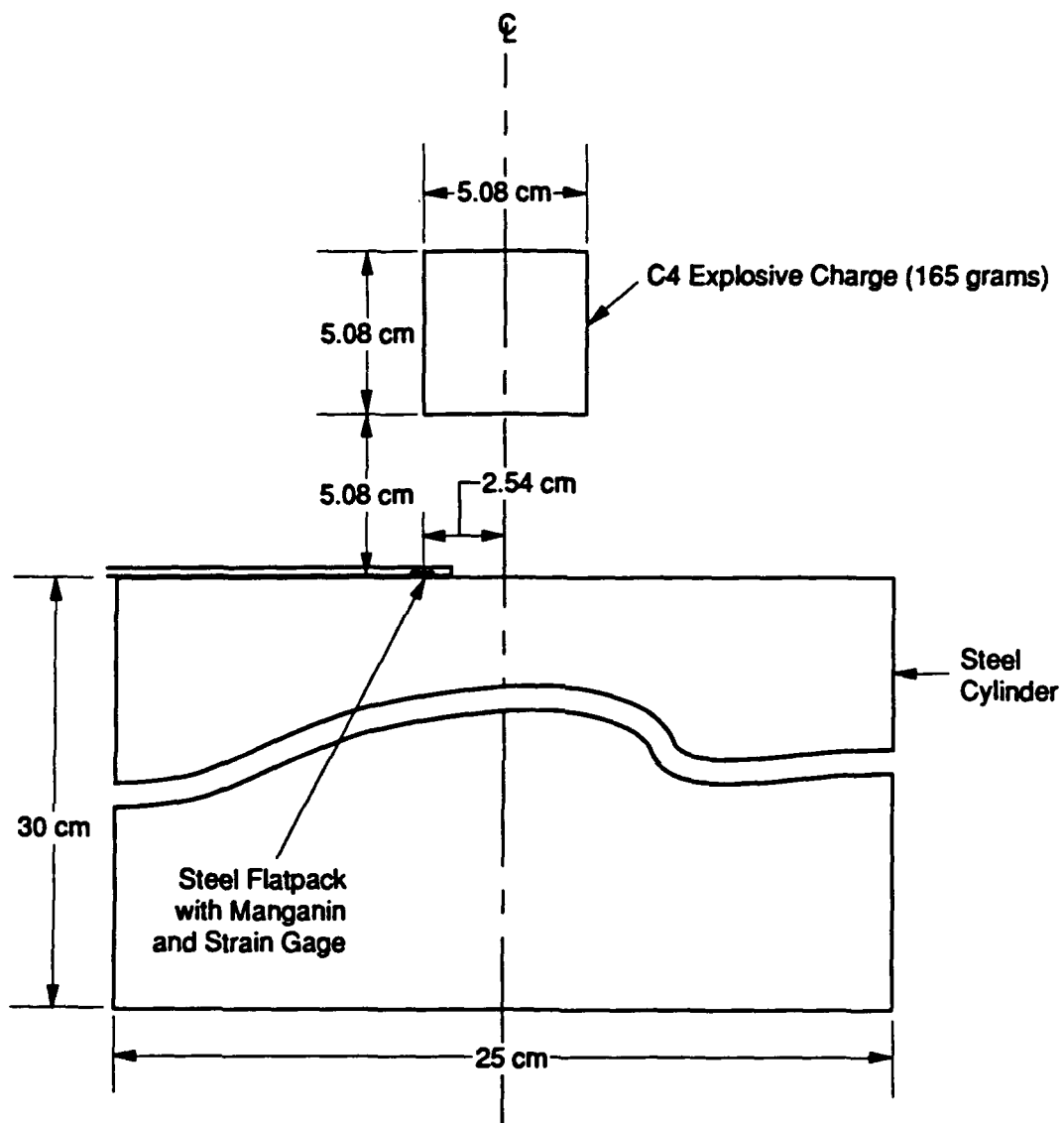
Figure D-9.   Configuration for Test 4.

RM-7422-15E

Figure D-10. Resistance histories from strain gages in flatpacks
in Tests 3 and 4.

surface of the plate, and the top surface of the cylinder. For Tests 3 and 4, we measured the shape of the top surface of the cylinder *after* Test 4. Thus, this shape contains the accumulated permanent deformation from Tests 3 *and* 4. In the plots shown below, these accumulated deformations were halved to approximate those from a single loading.

Figure D-11(a) shows the deformed profile of the top surface of the plate after Test 2. The depth of the depression at the center of the plate is about 0.016 cm (6.3 mil). The computed profiles are from the last time step in the computations (50 μs). Both computations (for a no-slip interface and a free-slip interface) predict a central depression of about the same diameter as measured, but the predicted depth of the depression is much larger than measured. The computations also predict much more deformation outside the central depression than is measured.

Figure D-11(b) shows the deformed shapes of the bottom of the plate and the top of the cylinder after Test 2. By spacing these profiles 0.020 cm (8 mil) apart at the outer radius, we have an approximate view of the residual shape of the epoxy layer. The epoxy layer apparently compressed quite a bit near the center, which must have significantly affected the deformation of the plate and cylinder. Also, the gradient in residual thickness of the epoxy layer suggests that the plate deformation produced radial flow in the epoxy layer, which could have affected the strain gages and manganin elements on the surface of the cylinder. Both computational simulations overpredict the deformation of the cylinder; the computations make no prediction of residual epoxy layer thickness because they both modeled the epoxy layer as an interface.

Figure D-11(c) shows the deformed shape of the top of the cylinder after Tests 3 and 4, with the measured deformations halved to approximate the result of a single loading. Again, the computational simulation (with the no-slip interface) overpredicts the depth of the central depression and predicts a deformed shape outside the central depression that is unlike the observed profile.

The deformed profile measurements from Tests 2 to 4 indicate that significant residual deformation occurs with a 4-cm radius, so it would be reasonable to expect large strains in that portion of the target. (In future experiments, we will scribe the targets with equally spaced lines before the test so that we can make posttest measurements of residual *strain* in addition to residual surface shape.) However, the computational simulations overpredict the deformation, suggesting that the computed strains are also greater than those experienced by the target. Thus, the strain-gage signals, which greatly exceed the predicted strains, apparently do not represent the actual strains in the target. Recall that an elastic perfectly plastic constitutive model was used for the cylinder and cover plate. Not allowing hardening could lead to an overestimation of the residual strains.

ASSESSMENT OF THE STRAIN-GAGE RECORDS

The strains predicted by L2D computations (Appendix C) are about an order of magnitude smaller than those indicated by the strain-gage records from Tests 2 and 3. However, as indicated in the previous subsection, it does not seem plausible that the target strains were 10 times larger than predicted because the measured residual deformations were considerably smaller than the L2D predictions. Thus, the strain-gage signals were not induced directly by target strains.

The magnitudes of normal stress oscillations that would be required to produce the observed strain-gage oscillations are *very* large. In the case of the circumferential strain gage at the 2.54-cm radius in Test 2, the stress oscillations would have to have been 25 kbar (2.5 GPa). Thus, the strain-gage signals were not induced by stress oscillations.
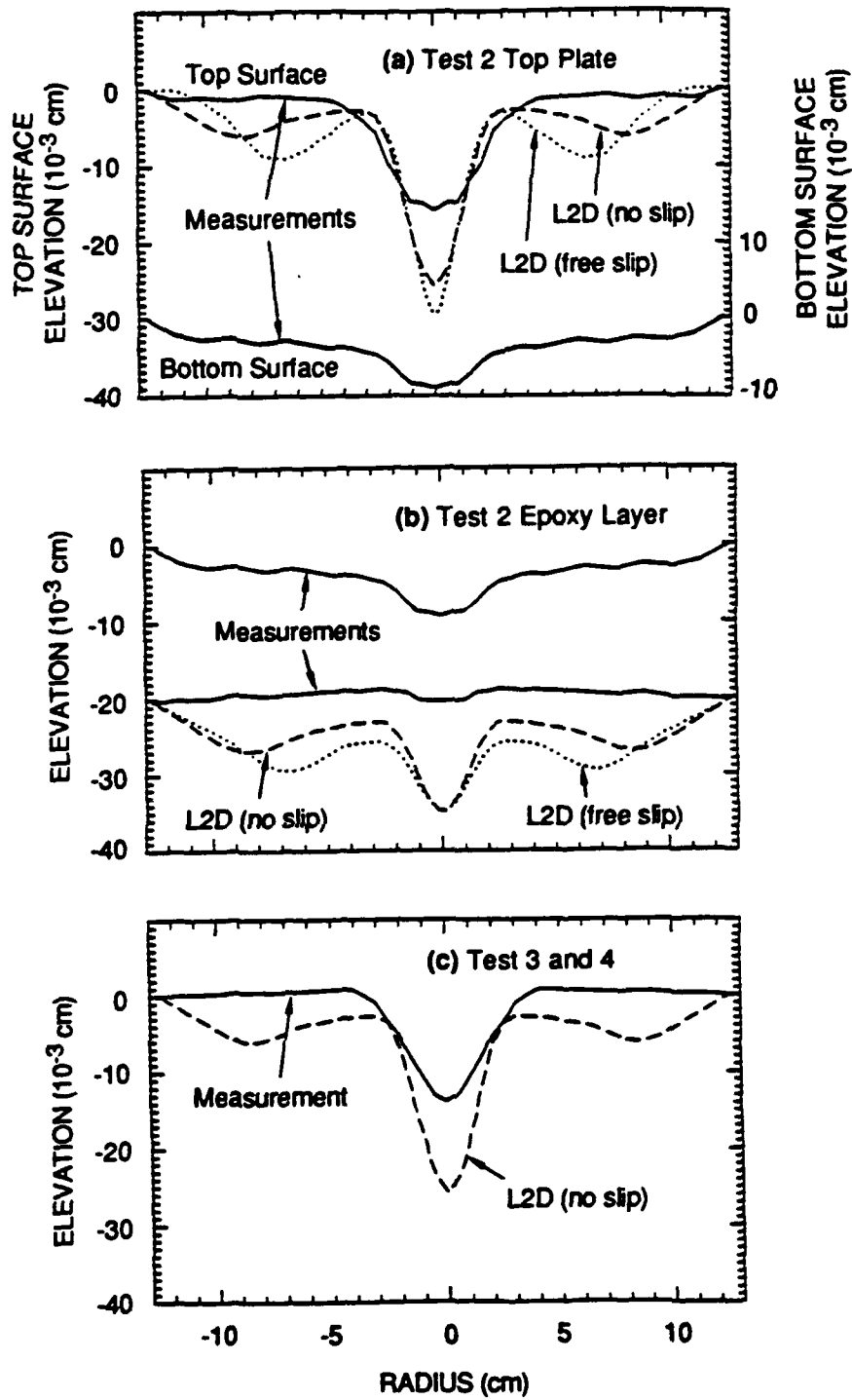
Figure D-11. Residual deformation profiles from Tests 2, 3, and 4.

Oscillations of the same frequency as those in the strain-gage signals also occurred in the manganin-gage signals in Test 3. Furthermore, the amplitudes of the oscillations in the manganin-gage signals are consistent with the assumption that the strain-gage signals represent elastic strain in the manganin element. Thus, it appears that the strain gages are recording the actual element environment.

The frequency of the oscillations in the strain-gage signals from Test 2 matches the frequency of stress oscillations in the epoxy layer predicted by a one-dimensional stress-wave computation (not shown). Also, the oscillations in the strain-gage signals from the flatpacks in Test 3 approximately match the calculated flexural frequency of the flatpack cover supported by an elastic layer of epoxy. Thus, it appears that package response (the plate on the epoxy layer or the flatpack on the surface) is inducing strains in the elements that are much different in character and magnitude from the local target strains.

In summary, the evidence indicates that the strain gages in Tests 2 and 3 provide records of element strains induced by the response of the element packages. That is, the strain-gage records represent strains in the epoxy layer in Test 2 and strains inside the flatpacks in Test 3. That these strain histories are so different (much larger amplitude) from the computational predictions of target strain implies that the elements need to be packaged or positioned differently to inhibit these strains.

TEST 5

The objectives of Test 5 were to

(1) Determine the relative magnitudes of strain in the longitudinal and transverse directions in flatpack gages.

(2) Find the dependence of these strains on the nature of the attachment of the flatpack to the target and the orientation of the flatpack to the explosive charge.

The 25-cm-diameter steel target and the 5-cm-diameter C4 explosive charge with a 5-cm standoff were the same as in the previous tests. Four flatpack gages were used, each with a pair of orthogonal strain-gage elements. Figure D-12 shows the flatpack gage configuration. Two flatpacks were welded to the target; two were bonded with epoxy. Two were oriented radially to the charge; two were oriented tangentially. The center of the sensing area of each flatpack was at a 2.75-cm radius from the axis of the explosive charge. (The slightly larger than 2.54-cm spacing was required to allow room for welding.)

The strain-gage records are plotted in Figures D-13 through D-16. In these plots, the recorded resistance histories have been digitally filtered at 1 MHz and converted to strain using the manufacturer's gage calibration without compensating for normal stress. In general, the strain in the transverse direction is comparable in magnitude to that in the longitudinal direction. Also, the welded flatpacks had slightly lower strains than those bonded with epoxy. Radially oriented and tangentially oriented flatpacks had about the same strain levels.
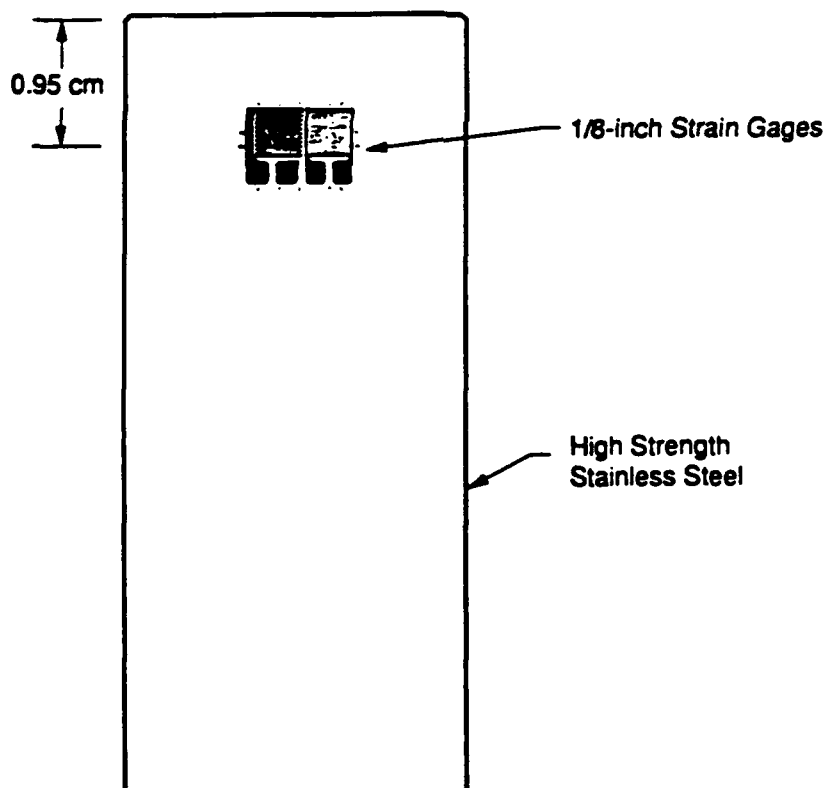
From these results we conclude that

(1) Both longitudinal and transverse strains are significant. Thus, both strains need to be measured to account for the effects of in-plane strain on manganin and ytterbium stress-sensing elements.
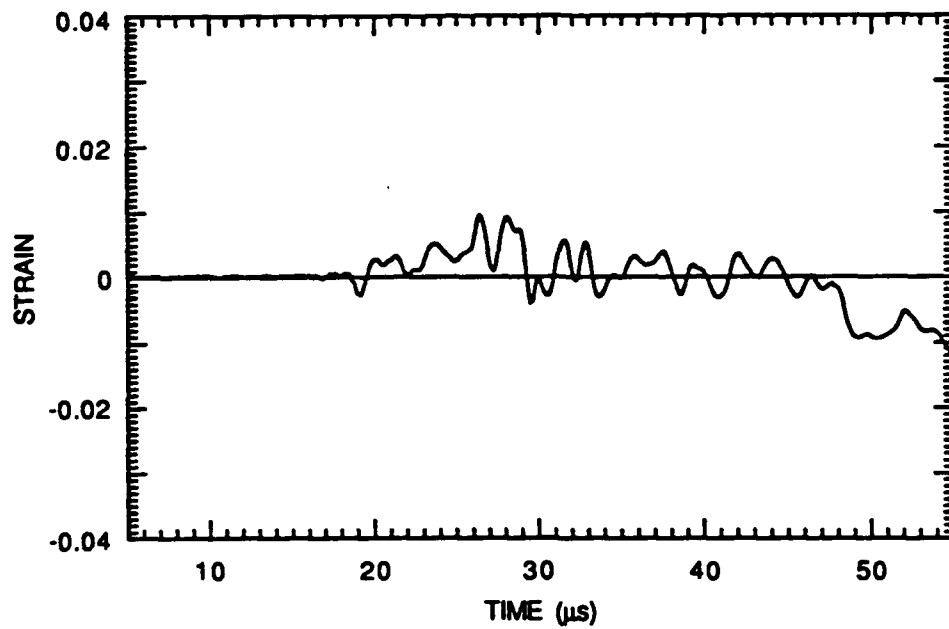
Figure 12

Weld

Explosive
Charge

2.75 cm

Epoxy
Bond
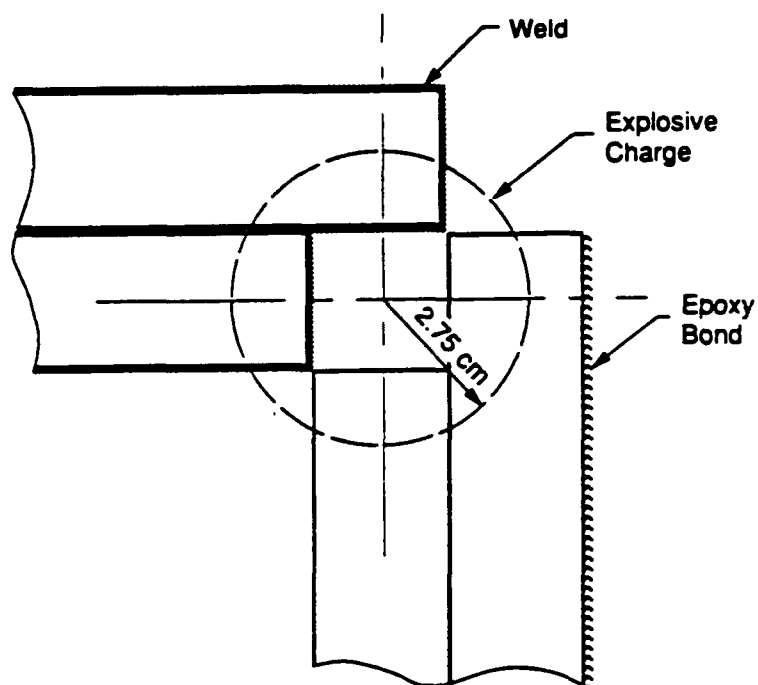
(a) Top view of gage arrangement

0.95 cm

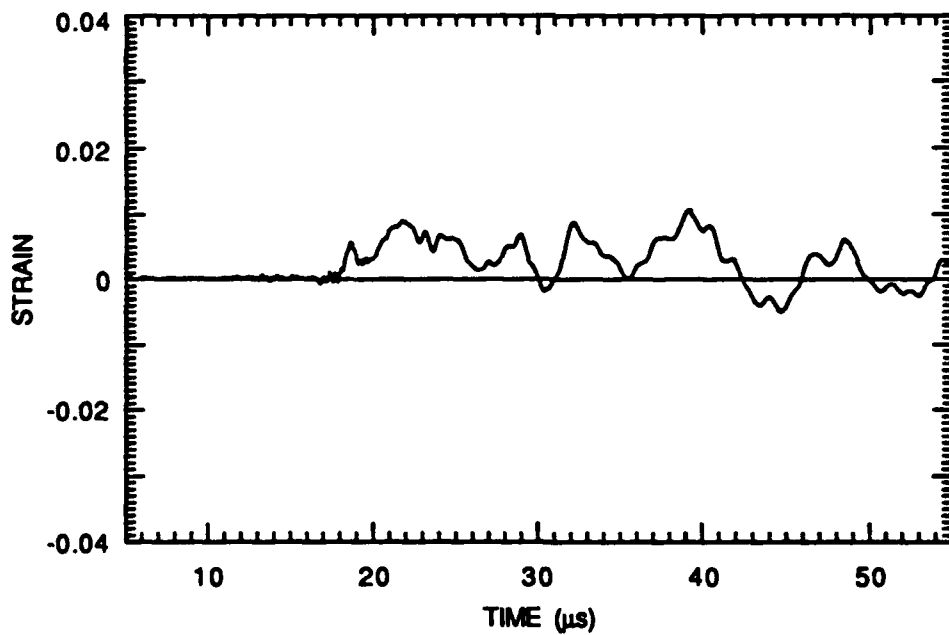1/8-inch Strain Gages

High Strength
Stainless Steel

(b) Flatpack design

RA-7422-29
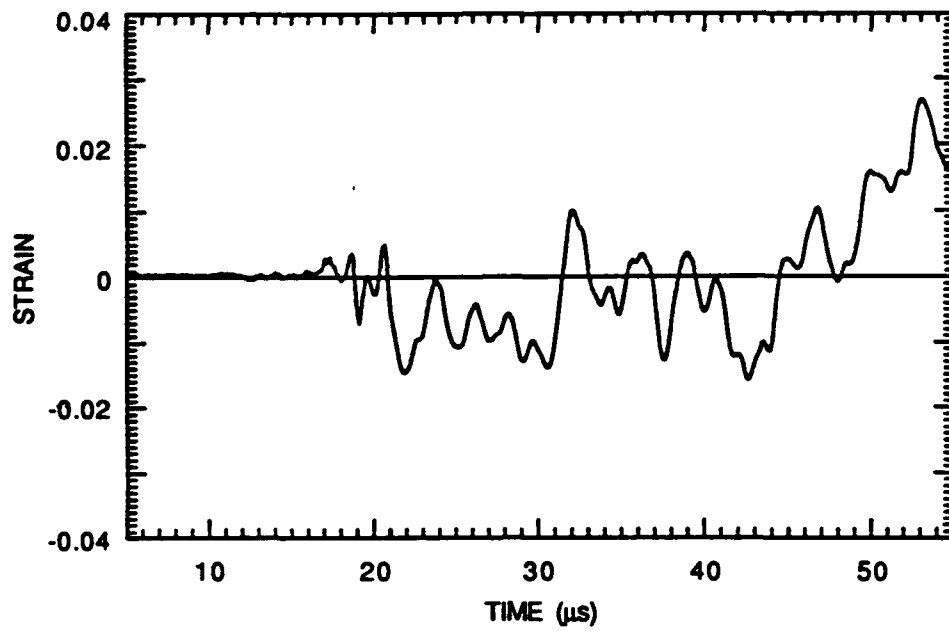
Figure D-12.   Flatpack gage configuration for Test 5.

D-17

(a) Longitudinal

(b) Transverse

RM-7422-41

Figure D-13. Test 5 strains from the welded flatpack in the radial orientation.
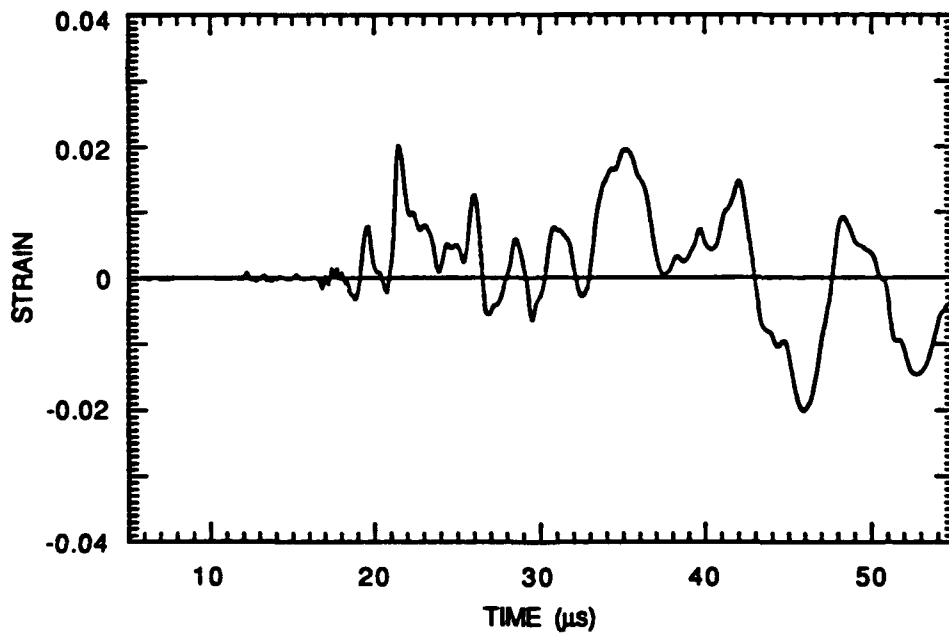
Figure D-14. Test 5 strains from the welded flatpack in the tangential orientation.

RM-7422-42

(a) Longitudinal

(b) Transverse

RM-7422-43

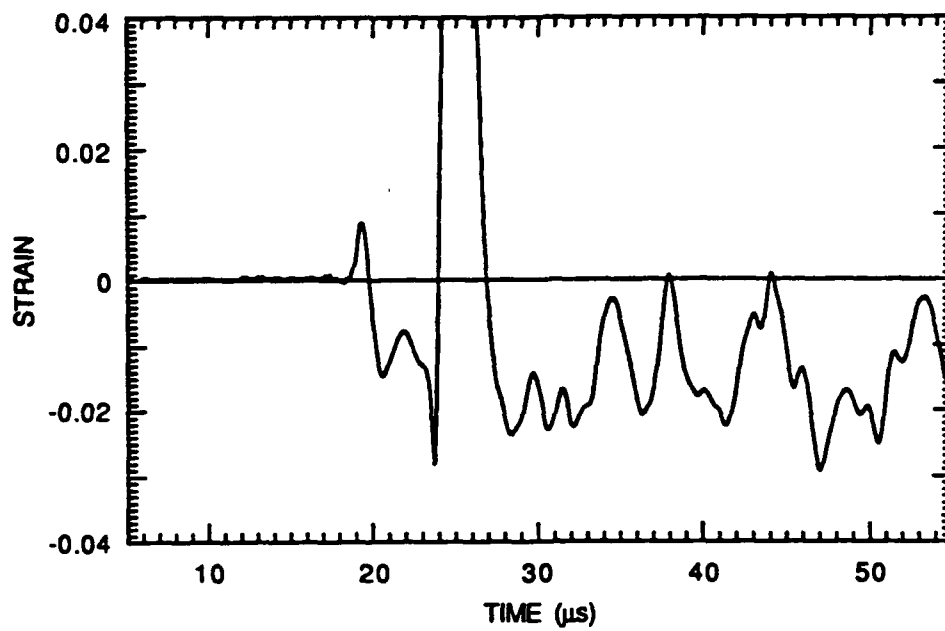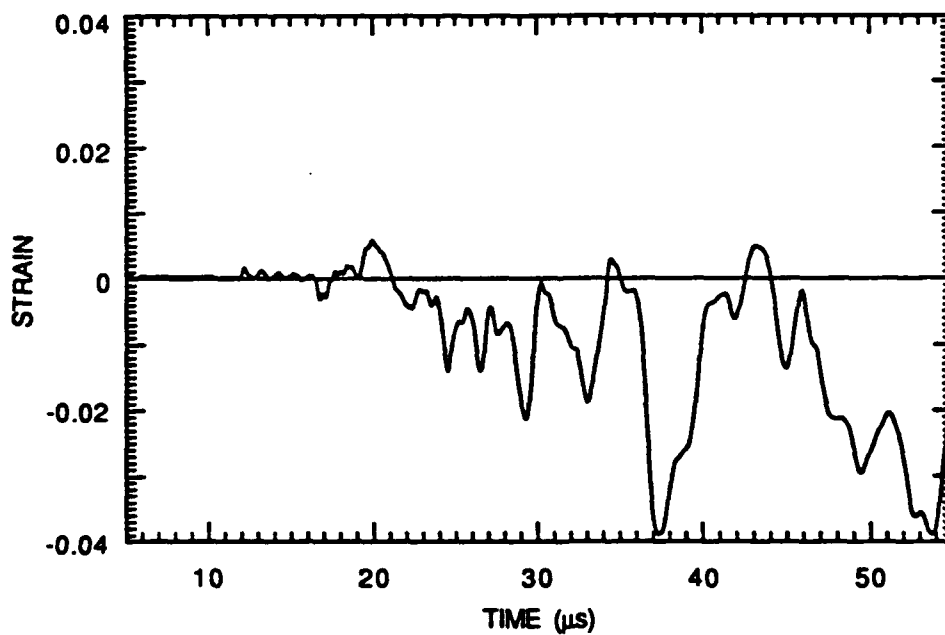Figure D-15. Test 5 strains from the epoxied flatpack in the radial orientation.

D-20
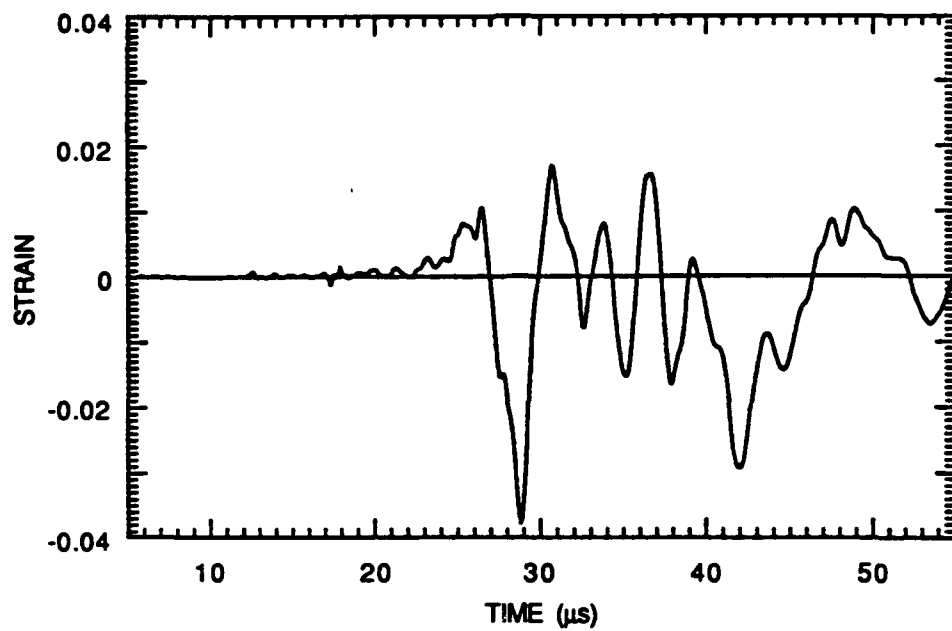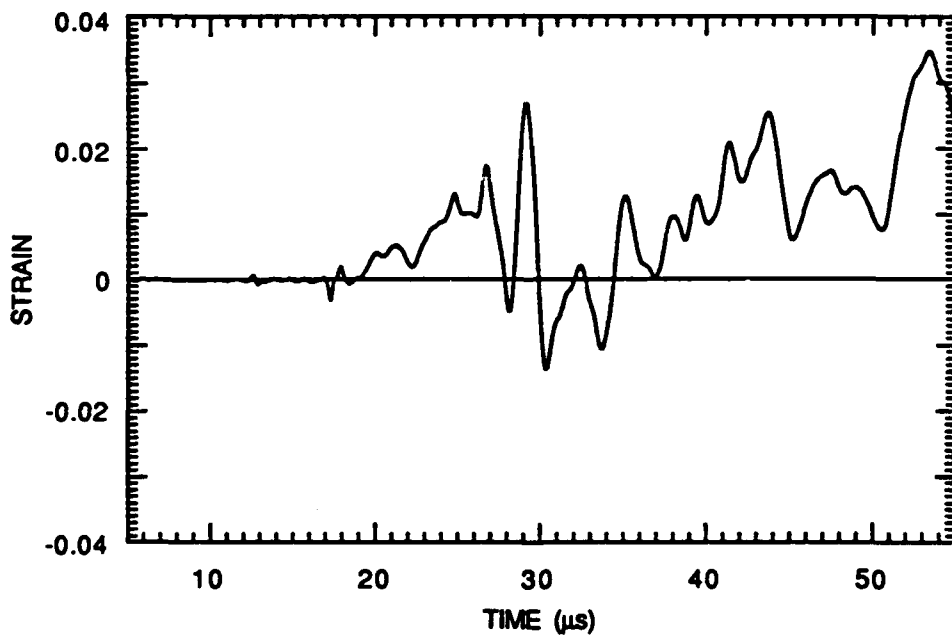
Figure D-16. Test 5 strains from the epoxied flatpack in the tangential orientation.

RM-7422-44

(2)   The strains in welded flatpacks are lower than those in epoxied flatpacks, but they are still large enough to significantly affect stress-sensing elements.

(3)   The orientation of the flatpack relative to the explosive charge is not important.

APPENDIX E

SIGNAL CONDITIONING

The pulsed bridge, shown schematically in Figure E-1, is a high-voltage version of an ordinary Wheatstone resistance bridge in which a change in resistance is determined by measuring the voltage due to bridge imbalance. The higher the voltage applied to the bridge, the higher the imbalance signal. The design of this circuit is described next; the relation between output voltage and gage resistance is discussed later.

To avoid destroying the piezoresistance gage element by the high current and resultant heating, the duration of bridge voltage application is limited to the time needed for the measurement. This can be done by discharging a capacitor (C_1) with a triggered silicon-controlled rectifier (SCR) switch to apply the voltage and a crowbar circuit to turn off the voltage, as done in SRI power supplies. Alternatively, one can use a field-effect transistor (FET) to control voltage, as done in SAIC* power supplies.

The apparent simplicity of the pulsed bridge circuit is deceptive. This is an AC circuit, designed to measure over a wide range of frequencies the change in resistance of a gage element located at the end of a long or short cable. Furthermore, the gage element is in a generally noisy environment, and the system must be optimized for noise rejection.

Referring to Figure E-1, R_1 and R_2 are 10 ohm resistors used to limit current through the crowbar SCR. They should be at least 5 watt resistors; 10 watt would be safer. They are not used or needed in the SAIC pulsed power supply, which uses a power FET rather than an SCR crowbar to turn the power off.

For signals traveling from the gage to the power supply, the capacitor C_1 appears as a short circuit. To properly terminate the gage cable, the sum of $R_1 + R_2 + R_8$ should be equal to the characteristic impedance of the gage cable (within 10%). Ideally, the gage cable should be a good quality balanced twin-ax such as RG22B. RG22B cable has a characteristic impedance of 95 ohms. With $R_1 = R_2 = 10$ ohms, one would choose a value of 75 ohms for R_8. With the SAIC supply, $R_1 + R_2 = 0$, and R_8 would be 95 ohms.

Gage element resistance is a design option. Since it is the relative resistance change that is related to the magnitude of the induced stress, the magnitude of the resistance change at a given stress will be simply proportional to the initial resistance of the gage element. If the current-handling capacity were independent of gage resistance, one would expect larger signals from higher initial resistance gage elements. However, if the area of the gage element is held constant, the current-handling capacity of the gage decreases proportionately as the resistance increases.

Gage cable resistance should be as low as practical; the sensitivity of the measurement system is inversely related to the gage cable resistance. Cable quality is important; it is imperative for accurate data reduction to capture the peak resistance changes by using high quality cable and/or shorter runs to the instrumentation.

---

*Sources for pulsed-power supplies are listed at the end of this section.
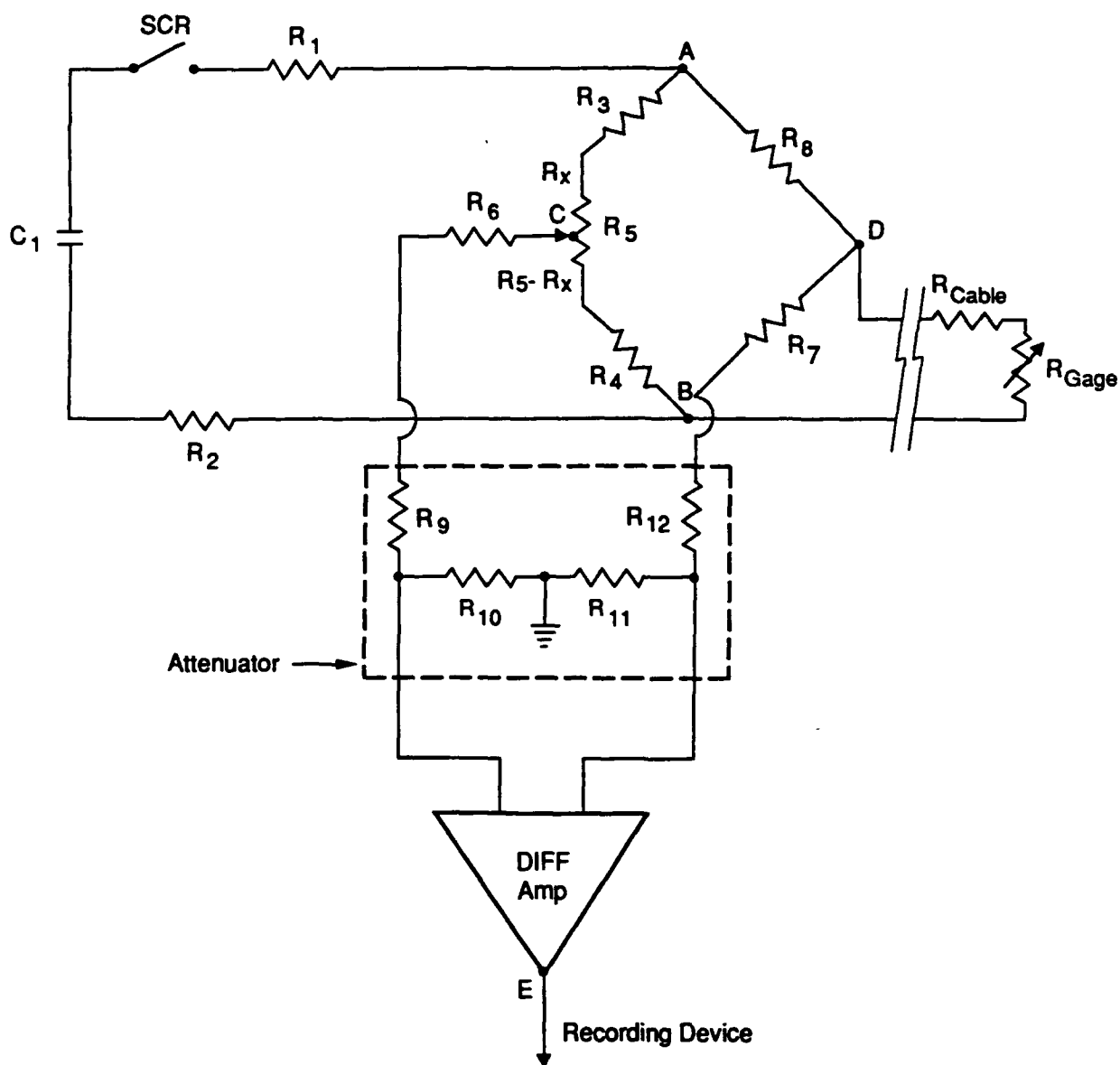
Figure E-1.   Pulse bridge power supply.

RM-7422-69

The sum of $R_3 + R_5 + R_4$ is generally in the range of 700 to 1500 ohms for most measurements. This range of values is a compromise: high enough to permit use of inexpensive one-watt ten-turn potentiometers but not so high that the high-frequency response of the system is degraded by stray capacitance. Two hundred ohms is a good value for R_5, the ten-turn pot. It is necessary to choose values of R_3 and R_4 compatible with the ratio of R_8 to the sum of gage and cable resistances. If the sum of gage and cable resistance is about 20 ohms and R_8 is 75 ohms (for impedance-matching reasons), then R_3 and R_4 could be 750 and 200 ohms, respectively. If the sum of gage and cable resistance is 100 ohms and R_8 is 75 ohms, R_3 and R_4 could be 500 and 600 ohms, respectively. We generally use two-watt resistors for R_3 and R_4. As mentioned, R_5 is a one-watt ten-turn pot.

R_6 is zero; we don't use a resistor here at all.

R_7 is the common mode balance resistor:

$$1/R_7 = 1/(R_1 + R_2 + R_3 + R_X) + 1/[R_4 + (R_5 - R_X)]$$

where R_X (the part of the pot resistance on the R_3 side of the slider) can be calculated from the relationship:

$$(R_3 + R_X)/(R_3 + R_5 + R_4) = R_8/(R_8 + R \text{ gage} + R \text{ cable}).$$

The purpose of R_7 is to balance the common mode signals on the gage cable with respect to the inputs to the differential amplifier. Noise generated in the test configuration will be coupled from the shield to the gage cable as common mode noise. If R_7 is zero, one side of the cable will be coupled directly to the input impedance of one side of the amplifier. The other side of the cable will be coupled to the other side of the amplifier through the parallel combination of $(R_1 + R_2 + R_3 + R_X)$ and $(R_4 + R_5 - R_X)$. If the input impedance of the amplifier is very high (megohms), R_7 may be omitted. If the input impedance is reduced to the Kilohm range, e.g., through use of attenuators, then the common mode balance obtained by choosing an appropriate value for R_7 can be critical in a noisy environment. Note that the value of R_7 was about 300 ohms and served to correct a 3% imbalance. A 10% error in the value of R_7 was acceptable, corresponding to an imbalance of 0.3%. R_7 may be a 1/8-watt resistor.

The purpose of the attenuator is to protect the amplifier from both common-mode and normal-mode overvoltages. Because of cable and system capacitance to ground, a decaying common mode voltage appears at the amplifier inputs when the bridge circuit is pulsed. The initial level of this common mode voltage is determined by the ratio of the gage and cable resistance to R_8 and can exceed the common mode voltage handling capabilities of the differential amplifier. Additionally, a large normal mode spike can be generated when the supply is pulsed because of the AC imbalance of the bridge. The attenuator reduces normal- and common-mode voltages to levels that can be handled by the amplifier. We typically use a 10:1 attenuator. Note that the attenuators are made up in matched pairs. Common mode rejection can be seriously compromised by mixing up the originally matched pairs. Our attenuator recipe is:

R_9 = R_{12} These resistors are nominally 9 k ohms and are matched to within 0.05%.

R_{10} = R_{11} These resistors are nominally 1 k ohm and are matched to within 0.05%.

1/8-watt resistors are adequate for the attenuators.

The attenuators are carefully matched so that the common mode noise will be attenuated equally at both amplifier inputs. In principle, matched capacitors should be added to the attenuators to improve their high frequency characteristics. However, after conducting tests at SRI with both capacitor-compensated and uncompensated attenuators, we concluded that the capacitors made no detectable difference, given the configuration with short cables between the power supplies and amplifiers. Note that R_7 must be included in an accurate calculation of the magnitude of the attenuation. With R_7 about 300 ohms, the attenuation will be increased by about 1.5%.

The source voltage V_s applied to the bridge circuit by the capacitor C_1 is given by

$$V_s = V_{so}e^{-t/\tau}$$

where V_{so} is the initial capacitor voltage, and τ is the time constant given by

$$\tau = R_1 + R_2 + R_{AB}$$

where R_{AB} is the resistance between A and B of the bridge, given by

$$R_{AB} = \frac{[R_{atten}(R_3+R_4+R_5)+(R_3+R_X)(R_4+R_5-R_X)](R_8+R_G+R_C)+R_8(R_G+R_C)(R_3+R_4+R_5)}{R_{atten}(R_8+R_3+R_4+R_5+R_G+R_C)+(R_8+R_3+R_X)(R_G+R_C+R_4+R_5-R_X)}$$

where $R_{atten} = R_6 + R_9 + R_{10} + R_{11} + R_{12} + R_7$

R_G = Gage resistance

R_C = Cable resistance

The time constant τ is determined at the arrival time ($t = t_0$) of the shock wave by assuming only the initial value of R_G. We have found that changes in R_G arising from the shock wave have no appreciable effect on V_s through changes in τ, at times greater than t_0.

The bridge voltage is V_{CD} is related to the differential amplifier output voltage V_E by

$$V_{CD} = V_E \times \frac{\text{Attenuation factor}}{\text{Amplifier gain}}$$

The attenuation factor is given by

$$\text{Attenuation factor} = \frac{R_{10} + R_{11}}{R_{atten}}$$

but attenuation factor and gain are usually determined by measurement.

We are interested in the effect of changes in R_G arising from the shock wave. Because we measure V_E and determine V_{CD}, we wish to determine R_G from V_{CD}, so we can then find the stress on the piezoresistance gage. The expression for R_G is given by

$$R_G = -R_C + \left\{ V_s\, R_{atten}\, (R_4 + R_5 - R_X)\, R_8 - V_{CD}\left[-2(R_3+R_X)\, R_{atten}\, (R_4+R_5-R_X) \right.\right.$$
$$+ (R_4+R_5-R_X+R_{atten})\, (R_8+R_X+R_3+R_{atten}) \cdot (R_3+R_4+R_5+R_1+R_2)$$
$$- (R_3+R_X)^2\, (R_4+R_5-R_X+R_{atten}) - (R_8+R_3+R_X+R_{atten})\, (R_4+R_5-R_X)^2$$
$$\left.\left. - R_{atten}^2(R_3+R_4+R_5+R_1+R_2) \right]\right\} \div$$

$$\left\{ V_s\, R_{atten}\, (R_3+R_X) + V_{CD}\left[(R_8+R_3+R_X+R_{atten})\, (R_3+R_4+R_5+R_1+R_2) \right.\right.$$
$$\left.\left. - (R_3+R_X)^2 \right] \right\}$$

In general, the bridge will not be perfectly balanced, because of limited resolution of the potentiometer, because of only an estimate for the expected change in R_G, and because of ambient heating resistance changes in cable and gage. The offset or reference voltage is referred to as V_{CDO}, observed at $t = t_0$. We can now obtain the change in gage resistance ΔR_G with respect to its reference value by the following expression:

$$\Delta R_G = R_G\, (V_{CD}(t),\, V_s(t),\, R_i) - R_G\, (V_{CDO},\, V_s(t_0),\, R_i)$$

assuming no further resistance heating changes occur in cable or gage (or elsewhere in the circuit). The relative change in gage resistance is then given by

$$\frac{\Delta R_G}{R_{GO}}$$

where R_{GO} is the gage resistance at $t = t_0$. If gage heating effects are negligible, R_{GO} will be the ambient temperature value of R_G.

SOURCES FOR PULSE POWER SUPPLIES

1. SAIC - Science Applications International Corporation, 3351 South Highland Drive, Suite 206, Las Vegas, NV 89109, Model SG-133A.

2. Dynasen, Inc., 20 Arnold Place, Goleta, CA 93117 (805) 964-4410, Model CK1-50-300.

INTENTIONALLY LEFT BLANK.

APPENDIX F

PRETEST CALCULATIONS OF THE PLATE-IMPACT EXPERIMENT

In the plate-impact experiment described in Section 5, a 25.4-mm-thick PMMA flyer plate impacted a 25.4-mm-thick buffer plate. Flatpack gages were placed at the interface between the buffer plate and a steel target plate. In the design of this experiment, the concern was that the flatpack gages might under-register the interface stress because they are more compliant than the solid steel target. In this appendix, we present the results of one-, two-, and three-dimensional pretest calculations performed for the specific purpose of predicting the response of the flatpacks.

In these calculations, the steel was modeled as an elastic-plastic material. The piezoresistance elements, the Kapton insulation, and the epoxy inside the flatpacks were modeled as a uniform layer with the elastic-plastic properties of the epoxy. The PMMA was linearly elastic. Table F-1 gives the properties of these materials. All the interfaces between materials were bonded. The impact velocity in the calculations was 51 m/s (higher than actually achieved in the experiment). The one-dimensional calculations were performed with SRI PUFF.[*] The two- and three-dimensional calculations were performed with DYNA3D.[**]

Table F-1. Material Properties for Pretest Calculations

Material	Density (g/cm^3)	Young's Modulus (GPa)	Poisson's Ratio	Yield Strength (GPa)	Hardening Modules (MPa)
Steel	7.85	200	0.3	1.24	1.0
PMMA	1.184	6.73[*]	0.345	—[*]	—
Epoxy	1.50	3.45[**]	0.35	0.069[**]	0.1

[*]The elastic behavior and the value of Young's modulus represent the estimated behavior for the strain rates involved. The static compressive strength is about 0.083 GPa.

[**]The manufacturer's recommended values are 3.17 and 0.083 GPa.

---

[*]L. Seaman, "SRI PUFF8 Computer Program for One-Dimensional Stress Wave Propagation," SRI International Final Report for U.S. Army Ballistic Research Laboratory, Contract DAAK11-77-C-0083, Vol. II (August 1978).

[**]J. Hallquist and D. Benson, "DYNA3D User's Manual (Nonlinear Dynamic Analysis of Structures in Three Dimensions)," Lawrence Livermore National Laboratory, Report UCID-19592, Rev. 2 (March 1986).

Figure F-1 shows the results of a pair of one-dimensional calculations. The first calculation did not include the flatpack gage. Figure F-1(a) shows the computed interface stress for this case. In the second calculation a one-dimensional flatpack was modeled with a 0.94-mm-thick steel layer and a 0.36-mm-thick epoxy layer between the PMMA buffer plate and the steel target. Figure F-1(b) shows that an overshoot and damped ringing of the stress inside the gage are predicted, but that the nominal equilibrium stress inside the gage is essentially equal to the interface stress.

Figure F-2 shows the results of a two-dimensional calculation in which the flatpack steel case and epoxy-filled cavity were included. The plane of this calculation included the normal and transverse axes of the flatpack, that is, it is a plane strain calculation with the longitudinal strain in the flatpack prohibited. The three cells for which the output is plotted are in the epoxy-filled cavity of the flatpack gage. One cell (A) borders the center of the sensing area, one cell (B) borders the outer edge of the sensing area, and one point (C) borders the edge of the cavity. The stress plots show that within the sensing area there is an overshoot followed by oscillations about the equilibrium stress level, but that the equilibrium stress level is essentially the same as the one-dimensional interface stress. Near the edge of the cavity the stress inside the gage is much lower. The strain plots show that the transverse strain is less that 0.002 within the sensing area and is only slightly larger near the edge of the cavity.

The results of a three-dimensional calculation are shown in Figure F-3. Both cells for which the output is plotted are in the epoxy-filled cavity of the flatpack. One cell (A) is at the center of the sensing area; the other cell (B) is 27.5 mm from the sensing area (toward the outer edge of the target). Both stresses show an overshoot and oscillations. The normal stress at A is slightly higher than the equilibrium stress predicted by the one- and two-dimensional calculations; the normal stress at B is slightly lower than those predictions. The longitudinal and transverse strains are less than 0.0005 except for one excursion of longitudinal strain at B to about 0.001.

In summary, the pretest calculations do not suggest that significant under-registration of stress by the flatpacks should occur in the plate-impact experiment. Additional analysis is necessary to fully understand the results of the experiment.
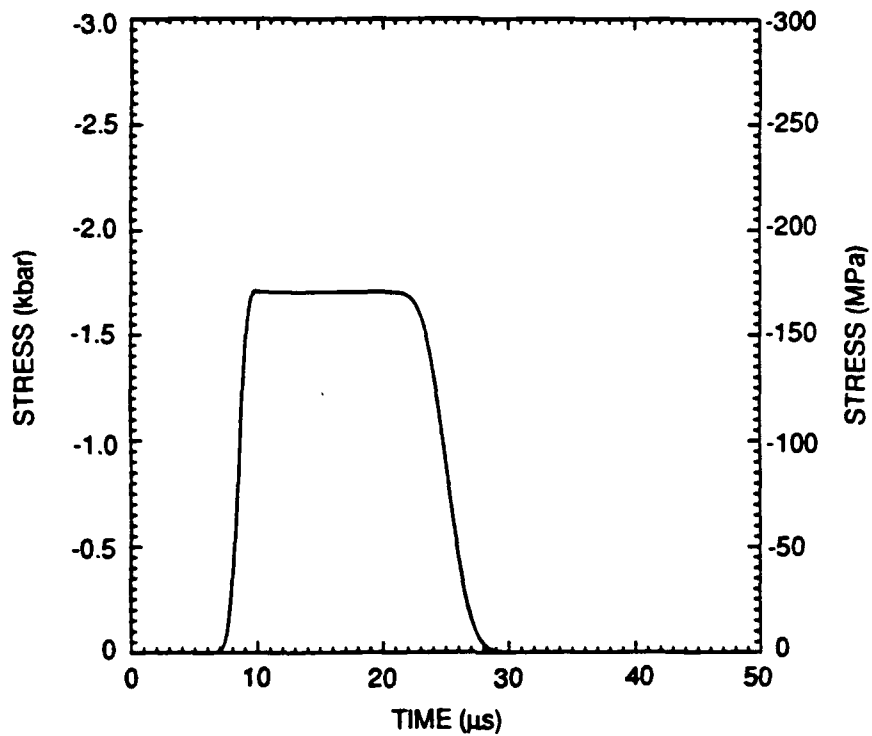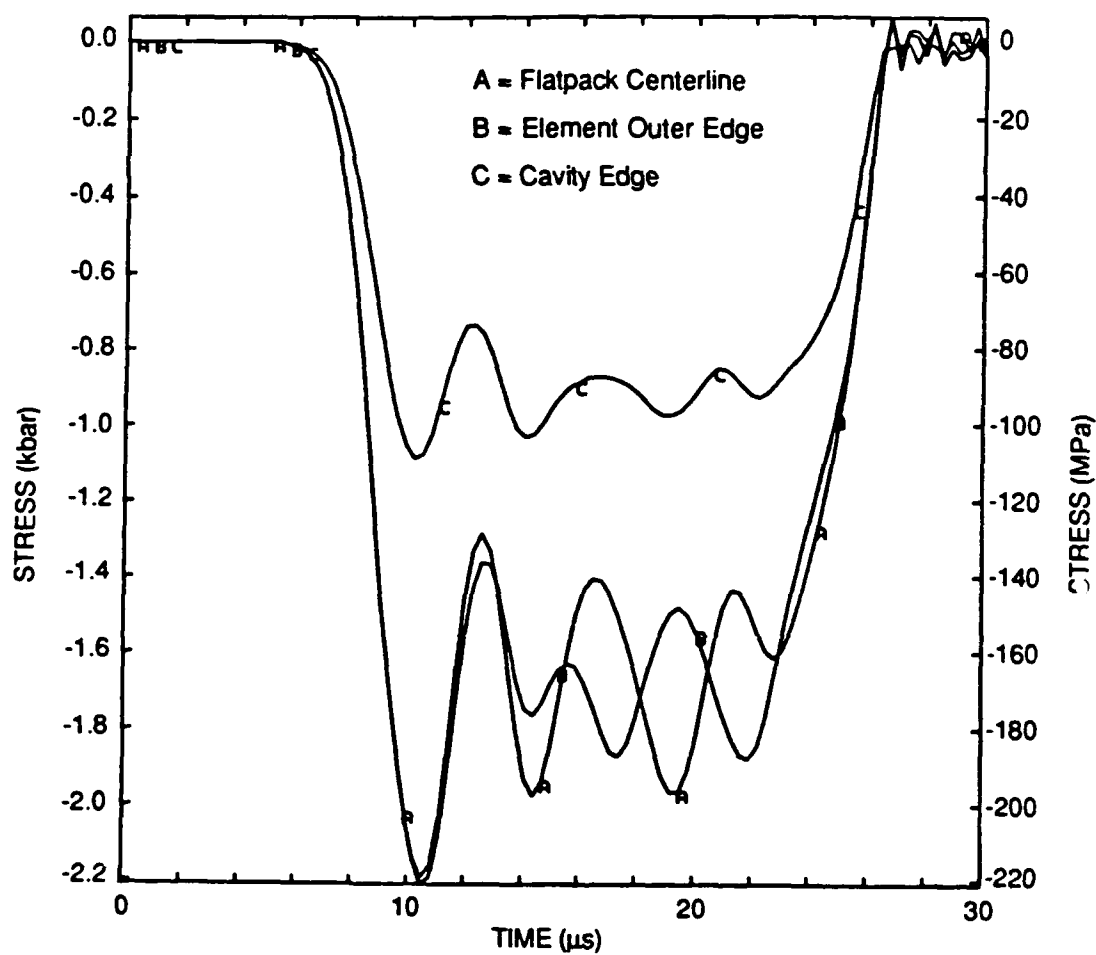
(a) PMMA/steel interface stress without the flatpack
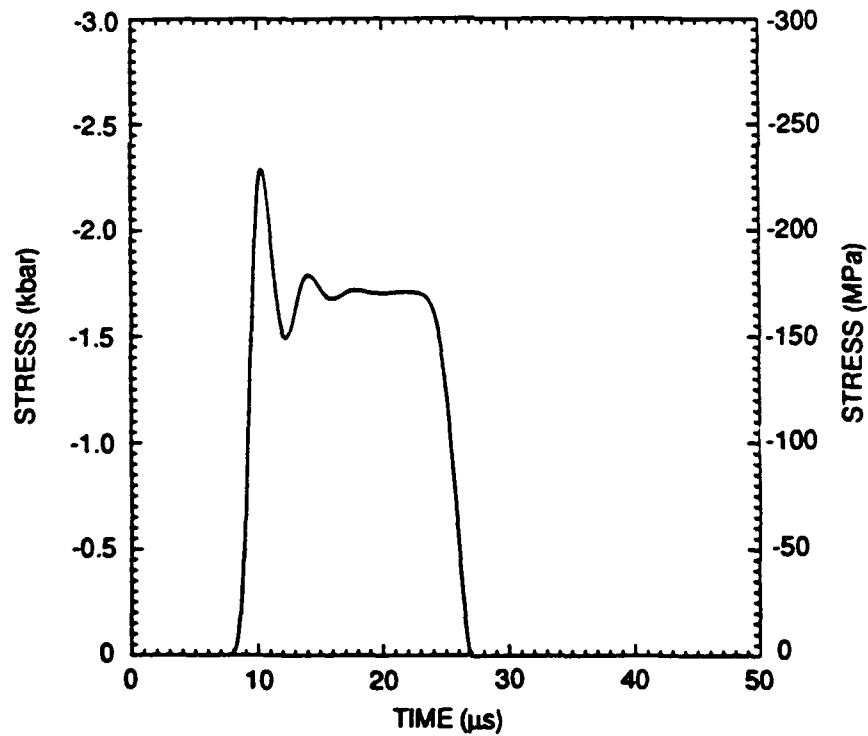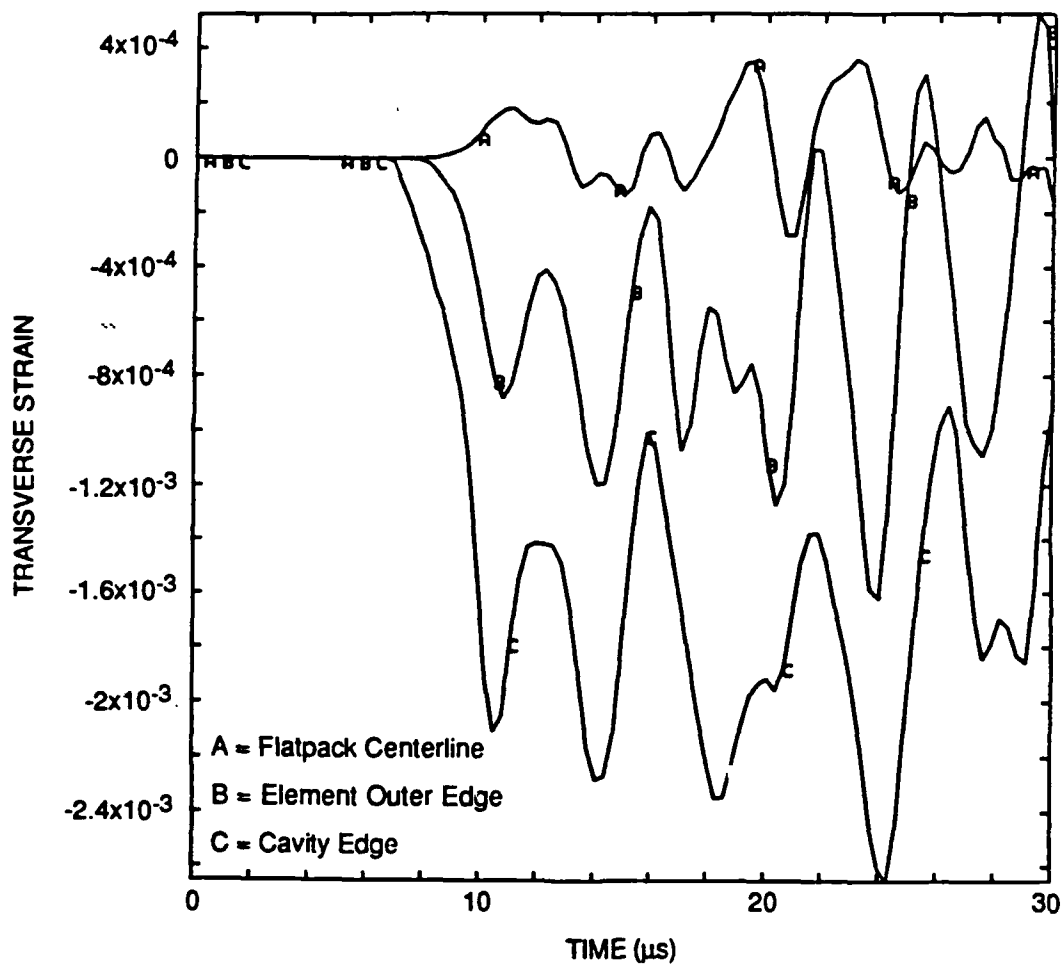
(b) Normal stress inside the flatpack

RA-7422-73

Figure F-1. One-dimensional finite-element pretest calculations
of the plate-impact experiment.

F-3

A = Flatpack Centerline
B = Element Outer Edge
C = Cavity Edge

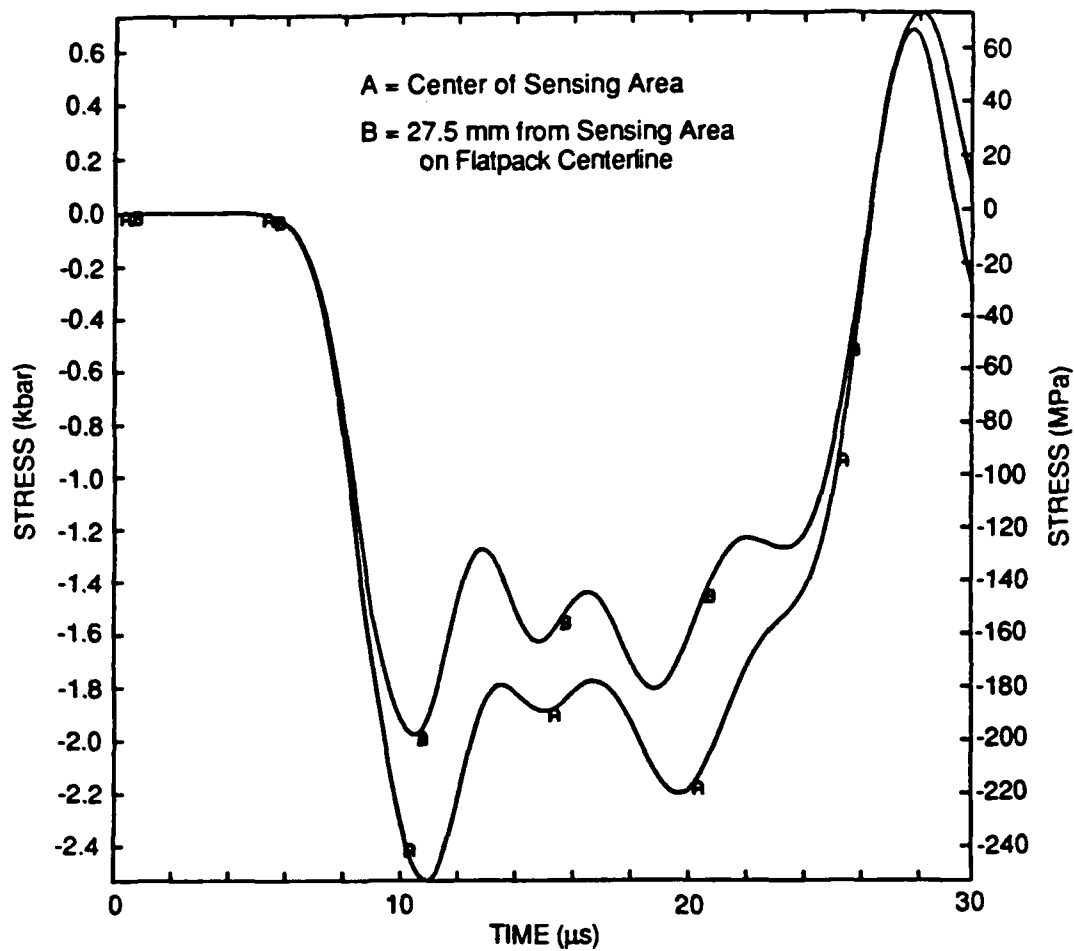(a) Normal stress inside the flatpack

RA-7422-74

Figure F-2. Two-dimensional finite-element pretest calculation
of the plate-impact experiment.

F-4

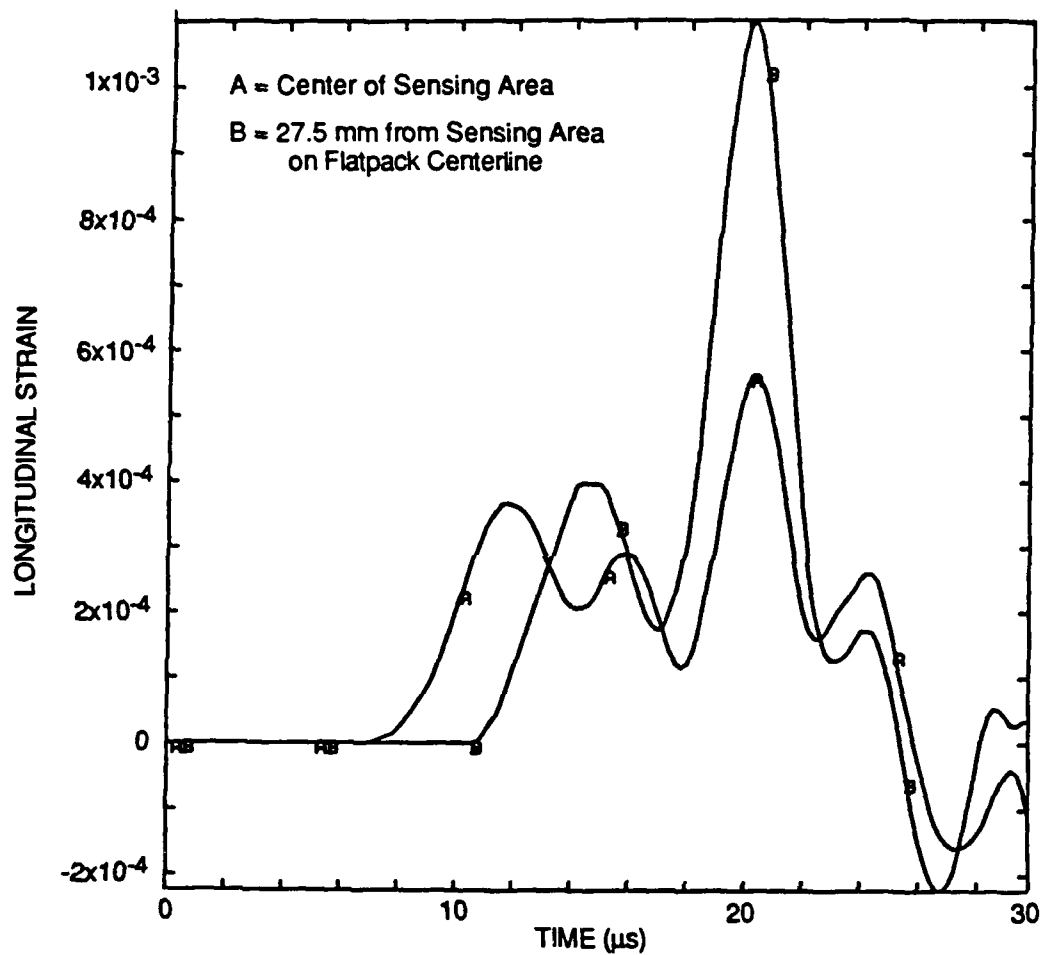(b) Transverse strain inside the flatpack

RA-7422-75

Figure F-2.   Two-dimensional finite-element pretest calculation
of the plate-impact experiment. (Concluded)

F-5

(a) Normal stress inside the flatpack

RA-7422-76

Figure F-3. Three-dimensional finite-element pretest calculation
of the plate-impact experiment.

(b) Longitudinal strain inside the flatpack

RA-7422-77

Figure F-3. Three-dimensional finite-element pretest calculation
of the plate-impact experiment. (Continued)

F-7
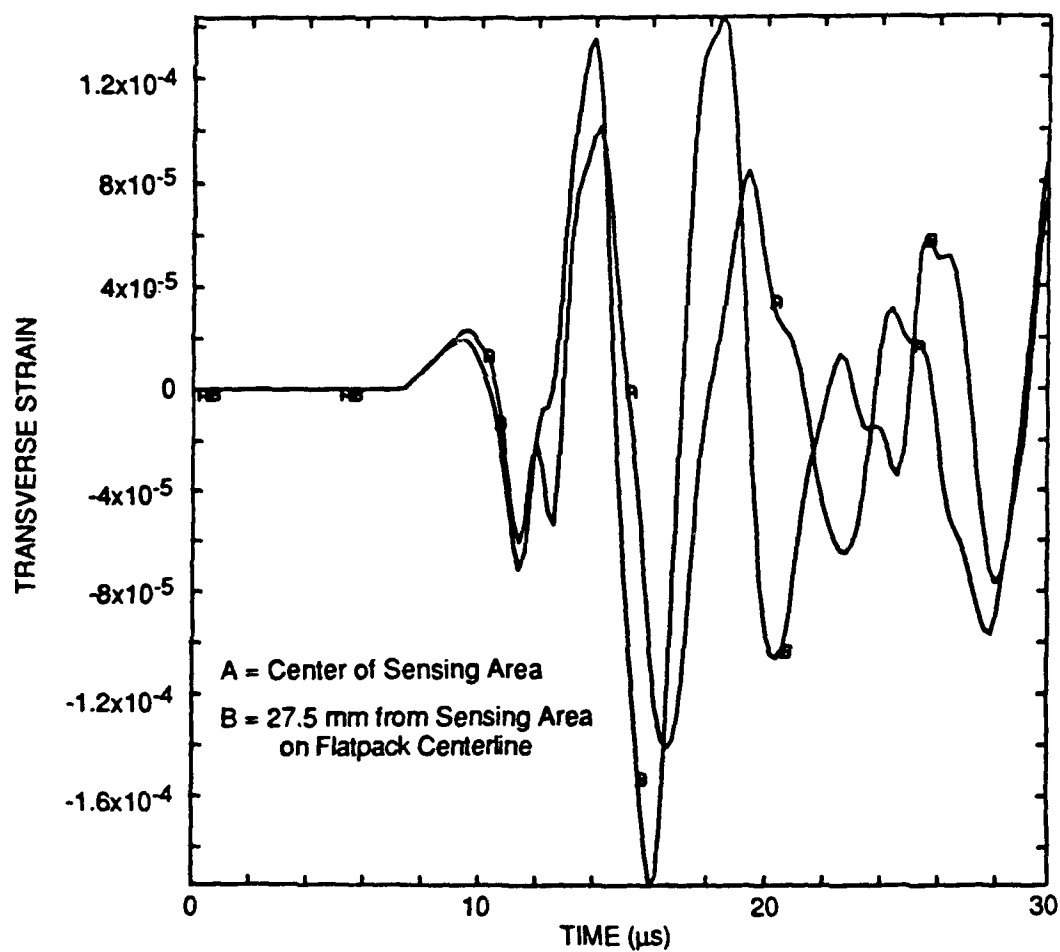
(c) Transverse strain inside the flatpack

RA-7422-78

Figure F-3. Three-dimensional finite-element pretest calculation
of the plate-impact experiment. (Concluded)

No. of Copies	Organization	No. of Copies	Organization
2	Administrator Defense Technical Info Center ATTN: DTIC-DDA Cameron Station Alexandria, VA 22304-6145	1	Commander U.S. Army Tank-Automotive Command ATTN: ASQNC-TAC-DIT (Technical Information Center) Warren, MI 48397-5000
1	Commander U.S. Army Materiel Command ATTN: AMCAM 5001 Eisenhower Ave. Alexandria, VA 22333-0001	1	Director U.S. Army TRADOC Analysis Command ATTN: ATRC-WSR White Sands Missile Range, NM 88002-5502
1	Commander U.S. Army Laboratory Command ATTN: AMSLC-DL 2800 Powder Mill Rd. Adelphi, MD 20783-1145	1	Commandant U.S. Army Field Artillery School ATTN: ATSF-CSI Ft. Sill, OK 73503-5000
2	Commander U.S. Army Armament Research, Development, and Engineering Center ATTN: SMCAR-IMI-I Picatinny Arsenal, NJ 07806-5000	(Class. only) 1	Commandant U.S. Army Infantry School ATTN: ATSH-CD (Security Mgr.) Fort Benning, GA 31905-5660
2	Commander U.S. Army Armament Research, Development, and Engineering Center ATTN: SMCAR-TDC Picatinny Arsenal, NJ 07806-5000	(Unclass. only) 1	Commandant U.S. Army Infantry School ATTN: ATSH-CD-CSO-OR Fort Benning, GA 31905-5660
1	Director Benet Weapons Laboratory U.S. Army Armament Research, Development, and Engineering Center ATTN: SMCAR-CCB-TL Watervliet, NY 12189-4050	1	WL/MNOI Eglin AFB, FL 32542-5000 Aberdeen Proving Ground
(Unclass. only) 1	Commander U.S. Army Rock Island Arsenal ATTN: SMCRI-TL/Technical Library Rock Island, IL 61299-5000	2	Dir, USAMSAA ATTN: AMXSY-D AMXSY-MP, H. Cohen
1	Director U.S. Army Aviation Research and Technology Activity ATTN: SAVRT-R (Library) M/S 219-3 Ames Research Center Moffett Field, CA 94035-1000	1	Cdr, USATECOM ATTN: AMSTE-TC
		3	Cdr, CRDEC, AMCCOM ATTN: SMCCR-RSP-A SMCCR-MU SMCCR-MSI
1	Commander U.S. Army Missile Command ATTN: AMSMI-RD-CS-R (DOC) Redstone Arsenal, AL 35898-5010	1	Dir, VLAMO ATTN: AMSLC-VL-D
		10	Dir, USABRL ATTN: SLCBR-DD-T

2   U.S. Army Materials Testing Laboratory
     ATTN: Ms. Kari Ofstedahl
            Dr. Shun Chin Chou
     Arsenal Street
     Watertown, MA 02172

1   Commander
     US Army Tank-Automotive Command
     ATTN: AMSTA-RSS, Mr. Bishnoi
     Warren, MI 48397-5000

2   FMC Corporation
     Advanced Systems Center
     ATTN: Ms. Carolyn Krebs
            Mr. James Drotleff
     2890 De La Cruz Boulevard
     Box 58123, MDP95
     Santa Clara, CA 95052

2   Ktech Corporation
     ATTN: Dr. E. S. Gafney
            Dr. David A. Hyndman
     901 Pennsylvania Avenue, N.E.
     Albuquerque, NM 87110

1   Naval Surface Warfare Center
     Dahlgren Division (G30)
     ATTN: Mr. W. S. Burnley III
     Dahlgren, VA 22448-5000

1   Commanding Officer
     Naval Research Laboratory
     ATTN: Code 6327, Dr. Robert Bayles
     Washington D.C. 20375-5000

2   Southwest Research Institute
     ATTN: Dr. Charles Anderson
            Mr. Scott Mullin
     6220 Culbera Road
     San Antonio, TX 78284

3   SRI International
     ATTN: Dr. Bayard S. Holmes
            Dr. James Gran
            Poulter Library
     333 Ravenswood Avenue
     Menlo Park, CA 94025

1   Sunburst Recovery, Inc.
     ATTN: Dr. Chapman Young
     P.O. Box 2129
     Steamboat Springs, CO 80477

3   University of Maryland
     Department of Mechanical Engineering
     ATTN: Dr. Richard Dick
            Dr. William Fourney
            Mr. Robert Gettings
     College Park, MD 20742-5141

Aberdeen Proving Ground

2   Cdr, USACSTA
     ATTN: STECS-DA-IL, Mr. Walton
            STECS-LI-V, Mr. Sokolis

46

USER EVALUATION SHEET/CHANGE OF ADDRESS

This laboratory undertakes a continuing effort to improve the quality of the reports it publishes. Your comments/answers below will aid us in our efforts.

1. Does this report satisfy a need? (Comment on purpose, related project, or other area of interest for which the report will be used.) _____
_____
_____

2. How, specifically, is the report being used? (Information source, design data, procedure, source of ideas, etc.) _____
_____
_____

3. Has the information in this report led to any quantitative savings as far as man-hours or dollars saved, operating costs avoided, or efficiencies achieved, etc? If so, please elaborate. _____
_____
_____

4. General Comments. What do you think should be changed to improve future reports? (Indicate changes to organization, technical content, format, etc.) _____
_____
_____

BRL Report Number __BRL-CR-693_____   Division Symbol _____

Check here if desire to be removed from distribution list. ____

Check here for address change. ____

Current address: Organization _____
                     Address   _____
                                  _____